Substrate Identification and Functional Analysis of α/ß Hydrolase Fold Epoxide Hydrolases

Author(s):
Hew, Bettina

Publication Date:
2019

Permanent Link:

https://doi.org/10.3929/ethz-b-000350557 →

DISS. ETH NO 25662

SUBSTRATE IDENTIFICATION AND FUNCTIONAL ANALYSIS OF α/β HYDROLASE FOLD EPOXIDE HYDROLASES

A thesis submitted to attain the degree of

DOCTOR OF SCIENCES of ETH ZURICH

(Dr. sc. ETH Zurich)

presented by

BETTINA HEW

MSc ETH in Pharmaceutical Sciences, ETH Zurich

born on 30.07.1987

citizen of Klosters-Serneus GR

accepted on the recommendation of

Prof. Dr. Hanns Ulrich Zeilhofer

Prof. Dr. Ursula Quitterer und Prof. Dr. Michael Arand

2019

PREAMBLE

The main project of the present work; “Deciphering the (patho)physiologic role of epoxide hydrolases by *ex vivo* cartography of their substrate landscape”, was a joined project of me together with Monika Dengler. Originally, it was planned to result in two independent projects after a joined part at the beginning, which did not work out. Thus, the research questions, methods and results were the same for both of us. We worked out the technical details, performed the experiments and analyzed the data with equal contributions. I particularly had the lead in AAV production and cell culture work, while M. Dengler had the lead in LC-MS/MS method development and analysis. In the two corresponding, individually written PhD dissertations the experimental parts were divided accordingly. For the sake of completeness missing sections were summarized and referred to the respective other work.
In contrast, the side project dealt with in this work; “The CYP blocker MS-PPOH is an inhibitor of sEH”, was my individual project.

SUMMARY

Epoxide hydrolases (EHs) are enzymes that convert epoxides to their corresponding vicinal diols. In mammals, they play a central role in the detoxification of genotoxic epoxides and have an important function in the regulation of physiological processes by hydrolyzing signaling epoxides. The best characterized EHs are the microsomal EH (mEH) and the soluble EH (sEH). mEH is generally considered to be primarily important in detoxification and only recently gained attention in signaling molecule metabolism. sEH, on the other hand, has long been recognized as the key enzyme in the hydrolysis of signaling fatty acid epoxides (FAEs), such as epoxyeicosatrienoic acids (EETs). The most recently discovered family member, EH3, was also shown to hydrolyze FAEs, thus a role in mammalian physiology seems likely. EH4 and mesoderm specific transcript (MEST) are also predicted to be mammalian EHs based on their primary structure, but their EH activity is not yet proven. Bacteria also possess EHs, sometimes with pathophysiologic consequences for host organisms as reported for the CFTR inhibitory factor (Cif), secreted by *P. aeruginosa*. However, the exact mechanism by which Cif fulfills its pathologic function is still unknown.

The knowledge about the aforementioned EHs is typically based on *in vitro* analysis of their substrate preference and does not allow direct conclusions on their real role in mammalian physiology. Thus, the general aim of the main project of this work was to identify the major (patho)physiologic roles of the six EHs via the identification of their preferred *in vivo* substrates. For this purpose, a novel unbiased *in vivo* substrate trapping approach, taking advantage of the characteristic molecular mechanism of EHs, was developed and applied. EH variants able to trap their substrate in a covalent ester-bond due to introduction of a point mutation, were expressed in target tissues of mice using adeno-associated virus (AAV) infection. The resulting enzyme-substrate complex was subsequently retrieved from tissue lysates by His-tag based affinity enrichment and analyzed using liquid chromatography-tandem mass spectrometry (LC-MS/MS) to identify the bound substrates.

A LC-MS/MS method to analyze bound substrates was successfully developed. The method could be confirmed by *in vitro* trapping experiments with sEH trapping mutant and its known substrate 14,15-EET. Moreover, successful AAV-mediated trapping EH expression was detected in different target organs of mice by Western blot and immunohistochemistry (IHC) stainings. However, in a comprehensive series of experiments, it was not possible to identify or verify any substrates with this novel trapping approach. The primary issues were the expression of non-functional trapping mutants unable to bind their substrate (i.e. mEH, MEST, Cif) and the selective loss of the peptides during sample

preparation for the LC-MS/MS analysis (i.e. sEH, EH3, EH4). Another shortcoming was that the selected AAV serotypes did not lead to transgene expression in the relevant organs for certain EHs (i.e. Cif, EH3). In addition, transgene expression for some EH trapping mutants was low and thus hindered their analysis (i.e. EH3, EH4). Finally, further optimization is required for the success of our developed trapping method. Moreover, trapping attempts *in vitro* could be a valuable alternative for Cif and EH3 substrate identification.

Unexpectedly, mice expressing the mEH trapping mutant in the brain developed a striking progressive trembling phenotype. This phenotype was not observed in any other group of AAV-infected mice. A potential underlying cause is a loss of dopaminergic neurons in the brain motor system of these mice, producing a pathology similar to Parkinson's disease. However, the exact mechanism remains unclear and needs further examination.

In a smaller side project pursued in parallel to the main project, a classic *in vitro* inhibitor screening was performed. The cytochrome P450 (CYP) inhibitor N-(methylsulfonyl)-2-(2-propynyloxy)-benzenehexanamide (MS-PPOH), which is generally used *in vitro* and *in vivo* to prevent EET formation, was examined for its potential to inhibit mEH and sEH activity. While it did not inhibit mEH, MS-PPOH inhibition of sEH was almost two orders of magnitude stronger compared to CYPs. This would lead to erroneous conclusions concerning the physiological EET functions when sEH inhibition is not considered in experiments using MS-PPOH. Nonetheless, additional studies to examine the consequences of these findings *in vivo* would be of major importance.

In the present work, novel insight into EH physiology has been obtained and a method has been established which has the potential to enable unbiased *ex vivo* substrate identification for EHs in the near future.

ZUSAMMENFASSUNG

Epoxidhydrolasen (EHs) sind Enzyme, die Epoxide zu ihren entsprechenden Diolen hydrolysieren. Sie spielen eine zentrale Rolle in der Entgiftung genotoxischer Epoxide und haben eine wichtige Funktion in der Regulation physiologischer Prozesse, indem sie Signalmoleküle hydrolysieren. Die bestcharakterisierten Säugetier-EHs sind die mikrosomale EH (mEH) und die lösliche EH (sEH). Die mEH wird hauptsächlich im Fremdstoffmetabolismus angesiedelt und erlangte erst vor Kurzem Aufmerksamkeit für ihre Funktion im Signalmolekülstoffwechsel. Die sEH hingegen ist das Schlüsselenzym im Umsatz von Fettsäureepoxiden (FAEs), wie Epoxyeicosatriensäuren (EETs). Auch für die erst kürzlich entdeckte EH3 wurde gezeigt, dass sie FAEs hydrolysiert, was eine physiologische Aufgabe nahelegt. Basierend auf ihren Primärstrukturen, sind auch EH4 und mesoderm specific transcript (MEST) potentielle Säugetier-EHs. Ihre EH Aktivität ist jedoch noch nicht erwiesen. Bakterien besitzen auch EHs, die pathophysiologische Konsequenzen für den Wirt mit sich ziehen können. Ein Beispiel dafür ist CFTR inhibitory factor (Cif), ein Virulenzfaktor sekretiert von *P. aeruginosa*. Der genaue Mechanismus, mit welchem Cif seine pathologische Funktion erfüllt, ist aber noch ungeklärt.

Das Wissen über die genannten EHs basiert typischerweise auf *in vitro* Untersuchen ihrer Substratpräferenz und erlaubt darum keine direkten Rückschlüsse auf ihre eigentliche physiologische Aufgabe. Das Ziel des Hauptprojekts dieser Arbeit war deshalb die Aufklärung der jeweiligen (patho)physiologischen Hauptaufgaben der sechs EHs, mittels Identifizierung ihrer bevorzugten *in vivo* Substrate. Dazu wurde eine neuartige, unvoreingenommene *in vivo* Substrat-Fangmethode entwickelt und angewendet. EH Varianten, die aufgrund einer Punktmutation ihr Substrat in einer kovalenten Esterbindung irreversibel festhalten (Trapping-Mutanten), wurden über Adeno-assoziierte Viren (AAV) in Zielorganen von Mäusen exprimiert. Die Enzym-Substrat Komplexe wurden anschliessend via His-Tag Affinitätschromatographie aus dem Gewebe angereichert und mit Flüssigchromatographie-Tandem Massenspektrometrie (LC-MS/MS) analysiert, um gebundene Substrate zu identifizieren.

Eine LC-MS/MS Methode für den Nachweis gebundener Substrate wurde erfolgreich entwickelt. Die Methode konnte durch *in vitro* Einfangexperimente mit Trapping-sEH und ihrem bekannten Substrat 14,15-EET bestätigt werden. Zudem konnte die AAV vermittelte Expression von Trapping-EHs in verschiedenen Zielorganen von Mäusen mittels Westernblot und immunohistochemischen (IHC) Färbungen nachgewiesen werden. Nichtsdestotrotz war es in einer umfangreichen Serie von Experimenten nicht möglich mit der neuartigen Methode neue Substrate zu identifizieren oder bekannte Substrate zu verifizieren. Die Hauptprobleme lagen darin, dass die exprimierten EH Trapping-

Mutanten nicht in der Lage waren ihr Substrat zu binden und festzuhalten (i.e. mEH, MEST, Cif) und im selektiven Verlust der Analyten während der Probenaufarbeitung für die LC-MS/MS Analyse (i.e. sEH, EH3, EH4). Ein weiteres Problem war, dass die verwendeten AAV Serotypen für manche EHs zu keiner Transgenexpression in den für sie relevanten Organen geführt haben (i.e. Cif, EH3). Zudem war die Transgenexpression mancher EH Trapping-Mutanten sehr gering, was die Analyse erschwerte (i.e. EH3, EH4). Weitere Optimierungen könnten jedoch zum Erfolg der entwickelten Methode führen. Ausserdem wären *in vitro* Substrat-Fangversuche eine gute Alternative für die Substratidentifizierung für Cif und EH3.
Unerwarteterweise entwickelten Mäuse, die die mEH Trapping-Mutante im Gehirn exprimierten ein auffälliges Zittern am ganzen Körper. Dieser Phänotyp konnte in keiner anderen Gruppe AAV-infizierter Mäuse beobachted werden. Eine mögliche Ursache ist ein Verlust dopaminerger Neuronen im motorischen System des Gehirns, was zu einem parkinsonoiden Erscheinungsbild führt. Der genaue Mechanismus ist jedoch unklar und benötigt weitere Untersuchungen.

In einem kleineren Nebenprojekt, welches parallel zum Hauptprojekt verfolgt wurde, wurde ein klassisches *in vitro* Inhibitor-Screening gemacht. Der Cytochrom P450 (CYP) Inhibitor MS-PPOH, welcher oft *in vitro* und *in vivo* zur Blockierung der EET-Synthese verwendet wird, wurde auf sein Potenzial der mEH und sEH Inhibition untersucht. Eine Inhibition der mEH konnte nicht gezeigt werden, aber die Inhibition der sEH durch MS-PPOH war um etwa zwei Grössenordnungen stärker als diejenige der CYPs. In Experimenten mit MS-PPOH würde diese Tatsache zu vollkommen falschen Schlussfolgerungen betreffend physiologischer EET Funktionen führen, wenn die sEH Inhibition nicht berücksichtigt wird. Weitere Untersuchungen zur Relevanz der Befunde *in vivo* sind deshalb von grösster Wichtigkeit.

In der vorliegenden Arbeit wurden neue Einblicke in die Physiologie von EHs geschaffen und es wurde eine Methode erarbeitet, die das Potential hat, schon in naher Zukunft unvoreingenommene *ex vivo* Substratidentifizierungen für EHs zu ermöglichen.

TABLE OF CONTENTS

GLOSSARY

AA	arachidonic acid
AAV	adeno-associated virus
ACN	acetonitrile
ACU	1-adamantyl-3-cyclohexylurea (sEH inhibitor)
Ala or A	alanine
ARDS	acute respiratory distress syndrome
Asn or N	asparagine
Asp or D	asparic acid
AUDA	12-(3-adamantan-1-yl-ureido)-dodecanoic acid (sEH inhibitor)
bp	base pairs
CA	cornu ammonis
CatNuc	catalytic nucleophile
CFTR	cystic fibrosis transmembrane conductance regulator
ChEH	cholesterol epoxide hydrolase
CID	collision induced dissociation
Cif	cystic fibrosis transmembrane conductance regulator inhibitory factor
Cif HQ	Cif trapping mutant
COX	cyclooxigenase
CYP	cytochrome P450
DHA	docosahexaenoic acid
DHET	dihydroxyeicosatrienoic acid
EpDPA	epoxydocosapentaenoic acid
EET	epoxyeicosatrienoic acid
EH	epoxide hydrolase
EH3	epoxide hydrolase 3
EH3 HQ	epoxide hydrolase 3 trapping mutant
EH3 KO	epoxide hydrolase 3 knockout
EH3k	epoxide hydrolase 3 missing the N-terminal membrane anchor
EH4	epoxide hydrolase 4
EH4 HQ	epoxide hydrolase 4 trapping mutant
EH4k	epoxide hydrolase 4 missing the N-terminal membrane anchor
EPA	eicosapentaenoic acid
EpDPA	epoxydocosapentaenoic acid
EpETE	epoxyeicosatetraenoic acid
ER	endoplasmic reticulum
ESA	epoxystearic acid
ESI	electron spray ionization
EST	expressed sequnece tag
FA	formic acid
FAE	fatty acid epoxide
FASP	filter aided sample preparation
FRET	Foerster resonance energy transfer
GFP	green fluorescent protein
Gln or Q	glutamine
Glu or E	glutamic acid
HETE	hydroxyeicosatetraenoic acid
His or H	histidine

HPLC	high pressure liquid chromatography
IHC	immunohistochemistry
IMAC	immobilized metal affinity chromatography
ITR	inverted terminal repeat
kb	kilobase
LC-MS/MS	liquid chromatography tandem mass spectrometry
LD	lipid droplet
LOX	lipoxigenase
LTA_4H	leukotriene A_4 hydrolase
mEH	microsomal epoxide hydrolase
mEH HQ	microsomal epoxide hydrolase trapping mutant
mEH KO	microsomal epoxide hydrolase knockout
MEST	mesoderm specific transcript (also known as peg1)
MEST HQ	mesoderm specific transcript trapping mutant
MEST KO	mesoderm specific transcript knockout
MOI	multiplicity of infection
MRM	multiple reaction monitoring
MS	mass spectrometer/mass spectrometry
MS-PPOH	N-(methylsulfonyl)-2-(2-propynyloxy)-benzenehexanamide
NADPH	nicotinamide adenine dinucleotide phosphate
OMV	outer membrane vesicle
ORF	open reading frame
PCR	polymerase chain reaction
peg1	paternaly exressed gene 1 (alternative name for MEST)
PLA2	phospholipase A2
PPOH	2-(2-propynyloxy)benzenehexanoic acid
Q1-Q3	quadrupole 1-3
QTrap	quadrupole linear ion trap
RPLC	reversed phase liquid chromathography
RT	room temperature
SAR	scaffold attachment region
SDS-PAGE	sodium dodecyl sulfate polyacrylamide gel electrophoresis
sEH	soluble epoxide hydrolase
sEH HQ	soluble epoxide hydrolase trapping mutant
sEH KO	soluble epoxide hydrolase knockout
Ser or S	serine
SN	substantia nigra
SNpc	substantia nigra pars compacta
SNpr	substantia nigra pars reticulata
SPE	solide phase extraction
St	striatum
SWATH	sequential window acquisition of all theoretical spectra
TFA	trifluoric acid
TH	tyrosine hydroxylase
TOF	time of flight
Tyr or T	tyrosine
vg	vector genomes
WT	wild type

1. introduction

1.1. Epoxide hydrolases

Epoxide hydrolases (EHs) are a small superfamily of functionally related enzymes that catalyze the hydrolytic cleavage of epoxides to their vicinal diols through addition of water (Figure 1) (Armstrong, 1999). EHs are present in many life-forms including microorganisms, plants, insects and mammals. In plants, EHs are mainly needed in host defense (Guo et al., 1998) and certain anabolic pathways like cutin biosynthesis (Heredia, 2003). In bacteria and insects EHs are primarily involved in catabolism of different compounds (van der Werf et al., 1998, Mullin, 1988) and regulation of signaling pathways (Slade and Zibitt, 1972). Furthermore, a bacterial EH was shown to function as a virulence factor in human respiratory infections (MacEachran et al., 2007). In mammals, EHs fulfill at least two functions. For a long time they were primarily considered to be typical detoxifying enzymes for exogenous and endogenous epoxides, as many epoxides tend to be electrophilic and thus are able to attack electron rich DNA potentially leading to DNA adducts, mutations and finally carcinogenesis (von der Hude et al., 1991, Beland and Poirier, 1993).

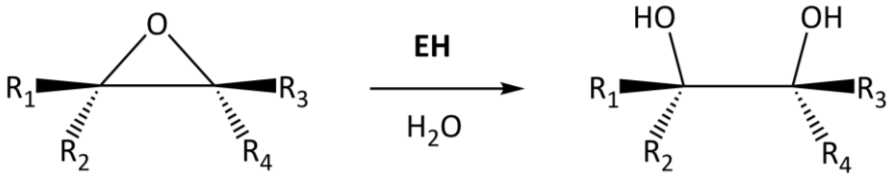

Figure 1: Enzymatic reaction of EHs. EHs hydrolyze epoxides to their vicinal diols under the addition of water. The intrinsic reactivity of the epoxide is generally dictated by the substituents at R_1-R_4.

Nonetheless, there is increasing evidence that especially fatty acid epoxides (FAEs), lacking electrophilicity, fulfill important signaling functions in the organism. This reveals the second important role of EHs in signaling molecule metabolism, thereby regulating a large variety of physiologic functions (Decker et al., 2009). At present, there are seven known mammalian EHs, namely microsomal EH (mEH), soluble EH (sEH), EH3, EH4, paternally expressed gene 1/ mesoderm specific transcript (peg1/MEST), leukotriene A_4 hydrolase (LTA_4H) and cholesterol EH (ChEH) (Decker et al., 2009). Of these, mEH, sEH, EH3, EH4, and MEST share structural characteristics classifying them as α/β hydrolase fold family members (see 1.1.1), whereas LTA_4H and ChEH do not. mEH and sEH are extensively characterized and much is known about their structure, substrate spectra and physiological relevance. While mEH is generally considered to be the major detoxifying EH (Oesch and Bentley, 1976, Oesch, 1974), sEH is known to be a key enzyme in endogenous signaling (Moghaddam et al., 1997b, Ota and Hammock, 1980).

1.1.1. Structure of α/β hydrolase fold epoxide hydrolases

The majority of the currently known EHs belong to the α/β hydrolase fold family, a large group of hydrolytic enzymes that share a common three-dimensional structure and a catalytic mechanism. The mammalian EHs (Figure 2) are a small superfamily within this large group of enzymes that also includes esterases, haloalkane dehalogenases, proteases and lipases (Holmquist, 2000).

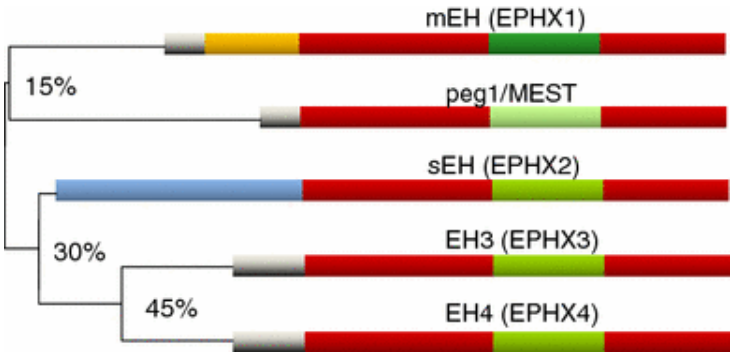

Figure 2: Phylogenetic tree of α/β hydrolase fold EHs. Percent sequence homology in the α/β hydrolase fold (red) is indicated on the branches. The lid domains are marked in green and different N-terminal extensions for mEH in yellow (meanders) and for sEH blue (phosphatase). Membrane anchors are depicted in grey. Figure taken from (Decker et al., 2009).

The α/β hydrolase fold was defined by Ollis et al. in 1992. All enzyme members are characterized by a core arranged of a central β-sheet of 8 parallel strands flanked by several α-helices that is interrupted by a variable lid domain. A highly conserved catalytic triad is situated on top of the hydrolase domain underneath the lid (Figure 3) (Arand et al., 2003c, Ollis et al., 1992). Consequently, the substrate binding pocket is formed at the interaction site of the core and the lid domain. The catalytic triad consists of an aspartic acid (Asp) side chain acting as catalytic nucleophile (CatNuc), a water activating histidine (His) and an acidic residue (usually Asp or glutamic acid (Glu) in mEH) forming a charge relay system together with the His. The CatNuc is located in a sharp turn called 'nucleophilic elbow', defined by the sequence motif Sm-X-Nu-X-Sm-Sm (Nu: nucleophile, Sm: small residue, X: any residue) (Arand et al., 1994), there it is easily accessible for the substrate and the activated water molecule (see 1.1.2) (Nardini and Dijkstra, 1999). Other conserved regions are the oxyanion hole (H-G-X-P) and the G-X-Sm-X-S/T motif, located between the oxyanion hole and the CatNuc. The oxyanion hole is responsible for the stabilization of the negatively charged transition state that appears during hydrolysis (Nardini and Dijkstra, 1999). In addition, two tyrosine (Tyr) residues pointing from the lid towards the catalytic triad distinguish EHs from other α/β hydrolase fold enzymes. These are especially relevant for epoxide hydrolysis as they orient and activate the epoxide substrate in the enzymatic pocket (Decker et al., 2009, Nardini et al., 1999). Apart from these highly conserved regions the amino acid sequences vary largely between the different EHs, as well as the N-terminal parts preceding the hydrolase fold (Figure

2) (Arand et al., 2003c, Decker et al., 2009). Nevertheless, putative EHs can be identified by means of the aforementioned structural motifs. The characteristic three-dimensional structure of α/β hydrolase fold EHs is depicted in Figure 3 based on *A. niger* EH, a close relative of mammalian mEH (Marowsky et al., 2010).

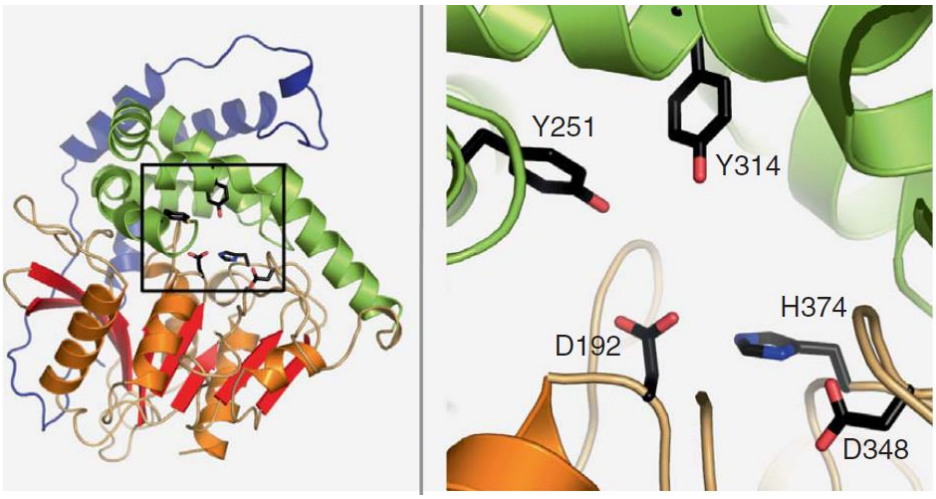

Figure 3: Three-dimensional structure of α/β hydrolase fold EHs. (A) The typical α/β hydrolase fold structure of *A. niger*, a close relative to mEH. The α/β hydrolase fold is shown in orange/red, the lid domain in green and the N-terminal meander in blue. (B) The catalytic triad consisting of an Asp as the CatNuc, and a His together with an Asp as the charge relay system. Figure taken from (Marowsky et al., 2010).

1.1.2. Reaction mechanism of α/β hydrolase fold epoxide hydrolases

EHs hydrolyze their epoxide substrates in a characteristic two step reaction mechanism, which is well understood thanks to several studies (Arand et al., 1996, Muller et al., 1997, Laughlin et al., 1998, Argiriadi et al., 1999, Armstrong and Cassidy, 2000, Zou et al., 2000, Arand et al., 2003a). The mechanism is explained in the following and visualized in Figure 4.

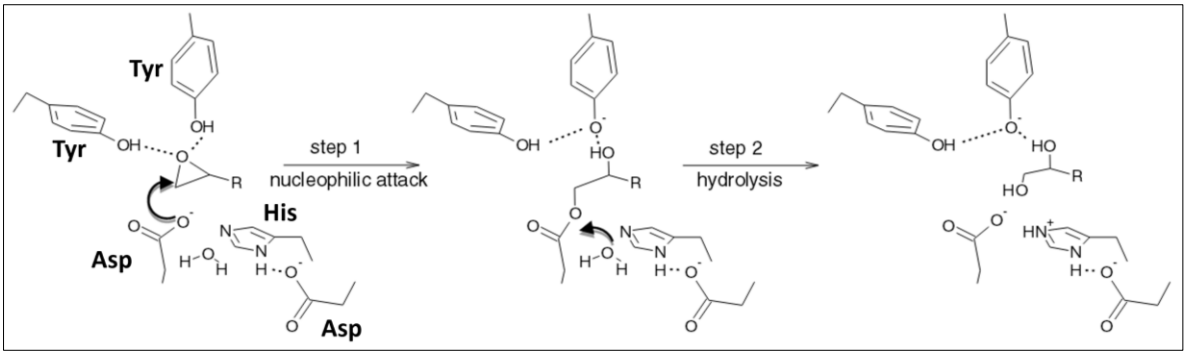

Figure 4: Characteristic two step reaction mechanism of α/β hydrolase fold EHs. The mechanism is described in detail in the text. Figure taken from (Decker et al., 2009).

In the first step, the CatNuc, which is an Asp side chain in all EHs, attacks one of the two electrophilic carbons of the epoxide ring, forming a covalent ester intermediate with the substrate stabilized by the

oxianione hole. This results in termination of the biologic function (mutagenicity or signaling) of the epoxide substrate. In a second, rate limiting step an activated water molecule attacks the ester bond leading to hydrolysis and release of the product. The water molecule gets activated through proton abstraction by the His of the charge relay system, while the supporting acidic residue of the charge relay system (Asp or Glu) orients and further activates the His by hydrogen bonding. Moreover, the resulting positive charge is neutralized by the acidic amino acid of the charge relay system (Decker et al., 2009, Armstrong, 1999).

1.2. Five mammalian α/β hydrolase fold epoxide hydrolases

1.2.1. Microsomal epoxide hydrolase

mEH was the first identified mammalian EH (Oesch, 1974) and has a length of 455 amino acids (Porter et al., 1986) encoded by the gene EPHX1. It is a membrane bound enzyme located on the cytosolic surface of the endoplasmic reticulum (ER) (Holler et al., 1997), where it is attached by an N-terminal membrane anchor (Friedberg et al., 1994). The mEH is the only mammalian EH with an N-terminal meander (Figure 2) which wraps around the protein and apparently holds the lid domain down to the α/β hydrolase fold (Arand et al., 2003c). The catalytic triad consists of the CatNuc Asp226 and the charge relay system Glu404 and His431 supported by the two catalytic tyrosines Tyr299 and Tyr374 (Armstrong and Cassidy, 2000). The mEH is highly expressed in liver and other organs like kidney, brain and heart (Coller et al., 2001). As mentioned before, it is generally accepted to be the major player in xenobiotic metabolism and detoxification of potentially carcinogenic epoxides (Oesch, 1974, Oesch and Bentley, 1976) with a broad substrate spectrum. The only observed major restriction is that mEH cannot efficiently hydrolyze *trans*-substituted epoxides. Otherwise, the shape and size of its substrates vary largely and range from 1,2-epoxibutene over benzo[a]pyrene-4,5-oxide to aflatoxin B1 8,9-exo-epoxide (Marowsky et al., 2010). In rare cases, however, hydrolysis by mEH indirectly increases the genotoxic potential of xenobiotics (e.g. benzo[a]pyrene) (Shimada, 2006). Compared to other EHs the mEH shows quite low hydrolysis rates, but because of the characteristic two step reaction mechanism mEH is still a fast detoxifier. The first, ester-forming step is up to three orders of magnitude faster than the second, hydrolytic step, thus mEH readily traps DNA-reactive epoxides before slowly hydrolyzing them, thereby acting like a sponge for toxic epoxides (Oesch et al., 2004). Faster turnover rates would actually not be of significant advantage as long as mEH is in excess over its substrate (Arand et al., 1999a), which is usually the case, especially in liver (Oesch et al., 2000).

Detoxification and physiologic relevance of mEH were also studied in different mEH KO mouse models. The mEH KO mouse line was first produced in 1999 by Miyata et al. It was fertile and showed no

phenotypic abnormalities indicating that mEH is not critical for reproduction and physiological homeostasis (Miyata et al., 1999). The carcinogenic potential, however, was heavily dependent on the chosen model substances (Miyata et al., 1999, Carratt et al., 2016, Liu et al., 2008). In general, mEH seems to be protective. Surprisingly, FAE hydrolysis was impaired in mEH KO mice (Marowsky et al., 2017, Edin et al., 2018).

In recent years mEH is also gaining attention for its role in endogenous signaling epoxide turnover, as it was shown to catalyze the hydrolysis of epoxyeicosatrienoic acids (EETs) (Marowsky et al., 2009, Marowsky et al., 2017). However, EET hydrolysis by mEH is slow compared to sEH *in vitro* and thus mEH is thought to contribute only marginally to EET metabolism. But it could be demonstrated that mEH actually contributes to EET turnover to a significant extend *in vivo* (Edin et al., 2018). This observation could probably be explained by its high affinity for EETs under non-saturating conditions and its widespread expression in different cell types lacking sEH (Marowsky et al., 2017). Moreover, the recently revealed unique subcellular localization of mEH in close proximity to the EETs producing cytochromes P450 (CYPs) on the cytosolic side of the ER membrane probably results in effective diol formation by substrate channeling (Orjuela Leon et al., 2017). The turnover of endogenous FAEs, however, is opening-up a whole new world of biologic functions for mEH (see also 1.2.2.1).

1.2.2. Soluble epoxide hydrolase

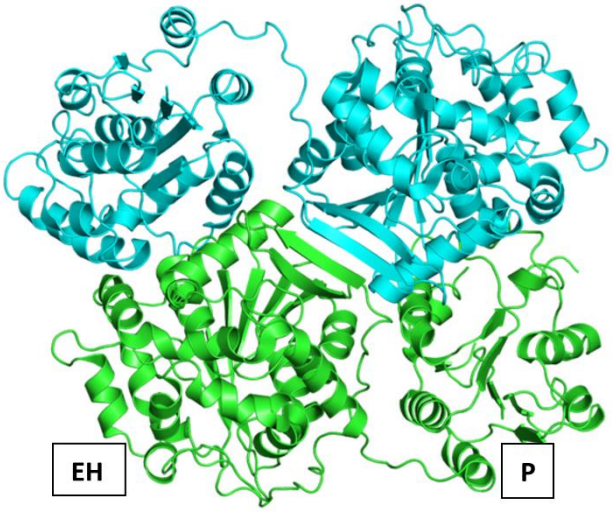

Figure 5: Three-dimensional structure of sEH. sEH is shown as a dimer, one subunit is shown in green and one in light-blue. The N-terminal phosphatase domain is marked with [P] and the C-terminal EH domain with [EH] for the green subunit. Figure taken from EMBL-EBI, Protein Data Bank in Europe (PDBe)[1] adapted from (Argiriadi et al., 1999).

The human sEH is an enzyme encoded by the gene EPHX2 and has a primary structure of 554 amino acids (Knehr et al., 1993). It was the second mammalian EH identified after mEH. The sEH forms a homodimer and each subunit consist of two functional domains linked by a short prolin-rich linker (Figure 5) (Argiriadi et al., 1999). The C-terminal domain features an EH activity with the catalytic triad

[1] https://www.ebi.ac.uk/pdbe/entry/pdb/1cqz, 15. October 2018

Asp335, Asp495 and His524 and the two catalytic tyrosines Tyr382 and Tyr465 (Morisseau and Hammock, 2005). The N-terminal domain exhibits phosphatase activity with the residues Asp9, Asp11, Thr123, Lys160, Asp184, Asp185 and Asn189 being important for its catalytic activity (Cronin et al., 2003, Newman et al., 2003, Cronin et al., 2008). The sEH is widely expressed in multiple tissues (Harris and Hammock, 2013, Decker et al., 2009, Newman et al., 2005), which fits quite well with its important role in signaling molecule turnover as a predominant role in xenobiotic metabolism would implicate a more focused expression in the liver. The sEH shows a dual subcellular localization in the cytosol and in peroxisomes (Mullen et al., 1999, Luo et al., 2008, Arand et al., 1991, Enayetallah et al., 2006). In rodents sEH is induced by peroxisome proliferator-activated receptor (PPAR) α agonists (Moody et al., 1985), but not in humans as the PPAR responsive element is not conserved in the human gene EPHX2 (Marowsky et al., 2010).

The catalytic site of the well-characterized hydrolase domain is situated at the base of a long L-shaped cavity (Argiriadi et al., 1999). Thus, the substrate pocket is well suited for long-chain, non-bulky substrates, which is in-line with the substrate preference of sEH. The sEH is not only complementing mEH in detoxification of *trans*-1,2-disubstituted epoxides, which are not mEH substrates (Krämer et al., 1991, Morisseau and Hammock, 2005, Hasegawa and Hammock, 1982), it is also widely accepted as the major signaling molecule metabolizing EH (Moghaddam et al., 1997a, Zeldin et al., 1993, Hammock et al., 1976). The CYP dependent arachidonic acid (AA) metabolites EETs seem to be the primary endogenous sEH substrates (Spector and Norris, 2006) and because of their various physiologic functions the most extensively studied ones (see section 1.2.2.1). Nevertheless, sEH also metabolizes other lipid epoxides, like those derived from docosahexaenoic acid (DHA) and eicosapentaenoic acid (EPA), as well as leukotoxin and isoleukotoxin (Zheng et al., 2001). In contrast to EETs, DHA-derived epoxides are dramatically anti-angiogenic with otherwise similar functions (Zhang et al., 2013, Morisseau et al., 2010) and EPA-derived epoxides inhibit endothelial cell proliferation (Cui et al., 2011).

1.2.2.1. Soluble epoxide hydrolase and epoxyeicosatrienoic acids

AA is a poly-unsaturated Ω-6 fatty acid and a normal constituent of membrane phospholipids. It is released from membrane phospholipids upon activation of phospholipase A2 (PLA2), making free AA available for the oxidative metabolism by several enzymes. The arachidonate cascade includes three main endogenous signaling pathways, the lipoxygenase (LOX) pathway producing leukotrienes, the cyclooxygenase (COX) pathway yielding prostaglandins and the CYPs leading to the formation of EETs and of hydroxyeicosatetraenoic acids (HETEs) (Figure 6) (Capdevila et al., 1992). In contrast to the well-studied LOX and COX pathways, not that much is known about the CYP pathway.

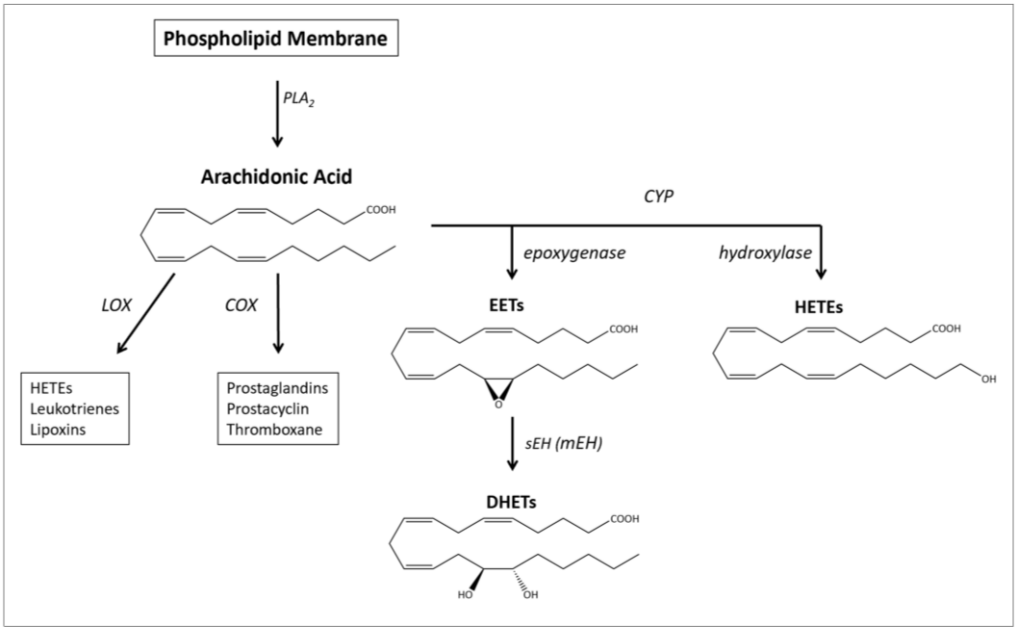

Figure 6: The arachidonate cascade. EETs are AA metabolites produced in the AA-CYP pathway and are rapidly hydrolyzed by sEH.

Nevertheless, it is established that many CYP subfamilies metabolize AA, either to one of the four EET regioisomers (5,6-, 8,9-, 11,12-, and 14,15-EET) with 11,12- and 14,15-EET being the predominant products or to 19- or 20-HETE. EETs, however, are rapidly hydrolyzed by sEH and to some extend by mEH (Marowsky et al., 2009, Marowsky et al., 2017) to their corresponding diols, dihydroxyeicosatrienoic acids (DHETs). The sEH can hydrolyze all EET regioisomers, preferring 14,15-EET (Morisseau and Hammock, 2005). EETs act as autocrine and paracrine effectors, regulating multiple biological processes (Campbell et al., 2017). They were shown to be anti-inflammatory (Node et al., 1999), pain-releasing (Inceoglu et al., 2007), anti-diabetic (Xu et al., 2010) and cardioprotective through vasodilatory effects (Fisslthaler et al., 1999). The exact mechanism of EET action is largely unknown. Reported potential molecular targets include the K_{ATP} channel, the calcium-activated BK channel and TRP channels (Campbell et al., 2017). Direct binding and activation of ion-channels by EETs, however, is rather unlikely. They might function via the activation of a G protein-coupled receptor, thus activating a signal transduction pathway which finally modulates ion channels. Most recently, 11,12-EET was reported to reduce excitation in CA1 pyramidal cells in the brain by opening up a G protein-gated ion channel (Mule et al., 2017).

Over the past decades, primarily CYP epoxygenases gained attention because of the diverse physiologic functions of EETs which could benefit human health (Spector and Norris, 2006). To elucidate the (patho)physiologic roles of EETs *in vivo*, selective inhibition of CYP epoxygenases is an important tool. The fact that CYPs exist in many isoforms with high homology and similar catalytic activity complicates this task, thus many CYP inhibitors lack selectivity (Capdevila et al., 1988, Gonzalez, 1988, VanAlstine and Hough, 2011). 2-(2-propynyloxy)benzenehexanoic acid (PPOH) and primarily its metabolically

stable congener N-(methylsulfonyl)-2-(2-propynyloxy)-benzenehexanamide (MS-PPOH) (Schaaf and Hess, 1979) are frequently used as selective CYP epoxygenase inhibitors *in vitro* and *in vivo* (Brand-Schieber et al., 2000, Wang et al., 1998, Bhardwaj et al., 2000, Zhu et al., 2000, Peng et al., 2002, Conroy et al., 2010).

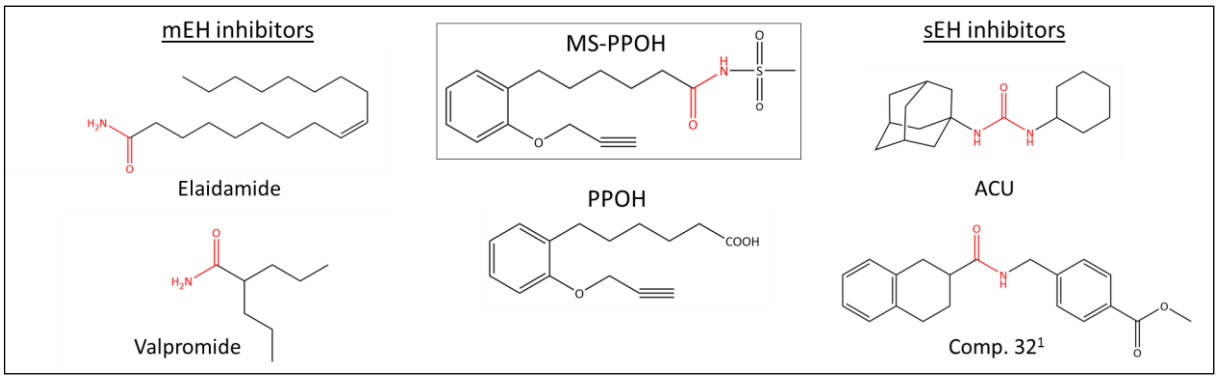

Figure 7: Chemical structures of MS-PPOH, PPOH and typical mEH and sEH inhibitors. The pharmacophore of each compound is marked in red. (Kim et al., 2011) [1]

Introduction of the amide group to obtain the metabolically stable MS-PPOH generated a product with high structural similarity to a certain class of mEH inhibitors (Morisseau et al., 2001) and to some extend to sEH inhibitors (Figure 7). This fact was ignored so far but is addressed in a side project of this work.

The beneficial effects of EETs in many pathologic conditions, are also intensively investigated in pharmaceutical drug development. As EETs are mainly metabolized by sEH to the supposed inactive DHETs, blocking sEH activity is expected to increase circulating EETs and thus potentiate their beneficial effects (Wagner et al., 2017). This is why many highly selective and potent sEH inhibitors, usually containing an urea moiety as a pharmacophore, were developed (Morisseau and Hammock, 2013). Two typical representatives are 12-(3-adamantan-1-yl-ureido)-dodecanoic acid (AUDA) and 1-adamantyl-3-cyclohexylurea (ACU) (Figure 7). Next to their use in basic research, sEH inhibitors are considered to be promising drug candidates and different inhibitors were tested in clinical trials, like GSK2256294 for the treatment of COPD (Yang et al., 2017) and AR9281 which targets hypertension and diabetes type 2 (Chen et al., 2012). sEH KO mice are also often used as models to study the beneficial effects of EET up-regulation *in vivo*, in particular in blood pressure regulation (Sinal et al., 2000, Luria et al., 2007, Sun et al., 2014a), renoprotection and inflammation (Manhiani et al., 2009). sEH KO mice did not show any behavioral or developmental phenotype (Sinal et al., 2000). However, the findings in blood pressure regulation were inconsistent (Sinal et al., 2000, Luria et al., 2007, Sun et al., 2014a). Additionally, sEH KO mice showed impaired FAE turnover (Edin et al., 2018, Sinal et al., 2000, Luria et al., 2007).

Although EETs seem to be generally beneficial, adverse effects cannot be circumvented when increasing their tissue levels upon sEH inhibition. While EETs commonly act as vasodilators, they do not in the lung, where they show the exact opposite effect (Pokreisz et al., 2006). Moreover, EETs were shown to be pro-angiogenic (Michaelis et al., 2005) and augmenting their levels could promote tumor growth and metastasis (Morisseau and Hammock, 2013, Imig, 2012).

1.2.3. Epoxide hydrolase 3 and epoxide hydrolase 4

EH3 and EH4 are closely related to each other. Both have been identified through data base searches for highly conserved regions of α/β hydrolase fold EHs (Decker et al., 2012). So far, there are no crystal structures available. Nevertheless, their amino acid sequences predict an N-terminal membrane anchor and at least EH3 is in fact membrane bound when expressed in insect cells (Decker et al., 2012). EH3 is encoded by the gene EPHX3 resulting in a protein with a length of 360 amino acids. Its catalytic triad consist of Asp173, His337 and Asp307 (Decker et al., 2012). Recombinant EH3 shows high turnover activity for fatty-acid derived epoxides like 8,9-, 11,12- and 14,15-EET, leukotoxin and isoleukotoxin, *cis*- and *trans*-epoxystearic acid and hepoxilin A and B (Decker et al., 2012). The impact of EH3 on FAE hydrolysis and EETs related physiology was further assessed by genetic disruption of EPHX3 in mice (Hoopes et al., 2017). The EH3 KO mice did not show an overt phenotype and FAE metabolism was not affected. EH3 expression throughout the whole organism is generally low, with the strongest expression detected in skin, lung, upper gastrointestinal tract and stomach (Decker et al., 2012). This expression pattern suggests a potential role for EH3 in barrier formation (Toulza et al., 2007), which is supported by the fact that EH3 is reported to be a candidate disease gene in ichthyosis (Ala et al., 2008) and by recent findings in skin water-barrier formation (Yamanashi et al., 2018).

EH4 consists of 362 amino acids encoded by the gene EPHX4 and its catalytic triad consists of Asp169, His336 and Asp307 supported by the conserved Tyr281. EH4 expression was revealed especially in brain tissue (Decker et al., 2009). There is nothing known about the substrate spectrum of EH4, as it was not possible to detect any enzymatic activity towards any tested substrate so far. Thus, EH activity is still speculative in case of EH4. If the lack in turnover was due to the expression of a misfolded protein lacking any activity or due to insufficient substrate specificity remains unclear, but because EH4 is potentially membrane bound it is difficult to discriminate on a physicochemical level between the correct and the misfolded enzyme after recombinant expression (Decker, 2010). However, because EH3 and EH4 share an amino acid sequence identity of 45 % (Figure 2) and the additional fact that their closest relatives are two EHs from the nematode *C. elegans* (Harris et al., 2008), it is highly probable that EH4 is also an active EH. In this light, the gene encoding EH4 and its name itself are already adapted to the EH nomenclature (Decker et al., 2012).

Taken together, the mentioned expression patterns suggest a specific role in the metabolism of endogenous compounds for both enzymes (Decker et al., 2009). Enzymes fulfilling a primary function in xenobiotic metabolism would be expected to be highly expressed in liver (Decker et al., 2012, Marowsky et al., 2010).

1.2.4. Mesoderm specific transcript

MEST is an imprinted gene expressed from the paternal allele and is widely expressed in mammals (Kobayashi et al., 1997). The expression is highest during early embryonic development particularly in mesodermal tissues and stays imprinted in adulthood with high expression in the nervous system (Lefebvre et al., 1998). Occasional loss of imprinting was reported to be related to diseases like invasive breast cancer (Pedersen et al., 1999) and lung adenocarcinoma (Nakanishi et al., 2004). MEST consisting of 335 amino acids, contains all sequence motifs of an α/β hydrolase fold EH (Kobayashi et al., 1997) and its structure suggests an N-terminal membrane anchor (Decker et al., 2009). Its catalytic triad is predicted to consist of the CatNuc Asp147, and the charge relay-system His314 and Asp284. With Tyr254 it at least contains one highly conserved tyrosine residue. The EH activity of MEST, however, still needs to be confirmed. Just as for the also membrane bound EH4, substrate screening with recombinant MEST were not successful so far.

At present a physiologic function for MEST has not been established, but it is highly conserved throughout mammalian species (Sado et al., 1993). As an imprinted gene with highest expression during early embryonic development it may fulfill an important role then (Decker et al., 2009). Furthermore, targeted disruption of MEST resulted in growth retardation, increased peri- and postnatal lethality and abnormal maternal behavior in mice (Lefebvre et al., 1998). More recently MEST has been related to lipid metabolism (Nikonova et al., 2008a) and early brain development specifically of dopaminergic neurons (Mesman et al., 2017).

1.3. The bacterial epoxide hydrolase CFTR inhibitory factor

The cystic fibrosis transmembrane conductance regulator (CFTR) inhibitory factor (Cif) is a virulence factor secreted by the opportunistic pathogen *P. aeruginosa* upon human airway infection. In patients with compromised pulmonary function, like in cystic fibrosis, *P. aeruginosa* often establishes permanent lung infections aggravating the disease outcome. Cif shows a typical α/β hydrolase fold structure (MacEachran et al., 2007) and has been described as a functional EH, with its catalytic triad consisting of the CatNuc Asp129 and the charge relay system His297 and Glu153 (Bahl et al., 2010). Unlike the other α/β hydrolase fold EHs Cif utilizes a histidine in position 177 in addition to Tyr239 to orient the epoxide in the active pocket (Bahl and Madden, 2012). Cif is the first EH reported as a

bacterial virulence factor, but *P. aeruginosa* is known to employ a wide variety of strategies to subvert host cell function (MacEachran et al., 2007). Cif is delivered into the cytosol of human airway epithelial cells by bacterial-derived outer membrane vesicles (OMVs) (Bomberger et al., 2009). There, Cif interferes with CFTR recycling through upregulation of its ubiquitination and lysosomal degradation (Bomberger et al., 2014). This leads to a reduced apical expression of the CFTR chloride channel, which results in a higher viscosity of the mucus layer in the airway tract, thus promoting *P. aeruginosa* colonization (Swiatecka-Urban et al., 2006, MacEachran et al., 2007). The exact mechanism herein is largely unknown but based on the findings that Cif is an EH, it would seem likely that an endogenous epoxide substrate or the diol product is involved in CFTR trafficking. In addition, inactive Cif variants did not affect CFTR recycling (Bahl et al., 2015), thus suggesting the EH function as a prerequisite. However, an epoxide substrate or diol product involved in CFTR trafficking has not been identified so far. Very recently Flitter et al. suggested that Cif also sabotages the production of 15-epi lipoxin A_4, a pro-resolving lipid mediator, by rapidly hydrolyzing 14,15-EET, which is responsible for 15-epi lipoxin A_4 formation, to its inactive diol. Thereby, Cif disrupts resolution pathways and substantiates pulmonary inflammation (Flitter et al., 2016). So far EH activity was only demonstrated against artificial surrogate substrates (MacEachran et al., 2007, Bahl et al., 2010) and most recently against endogenous FAEs, including 14,15-EET, 19,20-epoxydocosapentaenoic acid (EpDPA) and 17,18-epoxyeicosatetraenoic acid (EpETE) (Hvorecny et al., 2017, Flitter et al., 2016).

The treatment of *P. aeruginosa* is very difficult because of biofilm formation and antibiotic resistance. Thus, Cif seems to be a promising target for antibiotic treatment against this opportunistic pathogen in persisting lung infections. Cif inhibition might compromise *P. aeruginosa* colonization and reduce pulmonary infections.

1.4. Unbiased *in vivo* substrate trapping

Traditionally, EHs were isolated from tissue or recombinantly expressed and their substrate landscape was analyzed *in vitro*. Substrate screenings were performed, and kinetic analyses revealed the impact of the enzyme on the turnover of the respective substrates. This approach was used in the identification of EETs and kinetic analysis revealed that sEH outperforms mEH (Decker et al., 2009, Zeldin et al., 1993). However, recent results showed that the less efficient mEH still contributes to the EET turnover due to its cellular and subcellular localization and close proximity to the EET forming CYPs (Marowsky et al., 2009, Orjuela Leon et al., 2017), and the role of the two enzymes in EET turnover is still debated. Furthermore, classical substrate screenings were not successful for EH4 and MEST. These enzymes were recombinantly expressed, but activity could not be confirmed as they did not hydrolyze any offered substrate so far (Decker et al., 2012). With this approach, the analysis of the substrate

spectrum of a given EH is always limited to the set of compounds offered by the researcher. Thus, new unbiased approaches are required to evaluate substrate relevance in a tissue and context specific manner.

The aim of the main project was to identify the major (patho)physiologic functions of the six EHs mEH, sEH, EH3, EH4, MEST and Cif via the identification of their preferred *in vivo* substrates. To achieve this, a novel trapping approach was designed, taking advantage of the characteristic two step reaction mechanism of EHs (Figure 8 A). In the first step, the CatNuc Asp, attacks an electrophilic carbon of the epoxide ring of the substrate, forming a covalent ester intermediate. In the second, hydrolytic step the covalent enzyme-substrate intermediate is hydrolyzed by an activated water molecule, following activation through proton abstraction by the His of the charge relay system (for more details see 1.1.2) (Armstrong, 1999).

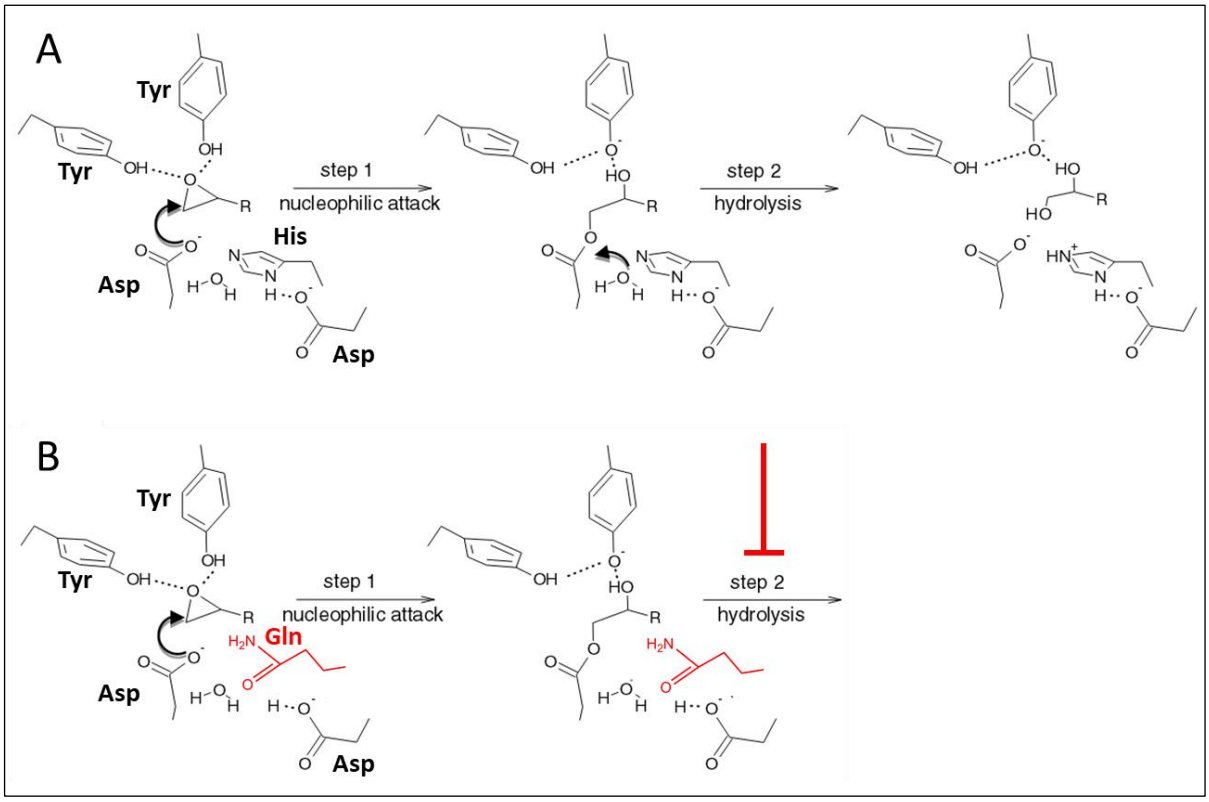

Figure 8: Substrate trapping mechanism by EH HQ variants. A) Characteristic two step reaction mechanism of α/β hydrolase fold EHs as described in the text. B) The EH trapping mutants have the catalytic His (H) replaced by Gln (Q), thus they are not able to perform the second hydrolytic step and consequently keep their substrates covalently bound to the CatNuc Asp.

By point mutating the His involved in the second catalytic step, we created an enzyme that can still nucleophilically attack the substrate with the CatNuc and form the covalent intermediate, yet is not able to perform the second, hydrolytic step (Figure 8 B), thus trapping the substrate via an ester bond. In the present work, these point mutated enzymes are called trapping mutants. To trap relevant *in vivo* substrates in an unbiased manner, trapping mutants of the different EHs are expressed in relevant

target tissues of mice via AAV infection. The substrate-enzyme complex can subsequently be retrieved from the tissue, potentially be enriched by His-tag based affinity chromatography and analyzed by liquid chromatography tandem mass spectrometry (LC-MS/MS) to identify the bound substrate.
Additionally, a proof of the trapping principle was successfully provided in a preliminary experiment using recombinant rat sEH and its known substrates epoxystearic acid (ESA) and 14,15-EET providing a predictable outcome. The modified peptides could be detected which eluted later and had the expected mass increases. After alkaline hydrolysis of the covalent ester bond the products could be detected. Recently, the trapping mutant approach was successfully applied to visualize the structure of the covalent Cif-substrate intermediate by protein crystallography (Bahl, 2016). Taken together, previous experiments showed that the trapping procedure should be sufficiently robust for the envisaged project.

1.4.1. Epoxide hydrolase expression patterns and expected substrates

In order to trap the physiologically relevant substrates, the trapping EHs need to be expressed in the same tissue/cell types as the natural enzymes occur. sEH and mEH are widely expressed in many different tissues, with highest expression in the liver primarily in hepatocytes, where xenobiotic metabolism as well as turnover of signaling molecules take place (Coller et al., 2001, Enayetallah et al., 2004). Therefore, the liver is the main target organ to gain insight into the contribution of mEH and sEH to the turnover of already known substrates (e.g. EETs). For sEH with its narrow substrate spectrum, we expect trapping of FAEs, with 14,15-EET probably being the most prominent representative, and less trapping of xenobiotic molecules. In case of mEH which has a broad substrate spectrum covering xenobiotic and endogenous molecules, we expected many different adducts adding up to the total substrate spectrum. Furthermore, with this approach, the contribution of mEH to the conversion of endogenous signaling epoxides can be analyzed, which may be bigger than presently appreciated (Marowsky et al., 2009, Marowsky et al., 2017). Furthermore, animals can be challenged with xenobiotic precursors of sEH and mEH substrates to analyze the extent to which they are occupied with detoxification.
Another organ of special interest is the brain, where sEH is expressed almost exclusively in astrocytes. mEH is abundantly expressed in structures forming brain-specific barriers, namely the epithelial cells of the choroid plexus and the endothelial cells of cerebral blood vessels. The enzyme is also present in smooth muscle cells and in specific neuronal populations, such as hippocampal pyramidal neurons, striatal neurons, central amygdala neurons and cerebellar granule cells as well as in a fraction of astrocytes (Marowsky et al., 2009). mEH substrates in neurons and astrocytes are of particular interest as in these cells, mEH might be involved in endogenous signaling as detoxification of xenobiotic

compounds is less relevant. In the barrier forming cells, detoxification might be the main function of mEH to protect the central nervous system. However, without xenobiotic challenge we expect mEH to trap endogenous epoxides as well. In addition to liver and brain, high expression of mEH and sEH is reported in the kidney and in the heart (Coller et al., 2001, Enayetallah et al., 2004). In both tissues trapping of EETs is expected (Harris and Hammock, 2013, Decker et al., 2009, Imig, 2015).

EH3 expression is rather low in any tissue. Nevertheless, organs with highest EH3 expression are lung, upper gastrointestinal tract and skin, where EH3 might be involved in barrier formation (Decker et al., 2012, Yamanashi et al., 2018). According to the expressed sequence tag (EST[2]) profile of the hitherto orphan mammalian EHs, EH4 is reported to be mainly expressed in the brain while MEST is widely expressed in many tissues. In the brain EH4 is primarily expressed in the cortex and hippocampus, while MEST is widely expressed throughout many brain structures with cortex and hypothalamus being the most intensively stained regions (Allen Brain Atlas). A behavioral phenotype has been reported in MEST deficient mice (Lefebvre et al., 1998). Thus, the search for new *in vivo* substrates for EH4 and MEST is primarily focused to the brain. For Cif, which is a secreted pathogenicity factor of *P. aeruginosa* during airway infection, the target organ is the lung. Previous studies (Hvorecny et al., 2017) propose 19,20-EpDPA to be the primary substrate of Cif. With the unbiased substrate trapping approach, we expect to identify new, so far unknown substrates and to gain information about the relevance of the already known substrates.

1.5. Adeno-associated viral vectors for gene delivery

The adeno-associated virus (AAV) is a family member of the *Parvoviridae*, generally known as parvoviruses. AAVs belong to the genus *Dependovirus*, meaning that they require a helper virus (usually adenovirus) to allow virus replication und thus reproductive infection (Ojala et al., 2015). AAVs are small (20-25 nm), non-enveloped, single-stranded (ss) DNA viruses (Mezzina and Merten, 2011). Their genome contains two open reading frames (ORFs, total 4.7 kb), *rep* which encodes proteins required for replication and packaging and *cap* which encodes capsid proteins. The ORFs are flanked by two inverted terminal repeats (ITRs), which are the only *cis*-acting elements. By formation of a hairpin structure, the ITRs initiate primase independent DNA synthesis and are also required for genome replication and packaging (Wu et al., 2006).

Recombinant AAV vectors are among the most widely used gene transfer tools for gene delivery and expression in different target tissues. AAVs possess highly advantageous characteristics including non-pathogenicity, low immunogenicity, long-lasting transgene expression, and the ability to transduce

[2] https://www.ncbi.nlm.nih.gov/UniGene/ESTProfileViewer.cgi?uglist=Hs.201555, 25. October 2018
https://www.ncbi.nlm.nih.gov/UniGene/ESTProfileViewer.cgi?uglist=Hs.270978, 25. October 2018

both dividing and non-dividing cells (Kaplitt et al., 1994, Lo et al., 1999, Mastakov et al., 2002). For AAV production, a recombinant AAV-vector (rAAV-vector) is cloned, in which the desired transgene and promotor are integrated between the two ITRs in a plasmid framework. The *rep* and *cap* genes and the adenoviral genes needed for replication (E2A, E4, VA,) are supplied in *trans* either in a combined helper plasmid (not shown) or in two individual helper plasmids, which are co-transfected together with the recombinant AAV vector into E1 positive (E1+) HEK293T cells for AAV production and packaging (Figure 9). The obtained recombinant AAV viral particles do not contain the *rep* genes and are thus not able to integrate into the host genome and remain as stable episomes leading to long-lasting transgene expression in infected cells (Mezzina and Merten, 2011, Grieger et al., 2006).

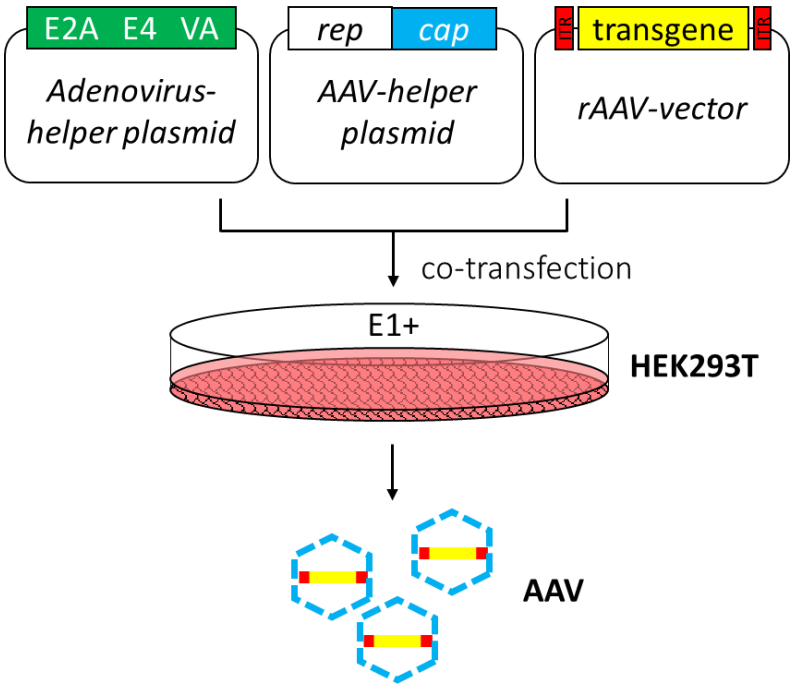

Figure 9: Recombinant AAV viral vector packaging in HEK293T. The recombinant AAV-vector, the AAV-helper plasmid and the adenovirus-helper plasmid are co-transfected into E1+ HEK293T cells. Three days post-transfection the cells are harvested and the AAV particles can be purified and enriched by iodixanol gradient ultracentrifugation.

To date, at least eleven AAV serotypes and hundreds of AAV variants have been isolated from humans and non-human primates, with new serotypes being discovered constantly. The serotype of an AAV determines its tropism, meaning the cell types it infects. The best examined and commonly used serotypes are AAV-1, -2, -5, -8 and -9 (Petrosyan et al., 2014). More recent serotypes are AAV-rh10 and AAV-PHP.B which are of major importance for this work as they are used for the *in vivo* substrate trapping experiments. AAV-rh10 is a natural AAV serotype shown to provide superior widespread transgene expression in mice after i.v. injection compared to the more commonly used serotypes (Hu et al., 2010). AAV-PHP.B is a capsid variant of AAV-9 generated by CREATE (Cre recombination-based

AAV targeted evolution), leading to particularly high transgene expression in the brain after i.v. injection compared to AAV-9 (Jackson et al., 2016, Deverman et al., 2016). In addition to astrocytes infected by AAV-9, AAV-PHP.B mediates transgene expression in endothelial cells, oligodendrocytes and neurons including several neuronal subtypes like midbrain tyrosine hydroxylase positive (TH^+) dopaminergic neurons (Deverman et al., 2016).

1.6. Liquid chromatography tandem mass spectrometry

In a LC-MS/MS system, analytes are separated with high-performance LC (HPLC) prior to mass analysis in a tandem MS. This synergistic system allows the analysis of very complex, biological samples with high specificity.

Protein analysis with LC-MS/MS typically includes proteolytic digestion by trypsin, as most peptide data libraries are trypsin based. The retention time of the tryptic peptides on the stationary phase of the HPLC is the first separation criterion. To separate peptides, reversed phase LC (RPLC) is used. In RPLC peptide analytes are separated based on their hydrophobicity on a C18-column. The electron spray ionization (ESI) source is the coupler between the HPLC system and the tandem MS. At this interphase the mobile phase is evaporated by heat under a stream of dry nitrogen and the analytes are ionized and drawn into the MS by electrical force (Fenn et al., 1989).

In a tandem MS, peptides are separated based on their mass-to-charge ratio (*m/z*). The tandem MS systems used in this work are a QTrap 4000 and a TripleTOF 6600. For convenience the basic principle of tandem MS analysis is explained here based on the primarily used TripleTOF 6600. More detailed information about the used LC-MS/MS techniques can be found in ETH Diss. No. 25663 from Monika Dengler (Dengler, 2019).

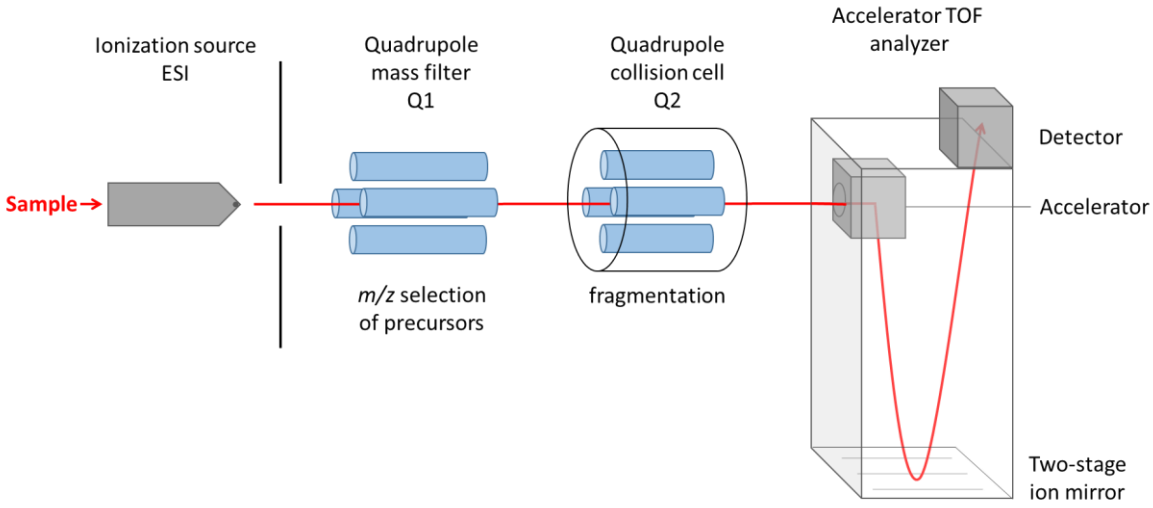

Figure 10: Principle of a TripleTOF MS. Visualization of the arrangement of the different modules in a TripleTOF device.

TripleTOF systems exhibit high resolution and mass accuracy (high resolution MS; HRMS). The system consists of an ESI source, a quadrupole mass filter (Q1) followed by a quadrupole collision cell (Q2), an accelerator time-of-flight (TOF) analyzer and a detector (Figure 10). Two frequently used MS/MS modes are multiple reaction monitoring (MRM) and product ion scan. In both, precursor ions (parent ions) are filtered in Q1 for their specific *m/z* by electrical fields. The selected precursor ions then enter Q2 were they get fragmented by a collision gas (collision induced dissociation (CID)). The typical predictable peptide fragmentation pattern is shown in Figure 11, as peptides usually break at certain points of their backbone.

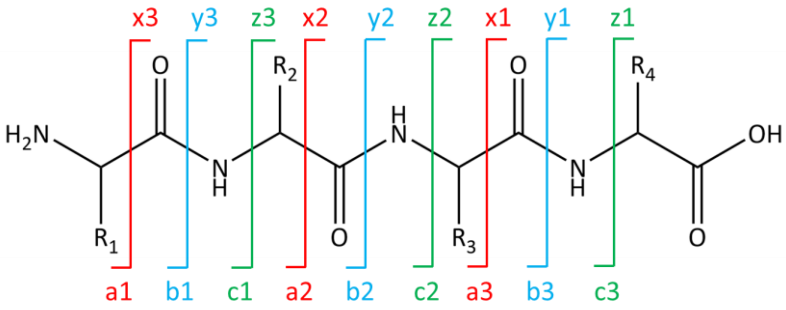

Figure 11: Typical peptide fragments in tandem MS analysis. C-terminal fragments are called x, y and z. N-terminal fragments are called a, b and c. The number stands for the number of amino acids.

The detector can only detect charged fragments. Using low energy CID mainly charged y and b fragments are generated. Depending on the scan type, the following accelerator TOF analyzer can again act as a filter for one specific product ion (multiple reaction monitoring (MRM) Figure 12 A) or it can scan all different product ions (product ion scan Figure 12 B). In the TOF analyzer the *m/z* of a fragment is deduced from its time of flight through a tube with a certain length under vacuum (Domon and Aebersold, 2006).

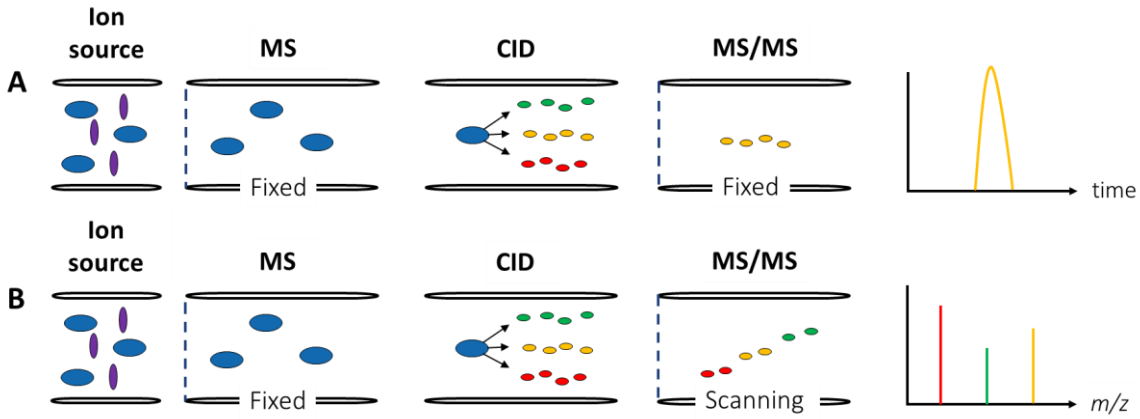

Figure 12: Two typically used MS/MS scan modes. (A) multiple reaction monitoring (MRM) and (B) product ion scan. CID = collision induced dissociation. Figure adapted from (Domon and Aebersold, 2006)

The aim of classical proteomics is to elucidate the entire protein content of a cell, organ, or organism. We, in contrast, are interested in one particular peptide of each trapping EH. Based on the aforementioned LC-MS/MS technique, a modified peptide would not only have different properties concerning the LC elution profile but also the *m/z* of the parent ion is different compared to the unmodified peptide. However, the key fragments of the fragmentation pattern of the peptide would stay the same. Thus, a substrate modified CatNuc peptide of our trapping EHs would show the same fragmentation pattern as the unmodified peptide but potentially have another retention time and for sure have a different parent ion mass (*m/z*). The substrate-peptide complex could therefore be identified by the known specific fragmentation pattern of the non-modified CatNuc peptide. The mass increase of the parent ion compared to the unmodified CatNuc peptide represents the substrate mass.

2. Aims

2.1. Deciphering the (patho)physiologic role of epoxide hydrolases by *ex vivo* cartography of their substrate landscape

The aim of the main project is to elaborate and use a novel substrate trapping method to elucidate the physiologic function of EHs by identifying which substrates they prefer *in vivo*.
Three major questions will be addressed:

1) What is the physiologic role of the hitherto orphan human EHs EH4 and MEST?

2) Which are the relevant *in vivo* substrates of the well-characterized sEH, mEH and EH3?

3) Is the EH activity of Cif, an enzyme secreted by the pathogen *P. aeruginosa*, a major contributor to the pathogenicity of the bacterium?

From answering these questions, we expect a fundamental gain in the understanding of the role of EHs in mammalian/human physiology and thus to create new leads for the development of novel therapeutic strategies. The development of the substrate trapping itself would be a breakthrough for the identification of the *in vivo* relevance of known substrates and for the identification of new substrates in an unbiased manner that could be applied for other enzymes.

2.2. The CYP blocker MS-PPOH is an inhibitor of sEH

The aim of the smaller side project is to answer the question if the selective CYP epoxygenease blocker MS-PPOH is an inhibitor of mEH and/or sEH, as a certain class of mEH inhibitors shows similar structure. Inhibition of mEH and/or sEH, would increase EET levels, as opposed to the expected drop in EET concentrations following CYP inhibition. Consequently, wrong conclusions concerning physiologic EET functions would be drawn from experiments using MS-PPOH as a CYP inhibitor.

3. Materials and methods

3.1. Chemicals and substances

Chemicals were obtained from Sigma-Aldrich (St. Louis, MO, USA) or Roth AG (Karlsruhe, Germany) if not stated otherwise. AA was purchased at Cayman Chemicals (Ann Arbor, MI, USA). The fluorescent EH substrates CMNMGC and CMNPC were kindly provided by Dr. Christoph Morisseau (Department of Entomology, University of California, Davis, CA, USA). EET and DHET regioisomers kindly provided by Dr. John Falck (Department of Biochemistry, UT Southwestern Medical Center, Dallas, TX, USA).

3.2. Vectors and Plasmids

Table 1: Plasmids

Abbreviations	Full name	Purpose
pRSET	pRSET A	Inclusion body expression in *E. coli* Mutagenesis PCR
pET	pET20b(+)	Active EH expression in *E. coli*
pAM-CAG	pAM-CAG-pl-His-WPRE	Virus production, rAAV-vectors Active EH expression in cell culture
AAV-5	AAV-5	Virus production, AAV-helper plasmid, (Pietropaolo et al., 2007)
AAV-rh10	pAAV2/rh10	Virus production, AAV-helper plasmid (Wilson et al. unpublished[3])
AAV-PHP.B	pUCmini-iCAP-PHP.B	Virus production, AAV-helper plasmid (Deverman et al., 2016)
adenovirus-helper plasmid	pBS-E2A-VA-E4	Virus production, adenovirus-helper plasmid, (Paterna et al., 2000)

The AAV-helper plasmid pAAV2/rh10 was kindly provided by Dr. James M. Wilson (Department of Medicine, University of Pennsylvania, Philadelphia, PA, USA; Addgene plasmid # 112866[3]). The AAV-helper plasmid pUCmini-iCAP-PHP.B was kindly provided by Dr. Benjamin Deverman (Division of Biology, California Institute of Technology, Pasadena, CA, USA). The adenovirus-helper plasmid was kindly provided by Dr. Jean-Charles Paterna (Viral Vector Facility, University of Zurich, Zurich, Switzerland).

[3] https://www.addgene.org/112866/, 14. December 2018

3.3. Primers

Table 2: Primers used to insert EHs into pRSET

Name	Sequence	Restric. site
sEHfor BamHI BstBI	*GATCGGATCC*GCCGCCATGACGCTGCGCGCGG	BamHI
sEHrev BamHI BstBI	*GATCTTCGAAGC*CATCTTTGAGACCACCGG	BstBI
EH3for Cla BstBI	*GATCATCGATGCGGCCGC*GCCGCCATGGCGGAGCTGGTGGTGA	ClaI
EH3rev NotI BstBI	*GATCTTCGAAGC*GTCCAGCAGGTCTTGCAAGAAGG	BstBI
EH4for BamHI BstBI	*GATCGGATCCGCCGCC*ATGGCGAGGCTGCGGGATTGCCTG	BamHI
EH4rev BamHIBstBI	*GATCTTCGAAGC*ATCTTTTTTTCTTGTTTCTTCTTTTAGAAATGTCCATATCAA	BstBI

Cursive, non-complementary sequence; underlined, restriction site.

Table 3: Mutagenesis primer

Name	Sequence
sEH D335A for	CATTGGCCATG***CA***TGGGGTGGCATGCTGGTG
sEH D335A rev	CACCAGCATGCCACCCCA***TG***CATGGCCAATG
sEH H524A for	GACTGTGGG***GC***CTGGACACAGATGGAC
sEH H524A rev	GTCCATCTGTGTCCAG***GC***CCCACAGTC
sEH H524Q for	GGACACATTGAGGACTGTGGGCA***G***TGGACACAGATGGAC
sEH H524Q rev	GTCCATCTGTGTCCA***C***TGCCCACAGTCCTCAATGTGTCC
EH3 D173A for	GTGGCCCATG***CA***TGGGGTGCCCTCCTTG
EH3 D173A rev	CAAGGAGGGCACCCCA***TG***CATGGGCCAC
EH3 H337A for	GCCAGGCATAGGG***GC***TTG***T***ATCCCACAGAG
EH3 H337A rev	CTCTGTGGGAT***A***CAA***GC***CCCTATGCCTGGC
EH3 H337Q for	GCCAGGCATAGGGCA***G***TG***T***ATCCCACAGAG
EH3 H337Q rev	CTCTGTGGGAT***A***CA***C***TGCCCTATGCCTGGC
EH4 D169A for	GTTCTTATTGGCCATG***CA***TGGGGGGGCATGATTGCTTGG
EH4 D169A rev	CCAAGCAATCATGCCCCCCCA***TG***CATGGCCAATAAGAAC
EH4 H336A for	GTCAGAAGCCAGT***GC***TTGGCTGCAGCAAGACCAAC
EH4 H336A rev	GTTGGTCTTGCTGCAGCCAA***GC***ACTGGCTTCTGAC
EH4 H336Q for	GTCAGAAGCCAGTCA***G***TGGCT***G***CAGCAAGACCAAC
EH4 H336Q rev	GTTGGTCTTGCTG***C***AGCCA***C***TGACTGGCTTCTGAC

Bold cursive, mutation; underlined, changed codon.

Table 4: Primers to insert EHs into pAM-CAG vector

Name	Sequence	Restric. site
sEHfor BamHI BstBI	*GGATCC*GCCGCCATGACGCTGCGCGCGG	BamHI
sEHrev BamHI BstBI	*GATCTTCGAAGC*CATCTTTGAGACCACCGG	BstBI
EH3for NotI BstBI	*GCGGCCGC*GCCGCCATGGCGGAGCTGGTGGTGA	NotI
EH3rev NotI BstBI	*GATCTTCGAAGC*GTCCAGCAGGTCTTGCAAGAAGG	BstBI
EH4for BamHI BstBI	*GGATCCGCCGCC*ATGGCGAGGCTGCGGGATTGCCTG	BamHI
EH4rev BamHIBstBI	*GATCTTCGAAGC*ATCTTTTTTTCTTGTTTCTTCTTTTAGAAATGTCCATATCAA	BstBI

Cursive, non-complementary sequence; underlined, restriction site.

Table 5: Oligonucleotides

Name	Sequence
Polylinker pAM-CAG sense1	GATCCGCTAGCGGTACCTTCG
Polylinker pAM-CAG sense2	AATCGCGAACATCATCATCATCATCATCGCGAGTA
Polylinker pAM-CAG antisense1	AGCTTACTCGCGATGATGATG
Polylinker pAM-CAG antisense2	ATGATGATGTTCGCGATTCGAAGGTACCGCTAGCG
Polylinker pAM-CAG sense3	GATCCGCGGCCGCCTGCAGCTCGAGGAATT
Polylinker pAM-CAG antisense3	CGAATTCCTCGAGCTGCAGGCGGCCGCG

Table 6: Sequencing primer

Name	Sequence
AAV8-SAR120514	TGACGTCAATGGAAAGTCCC
AAV-pl-for	GTGGCTGCGTGAAAGCCTTGA
CAGfor	GCCCAGTACATGACCTTA
VP1.5	GGACTTTCCAAAATGTCG
XL39	CCACCAGCCTTGTCCTAATA

3.4. Synthetic peptides

Table 7: Properties of the six tryptic, synthetic CatNuc peptides

Name	Sequence	Mass [Da]
mEH	LGFQEFYIQGGDWGSLIC[CAM]TNMAQLVPSHVK	3396.88
sEH	LGLSQAVFIGHDWGGMLVWYMALFYPER	3257.82
EH3	C[CAM]ILVAHDWGALLAWHFSIYYPSLVER	3117.64
EH4	C[CAM]VLIGHDWGGMIAWLIAIC[CAM]YPEMVMK	3064.75
MEST	INLLSHDYGDIVAQELLYR	2232.53
Cif	QFSPDRPFDLVAHDIGIWNTYPMVVK	3046.50

Underlined, CatNuc and site of modification with trapped substrates.

The synthetic CatNuc peptides of the six EHs were purchased from JPT Peptide Technologies (JPT Peptide Technologies, Berlin, Germany).

3.5. Antibodies

Table 8: Primary antibodies

Abbreviation	Supplier information
anti His-tag	Anti-6X Histag® antibody-ChIP Grade (ab9108), polyclonal, Abcam
anti GFP	GFP Polyclonal Antibody (A6455), polyclonal, Invitrogen
anti-human mEH	Rabbit 2 Anti-mix mEH, polyclonal, in-house

Table 9: Secondary antibodies

Abbreviation	Supplier information
anti rabbit AP	Anti-Rabbit IgG (whole molecule), F(ab')2 fragment−Alkaline Phosphatase antibody produced in goat (A3937), Sigma Aldrich
Odyssey 680	IRDye® 680RD Donkey anti Rabbit Antibody (926-68073), polyclonal, Li-Cor
Odyssey 800	IRDye® 800CW Donkey Anti-Rabbit IgG (H+L) (926-32213), polyclonal, Li-Cor
Cy3	Cy™3 AffiniPure Donkey Anti-Rabbit IgG (H+L) (711-165-152), polyclonal, Jackson Immuno Research

3.6. Microbiological methods

3.6.1. Polymerase chain reaction

Polymerase chain reaction (PCR) was used to amplify specific DNA segments from plasmid DNA or from genomic DNA. PCR reaction mix and PCR program are summarized in Table 10. Primers were ordered desalted and lyophilized from Microsynth (Balgach, Switzerland). They were resuspended in water to obtain a concentration of 100 µM and stored at -20 °C. Primers were prediluted to 25 µM in water before use. Homemade proofreading Pfu DNA polymerase was used (2.5 U). 10 x dNTP mix consisted of 2.5 mM dNTPs (Thermo Fisher Scientific, Waltham, MA, USA) and 10 x Taq buffer consisted of 200 mM Tris, 100 mM $(NH_4)_2SO_4$, 100 mM KCl, 20 mM $MgSO_4$, 1% Triton X-100, 1 mg/mL BSA, Tris pH 7.4. The PCR was performed in a thermal cycler (T100 thermal cycler; Bio-Rad Laboratories, Inc., Hercules, CA, USA). Hot-start PCR was used, meaning that the Pfu polymerase was added last to the PCR reaction after it was heated up to 95 °C. With a hot-start, unspecific primer binding and amplification is reduced.

Table 10: PCR reaction mix and PCR program

PCR reaction mix		PCR program		
Plasmid DNA	40 ng	95 °C	5'	add Pfu
Reverse primer	0.5 µl	95 °C	30''	
Forward primer	0.5 µl	60 °C*	10''	30 x
10 x dNTP mix	5 µl	72 °C	2'	
10 x Taq buffer	5 µl	72 °C	5'	
Pfu polymerase	1 µl			
Water	ad 50 µl			

* Gradient PCR 55-65 °C: 3-5 tubes of the same PCR-mix were run at different temperatures. Adapted from Monika Dengler ETH Diss. No. 25663 (Dengler, 2019).

3.6.2. Site-directed mutagenesis PCR

Site-directed mutagenesis PCR was used to introduce point mutations into double stranded DNA. Two complementary primers including the desired point mutation were designed allowing amplification of the entire plasmid. The point mutation should be flanked by at least 10-15 bases on each side. Because of its bacterial origin, the template plasmid is methylated and can be selectively digested with the restriction endonuclease DpnI. The PCR amplified plasmid which contains the mutation is not digested and was transformed into *E. coli* for amplification and analysis. All site-directed mutagenesis PCRs were done using the hot-start method.

Table 11: Site-directed mutagenesis PCR reaction mix and PCR program

PCR reaction mix		PCR program		
Plasmid DNA	40 ng	95 °C	3’	add Pfu
Reverse primer	0.3 µl	95 °C	1’	
Forward primer	0.3 µl	60 °C*	1’	30 x
10 x dNTP mix	3 µl	72 °C	10’	
10 x Taq buffer	3 µl	72 °C	15’	
ATP	0.5 µl			
Pfu polymerase	0.6 µl			
Water	ad 30 µl			

* Gradient PCR 55-65 °C: 3-5 tubes of the same PCR-mix were run at different temperatures. Adapted from Monika Dengler ETH Diss. No. 25663 (Dengler, 2019).

3.6.3. Cloning

To transfer a gene or a segment from one vector to another, the segment was amplified using PCR. Primers were designed complementary on the 3’-end and at the 5’-end up to 24 non-complementary base pairs were added to change the final vector sequence or to introduce a new endonuclease restriction site. The amplified fragments and the desired vector backbones were cleaved with the respective restriction endonuclease(s) (New England Biolabs (NEB), Ipswich, MA, USA) and BSA (if required) in the corresponding NEB buffer for 1 h. If required, the vector backbone was dephosphorylated to avoid self-ligation by adding calf intestinal phosphatase (NEB) to the restriction endonuclease digest for 1 h at 37 °C. Subsequently, both fragments were gel-purified with a preparative 0.7-1% agarose gel using the QIAquick Gel Extraction Kit (Qiagen, Hilden, Germany) according to the manual.

For ligation, 40 ng vector backbone and the respective amount of insert leading to a molecular weight ratio of 1:3 (backbone to insert) were added to the ligation reaction together with 1 µl of 10 x T4 ligation buffer and 1 µl T4 DNA ligase (1:10 dilution in water) (Thermo Fisher Scientific, Waltham, MA,

USA) and filled up to 10 µl with water. The reaction was incubated for 30 min at RT in the dark, heat inactivated for 10 min at 65 °C and transformed into TOP10 or MDS42 electro-competent *E. coli*.

3.6.4. Transformation and plasmid amplification

1-2 µl of plasmid or ligation mix were added to 40 µl of freshly thawed electro-competent TOP10 or MDS42 *E. coli* and transferred into a sterile, precooled 0.1 cm gap cuvette (Bio-Rad Laboratories, Inc., Hercules, CA, USA). After incubation on ice for 5 min electroporation was performed at 1.35 kV for one pulse of 5 ms with a Gene Pulser™ (Bio-Rad Laboratories). The bacteria were then suspended in 500 µl of LB medium and incubated for 1 h at 37 °C shaking with 220 rpm. Subsequently 100 µl of the cell suspension was plated on a 10 cm LB agar plate containing the respective selection antibiotic and incubated overnight at 37 °C.

3.6.5. Plasmid isolation

E. Coli colonies from a LB agar plate containing the plasmid of interest were used to inoculate a 4 ml LB medium starter culture which was incubated overnight. Depending on the desired plasmid amount, 4-250 ml LB medium containing ampicillin (100 µg/ml) was inoculated with the starter culture and plasmid DNA isolated using a Qiagen DNA isolation kit according to the manufacturers' protocol (QIAprep Spin Miniprep Kit, HiSpeed Plasmid Midi Kit, HiSpeed Plasmid Maxi Kit; Qiagen, Hilden, Germany) and quantified by Nanodrop.

3.7. Recombinant protein expression

Wild type (WT) and mutant (HQ) EHs were recombinantly expressed as inclusion bodies or active protein in *E. coli* or mammalian cell lines for the LC-MS/MS method development as well as for *in vitro* trapping experiments.

3.7.1. Recombinant expression in *E. coli*

EHs in the pRSET or pET expression vector were transformed into the arabinose inducible *E. coli* strain BL21-AI and a 4 ml LB medium starter culture was incubated overnight at 37 °C, shaking at 220 rpm. 1-4 ml of the starter culture was spun down and washed twice with LB medium before inoculation of 100-250 ml of LB medium containing ampicillin (100 µg/ml). The culture was incubated at 37 °C until an OD_{600} of 0.4-0.6 was reached. Protein expression was induced by adding arabinose to a final concentration of 10 µM for active enzyme expression and 1 mM for inclusion body production. The culture was incubated overnight (22 h) at RT (active enzyme) or 30 °C (inclusion bodies), shaking at 220 rpm.

The following day bacterial culture was harvested by centrifugation at 4000 g for 15 min (Heraeus Megafuge 1.0R, rotor #2704; Heraeus Instruments GmbH, Hanau, Germany) and the pellet was either resuspended in Tris-buffer (20 mM Tris, 100 mM NaCl) for further purification or alternatively stored at -80 °C until further use.

3.7.2. Recombinant expression in mammalian cells

For recombinant protein expression in mammalian cells, HEK293T, U87 and SH-SY5Y were transiently transfected or virally transduced.

3.7.2.1. Cultivation of mammalian cell lines

HEK293T cells were cultivated in DMEM low glucose medium (Gibco) supplemented with 5% FBS at 37 °C with 5% CO_2. Cells were grown until they reached 80% confluency and detached by incubation with trypsin (Gibco, 0.125% w/v) and reseeded at a dilution of 1:20 (frequency: 2-3 times per week).
U87 glioma cells were cultivated in EMEM medium (Gibco) supplemented with 10% FBS at 37 °C with 5% CO_2. Cells were grown until they reached 80% confluency and detached by incubation with trypsin (Gibco, 0.125% w/v) and reseeded at a dilution of 1:5 (frequency: 2-3 times per week).
SH-SY5Y neuroblastoma cells were cultivated in DMEM:F12 medium (1:1) complemented with 5% FBS at 37 °C with 5% CO_2. Cells were grown until they reached 80% confluency and detached by incubation with trypsin (Gibco, 0.125% w/v) and reseeded at a dilution of 1:10 (frequency: 2-3 times per week).

3.7.2.2. Transient transfection

Transient transfections were done according to the JetPEI® user guide (Polyplus-transfection®, Strasbourg, F) but instead of JetPEI® the transfection reagent PEI MAX (1 µg/µl in ddH_2O) (Polysiences, Inc., Warrington, PA, USA) was used.
In brief, for a 10 cm dish 2-3 x 10^6 HEK293T cells were seeded 24 h before transfection to reach 70% confluency. 15 µg of plasmid DNA was diluted in 600 µl of 150 mM NaCl and 45 µg of PEI MAX (DNA:PEI MAX was always 1:3) was diluted in another 600 µl 150 mM NaCl solution and both vortexed. The PEI MAX solution was then added dropwise to the plasmid DNA mix, vortexed briefly and incubated for 20-25 min at RT. Subsequently, the 1200 µl DNA/PEI MAX mix was gently added to the cell covering medium, avoiding detachment of the cell layer, and slewed with caution. Transgene expressing cells were harvested 48-72 h post-transfection.

3.7.2.3. Fluorometric quantification of GFP expression in transfected cells

HEK293T cells were transiently transfected with pAM-CAG-SARsense GFP, pAM-CAG-SARantisense GFP or pAM-CAG GFP in a 24-well plate and harvested 48 h post-transfection (see 3.7.2.2). Medium was removed and 200 µl of EBC lysis buffer (500 mM Tris, 120 mM NaCl, 0.5% (v/v) Nonidet P-40, pH 8.0) were added to each well. Cells were incubated on ice for 1 h and subsequently transferred into a 96-well plate. The GFP fluorescence was quantified in a plate reader (SpectraMAX GeminiXS microplate fluorescence reader; Molecular Devices, LLC, CA, USA) at the excitation wavelength 480 nm and the emission wavelength 510 nm. Measurements were done in triplicates.

3.7.2.4. Viral transduction and transgene analysis in a microplate reader format

For the viral transduction, 10'000 cells were seeded per well (96-well plate) and incubated overnight to reach 70% confluency. The viral solution was added at a multiplicity of infection (MOI) of 100'000 or 1'000'000 which corresponds to 100'000 resp. 1'000'000 viral genomes (vg) per cell. Cells were harvested 72 h post-infection. Medium was aspirated, and cells were resuspended in 1 x Lämmli buffer (50 mM Tris pH 6.8, 2% SDS, 0.1% Bromphenol blue, 10% Glycerol, 2.5% ß-Mercaptoethanol). Transgene expression was analyzed with SDS-PAGE followed by Western blot.

3.8. Protein purification

All protein expression constructs contain an in-frame C- or N-terminal His-tag for the following retrieval of recombinant protein out of cell, bacteria or mouse tissue homogenates.

3.8.1. Protein purification from *E. coli*

3.8.1.1. French Pressure Cell

Bacterial cell pellets were resuspended in a 25-fold reduced volume of Tris-buffer compared to the bacterial culture volume. The homogenous disruption of bacterial cells was achieved using a French® Pressure Cell press (Slm Aminco, Thermo Fisher Scientific, Waltham, MA, USA) with a pressure of 30'000 psi. Outflowing lysates were chilled on ice.

3.8.1.2. Immobilized metal ion chromatography on an ÄKTA setup

Immobilized metal ion chromatography (IMAC) on an ÄKTA setup was used to purify and enrich His-tagged proteins expressed in *E. coli*. For membrane bound enzymes like mEH, 0.5% (v/v) Genapol® X-100 was added to the bacteria lysates and incubated for 1 h on ice to solubilize the enzyme. Bacteria lysates were centrifuged for 20 min at 4000 g, 4 °C (Heraeus Megafuge 1.0R, rotor #2704, Heraeus

Instruments GmbH, Hanau, Germany) and subsequently, the His-tagged EHs were purified from the supernatant by IMAC using a 1 ml HisTrap FF column in an ÄKTA Explorer setup (both GE Healthcare Life Sciences, UK). The recombinant His-tagged protein binds the immobilized Ni^{2+} ions on the column (stationary phase) and can be eluted by increasing imidazole concentration in the elution buffer (mobile phase). The HisTrap FF column was first primed with 100% buffer A (20 mM Tris, 500 mM NaCl, 20 mM Imidazole, pH 7.4) for 5 min with a flow of 1 ml/min. The sample was loaded with a 0.5 ml/min flowrate and an isocratic flow of 100% buffer A with 1 ml/min was maintained until no protein elution was visible anymore with the UV (280 nm) detector. The bound protein was then eluted with a linear gradient of 1% per 2 min of buffer B (20 mM Tris, 500 mM NaCl, 500 mM Imidazole, pH 7.4) at a flowrate of 0.5 ml/min and 0.5 ml fractions were collected which was monitored by UV. The fractions containing the protein were analyzed by SDS-PAGE and Western blot or Coomassie staining.

3.8.2. His-tagged protein enrichment from mouse tissue by IMAC

1 ml homogenization buffer (0.125 M KCl, 0.25 M sucrose, 1 mM EDTA, 0.1 M potassium phosphate, pH 7.4) was submitted in a glass tissue grinder on ice. Up to 400 mg of mouse organ (stored at -80 °C) was added and homogenized with 6-8 strokes. For membrane bound enzymes the homogenization buffer was supplied with 0.5% (v/v) Genapol® X-100 prior to tissue homogenization. After centrifugation (15 min at 10'000 g, 4 °C; Eppendorf Centrifuge 5430R, rotor FA-45-30-11, Eppendorf AG, Hamburg, Germany) the cleared supernatant was loaded on a ready-to-use primed 1 ml HisTrap FF column using a syringe pump (Harvard Apparatus 11 Plus Syringe Pump) at a flow rate of 0.5 ml/min. Subsequently, the column was washed with 6 column volumes (6 ml) of buffer A (20 mM Tris, 500 mM NaCl, 20 mM Imidazole, pH 7.4) and the His-tagged protein was eluted immediately with 3 column volumes (3 ml) of buffer B (20 mM Tris, 500 mM NaCl, 500 mM Imidazole, pH 7.4). The eluting fractions (0.5-1 ml) were analyzed by SDS-PAGE and Western blot or Coomassie staining.

3.9. Protein analytics

3.9.1. Bradford assay

His-tag purified protein, expressed in *E. coli,* was quantified by the Bradford assay. The BSA calibration curve was prepared in a 96-well plate according to the following pipetting scheme (Table 12) using a BSA stock solution of 1 mg/ml.

Table 12: BSA calibration curve

Final BSA conc. [µg/ml]	66.7	53.3	40.0	26.7	13.3	6.7	0
BSA stock solution [µl]	20	16	12	8	4	2	0
H_2O [µl]	80	84	88	92	96	98	100

The Bradford working solution was prepared by diluting Bradford reagent (Roti®-Quant 5x concentrated Bradford Reagent K015) 1:2.33 in water. 100 µl of protein sample, diluted to a concentration within the range of the calibration curve, was provided in the 96-well plate. After the addition of 200 µl Bradford working solution to each well of the standard curve and the sample the plate was shacked carefully and absorbance was measured in a plate reader at 595 nm (SpectraMAX GeminiXS microplate fluorescence reader; Molecular Devices, LLC, CA, USA). All measurements were done in duplicates.

3.9.2. Sodium dodecyl sulfate polyacrylamide gel electrophoresis

Sodium dodecyl sulfate polyacrylamide gel electrophoresis (SDS-PAGE) was used for protein separation. The used gels were self-casted according to the composition specified in Table 13. One part of sample (v) was mixed with 3 parts (v) of 4 x Lämmli buffer (200 mM Tris pH 6.8, 8% SDS, 0.4% Bromophenol blue, 40% Glycerol, 10% ß-Mercaptoethanol) and incubated for 5 min at RT (heat sensitive EH3) or 85 °C. Gel pockets were loaded with 1-60 µl of sample. The gel was run with 1 x PAA buffer (25 mM Tris, 250 mM Glycine, 0.1% SDS, pH 8.3) at 80-100 V for 1-3 h (Bio-Rad PowerPac™ Basic Power Supply; Bio-Rad Laboratories, Inc., Hercules, CA, USA).

Table 13: Self-casted 12.5% SDS-PAGE gels

	12.5% Running gel [ml]	5% Stacking gel [ml]
Water	24.8	20.6
Rotiphorese® Gel 30	33.3	5.0
1 M Tris pH 6.6	20	-
1.5 M Tris pH 8.8	-	3.75
10% SDS	0.8	0.3
10% APS	0.8	0.3
TEMED	0.032	0.032

The specified volumes are adequate to cast 7 gels of 8 x 9 cm size.

3.9.3. Coomassie staining of proteins

Proteins separated by SDS-PAGE were visualized with Coomassie brilliant blue solution (0.25 g Brilliant blue R250, 0.25 g G250 in 45% (v/v) methanol and 10% (v/v) acetic acid). Gels were incubated in the

Coomassie solution for at least 20 min (RT) and destained in destaining solution (15% isopropanol, 10% acetic acid) for 12-18 h. The destaining solution was changed 2-3 times during this time.

3.9.4. Western blot analysis of proteins

Proteins expressed in bacteria, cell culture or mouse tissue were detected and semi quantified by Western blot. The semi-dry blotting technique was used to blot SDS-PAGE separated proteins onto a polyvinylidene difluoride membrane (Immobilion-P, Merck Millipore, Burlington, MA, USA). The membrane was first activated for 5 min in methanol and in the following equilibrated in blotting buffer (25 mM Tris, 250 mM glycine, 0.1% SDS, pH 8.3, 20% methanol), both at RT. One blotting buffer-soaked filter paper was placed into the transfer chamber and the activated membrane placed on top. Air bubbles were removed using the blot roller. Subsequently, the SDS-PAGE gel was placed on top of the membrane and air bubbles were removed for a second time. Finally, the gel was covered with a second blotting buffer-soaked filter paper and the chamber was closed with the lid and blotting was performed for 30 min at 25 V and 1 A (Bio-Rad Trans Blot Turbo Transfer System, USA). After blocking the membrane for 1 h in either Odyssey Blocking Buffer (LI-COR Biosciences) for Odyssey secondary antibodies or 2.5% skimmed milk powder in TBST (10 mM Tris, 150 mM NaCl, 0.05% TWEEN 20, pH 8.0) for alkaline phosphatase (AP) conjugated secondary antibodies, it was incubated for 1 h at RT or overnight at 4 °C with the primary antibody (1:1000 in the respective blocking buffer, if not specified otherwise). The membrane was washed 3 x 15 min in TBS (10 mM Tris, 150 mM NaCl, pH 8.0) (or TBST for AP detection) to remove residual antibody. Subsequently, the membrane was incubated for 1 h at RT with the secondary antibody (1:8000 in TBS or TBST, if not specified otherwise). The membrane was washed 3 x 15 min with TBS (or TBST for AP detection) before it was scanned with the Odyssey reader (LI-COR Biosciences, Lincoln, NE, USA) or developed by AP.

3.10. Virus production

The AAV production was done in collaboration with the Viral Vector Facility. All used protocols for in-house production were kindly provided by Jean-Charles Paterna (Viral Vector Facility VVF, University of Zurich, Irchel Campus, Zurich). Two plasmids were co-transfected in HEK293T cells, the sample plasmid which provides the gene of interest and the helper plasmid with the *rep* and *cap* genes for virus particle assembly. The virus particles were then purified from the HEK293T cells by iodixanol gradient ultracentrifugation and quantified using a Qubit™ 2.0.

3.10.1. Plasmid-DNA co-transfection

For the AAV production, HEK293T cells were co-transfected with AAV-helper plasmid (AAV-PHP.B, AAV-rh10 or AAV-5) adenovirus-helper plasmid and the respective rAAV-vector (pAM-CAG construct) in a molar ratio of 1:1:1. Therefore, helper plasmids and sample plasmid were diluted in 1500 µl of 150 mM NaCl and PEI MAX (total DNA:PEI = 1:3 (w)) was diluted in another 1500 µl 150 mM NaCl solution and both vortexed. The PEI MAX solution was added dropwise to the sample DNA mix, was vortexed and incubated for 20 min at RT. Subsequently, 3 ml of the DNA/PEI MAX mix were gently added to a 15 cm dish of 60% confluent HEK293T cells and slewed with caution. 72 h post-transfection, cells were harvested by flushing them with their own DMEM medium using a 25 ml cell culture pipette. The cell suspension was transferred into a 50 ml Falcon tube and pelleted for 15 min at 600 g, 4 °C (Eppendorf Centrifuge 5702, rotor A-4-38; Eppendorf AG, Hamburg, Germany). The HEK cell pellet and supernatant were stored at -80 °C until further processing.

3.10.2. Cell lysate

To lyse the harvested HEK cells, the cell pellet derived from up to two 15 cm cell culture dishes were resuspended in 1 ml of AAV resuspension buffer (RB) (150 mM NaCl, 50 mM Tris, pH 8.5). A total volume of 3 ml AAV RB was used to resuspend HEK cell pellets derived from more than 2 (but less than 16) 15 cm cell culture dishes. The suspension was transferred into 1.5 ml Eppendorf tubes with a maximum volume of 500 µl and cells were lysed using the Bullet Blender Storm 24 (Next Advance, Troy, NY, USA) without beads at speed 8 for 3 x 3 min. The crude cell lysate was than centrifuged for 10 min at 17'000 g, 4 °C (Eppendorf Centrifuge 5430R, rotor FA-45-30-11, Eppendorf AG, Hamburg, Germany), to remove most of the insoluble cellular debris and the supernatant was transferred directly into a 35 ml PA Ultracrimp tube (Thermo Fisher Scientific, Waltham, MA, USA) using 1 ml filter tips for iodixanol ultracentrifugation (see 3.10.4).

3.10.3. PEG precipitation

The cleared supernatant from step 3.10.1 (70% V_{tot}) was PEG precipitated overnight at 4 °C by adding 20% V_{tot} 40% PEG 8000 solution (final PEG concentration 8%) and 10% V_{tot} 5 M NaCl solution (final NaCl concentration 0.5 M). The PEG precipitated supernatant was centrifuged the next day for 30 min at 4000 g, 4 °C (Heraeus Megafuge 1.0R, rotor #2704, Heraeus Instruments GmbH, Hanau, Germany) and the supernatant was aspirated completely. The pellet was resuspended in 1.6 ml AAV RB and stored at 4 °C until iodixanol ultracentrifugation together with the supernatant from step 3.10.2 in a PA Ultracrimp tube.

3.10.4. Iodixanol ultracentrifugation

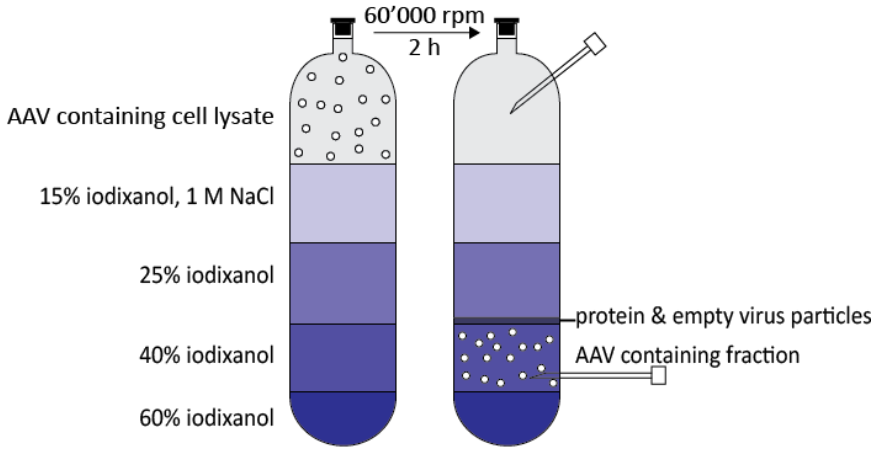

Figure 13: Iodixanol gradient composition before and after ultracentrifugation. A description of the procedure is given in the text.

The cell lysate and PEG precipitate in the PA Ultracrimp tube from steps 3.10.2 and 3.10.3 was underlayed with an increasing iodixanol gradient using a sterile 14-gauge needle starting with 9 ml 15% iodixanol in 1 M NaCl (60% Optiprep™ in PBS pH 7.4, 1 mM $MgCl_2$ • 6 H_2O, 2.5 mM KCl, 1 M NaCl), which was then underlayed by 9 ml of 25% iodixanol (60% Optiprep™ in PBS pH 7.4, 1 mM $MgCl_2$ • 6 H_2O, 2.5 mM KCl), followed by 8 ml 40% iodixanol and finally with 4 ml 60% iodixanol (60% Optiprep™ undiluted in ddH_2O) (Figure 13). If necessary, the tube was filled up with 1 M NaCl pH 8.5 to 1 mm bellow the inserted plug. The plug was inserted, the PA Ultracrimp tube sealed with a cap and centrifuged for 2 h at 60'000 rpm (366000 g), 15 °C (Sorvall WX 80 Ultra Centrifuge, T-865 fixed angle titanium rotor). After centrifugation, the tube was carefully removed from the rotor avoiding dispersing the gradient and was fixed in a tube holder on the sterile bench. The AAV containing 40% iodixanol fraction was collected using a syringe (18 G needle) whereupon vacuum formation and subsequent dispersion of the gradient was prevented by stinging another 18 G needle into the top of the Ultracrimp tube (Figure 13).

3.10.5. Diafiltration

Diafiltration was used to exchange the buffer of the collected AAV containing 40% iodixanol fraction from step 3.10.4. and to concentrate the sample. A Vivaspin® 20 ultrafiltration device (Sartorius/ VWR, MWCO 100'000 Da) was first flushed with 18 ml of PBS-MK (PBS pH 7.4, 1 mM $MgCl_2$ • 6 H_2O, 2.5 mM KCl) for 2 min at 3000 g, 20 °C (Heraeus Megafuge 1.0R, rotor #2704; Heraeus Instruments GmbH, Hanau, Germany) and then loaded with 13 ml of PBS-MK and the collected 6-8 ml 40% iodixanol fraction. The Vivaspin® was alternately centrifuged (3000 g, 20 min, 20 °C) and replenished up to 4 times with PBS-MK to 20 ml so that the retentate at the end was about 2 ml. The viral genome

containing particles were quantified using a Qubit™ 2.0 with the Qubit™ dsDNA HS Assay Kit (Thermo Fischer Scientific, Waltham, MA, USA). The purified AAV in PBS-MK was aliquoted and stored at -80 °C.

3.11. Peptide analysis by LC-MS/MS

All used methods for the peptide analysis by LC-MS/MS are described in detail in the ETH Diss. No. 25663 from Monika Dengler (Dengler, 2019). In brief, recombinant proteins expressed in HEK293T cells, *E. coli* or mouse tissue were, if possible, enriched (His-tag purification see sections 3.8.1 and 3.8.2) and trypsin digested prior to LC-MS/MS measurement. Trypsin digestion was accomplished either using in solution digestion, in-gel digestion or filter aided sample preparation (FASP) digestion of the protein samples. Peptide samples still containing high salt amounts (e.g. in solution digestion of inclusion bodies) were desalted by solid phase extraction (SPE) prior to injection into the LC-MS/MS system. After first unsatisfactory trials on our in-house QTrap 4000 MS system (Sciex, Concord, Ontario, Canada), peptide samples were analyzed in full extend using a TripleTOF 6600 HRMS (Sciex) operated in sequential window acquisition of all theoretical spectra (SWATH) MS/MS (high-resolution mode).

3.12. Fluorometric assay for the analysis of trypsin performance

Unspecific cleavage or inactivity of the used trypsin was checked using a Foerster resonance energy transfer (FRET)-based assay established in our group. The detailed method can be found in the ETH Diss. No. 25663 from Monika Dengler (Dengler, 2019). In brief, two fusion proteins of the FRET-pair Ruby and Cerulean differing in their polypeptide linkers, one including the trypsin restriction site and one not, were digested by the tested trypsin and FRETing was monitored in a fluorescence reader (Tecan Infinite 200 Pro; Tecan Group, ZH, Switzerland).

3.13. *In vitro* trapping

The detailed methods including the MS settings can be found in the ETH Diss. No. 25663 from Monika Dengler (Dengler, 2019). In brief, either purified trapping mEH or sEH expressed in *E. coli* or HEK293T cells transiently transfected with the trapping EHs (pAM-CAG vector constructs) were incubated with 5 µM of the respective EET (11,12-EET for mEH, 14,15-EET for sEH). Subsequently, the proteins were in-gel digested with trypsin and analyzed using SWATH MS/MS on the TripleTOF 6600 MS. Data was filtered for the known EH and EET masses (*m/z*).

3.14. Animal experiments

The used mice were C57BL/6J WT and C57BL/6J mEH KO females at the age of 6-11 weeks. CL57BL/6 is an inbred mouse strain whose genetic background is most widely used for genetically modified mice especially in human disease models. They were originally purchased from The Jackson Laboratory (Bar Harbor, ME, USA) and colonies were maintained by the Laboratory Animal Service Center (LASC) of the University of Zurich. C57BL/6J mEH KO is a mouse strain genetically modified on a genetic background of C57BL/6J. They were originally kindly provided by Dr. F. J. Gonzalez, NH Bethesda, MD, USA and colonies were maintained by the LASC of the University of Zurich.
Animals were kept in a 12 h light/ dark cycle and received food ad libitum. All animal experiments were approved by the Swiss cantonal veterinary office (Zurich, license number 005/2016).

3.14.1. *In vivo* trapping

Mice were injected via tail vein (100 µl, 1-4 x 10^{12} vg/ml) and transgene expression was allowed for up to 14 days. Subsequently, mice were euthanized, organs excised and snap frozen at -80 °C for Western blot and LC-MS/MS analysis. Mice used for native tissue section analysis (GFP fluorescence) and for immunohistochemistry (IHC) analysis of tissue sections were transcardially perfused with PBS (pH 7.4) and tissues post-fixed for 2 h with 4% paraformaldehyde (PFA) on ice. Post-fixed tissue was briefly washed with PBS (pH 7.4) and then incubated in 30% sucrose (in PBS, pH 7.4) overnight at 4 °C.

3.14.2. GFP fluorescence in tissue sections

Cryoprotected tissue was cut at 40 µm on a Hyrax S30 sliding microtome (Zeiss, Oberkochen, Germany), transferred to antifreeze solution (50 mM PB, 30% glucose (m/v), 30% ethylene glycol (v/v), 6.7 mM sodium azide, pH 7.4) and stored at -20 °C until further use. Sections were washed three times in PBS with 274 mM NaCl 10 min each and directly mounted on Superfrost Plus glass slides (Thermo Scientific, Zurich, Switzerland) and stored at 4 °C. Tile scans of GFP fluorescence in tissue sections were recorded on a Zeiss Apotome.2 (Zeiss, Oberkochen, Germany).

3.14.3. IHC staining of liver and brain sections

Cryoprotected tissue was cut at 40 µm for free-floating sections on a Hyrax S30 sliding microtome. Sections were transferred to antifreeze solution and stored at -20 °C until further use. Free-floating sections were washed three times in 50% ethanol for 10 min each, then washed twice in PBS with 274 mM NaCl and blocked for 1 h in 0.3% Triton X-100, 10% normal donkey serum (NDS) in PBS with 274 mM NaCl. Sections were incubated overnight with primary antibodies (anti His-tag or anti human mEH, 1:3000) in the NDS blocking solution at 4 °C. Sections were then washed in PBS and subsequently

incubated with secondary antibody cyanine 3 (Cy3) (1:700) and DAPI (1:10'000) in 0.3% Triton X-100, 10% NDS in PBS with 274 mM NaCl for 45 min at RT. Sections were washed three times in PBS 274 mM NaCl 10 min each and directly mounted on Superfrost Plus glass slides and stored at 4 °C. Tile scans of fluorescent tissue sections were recorded on a Zeiss Apotome.2.

3.14.4. Rotarod performance test

Mice were placed on the rotarod (IITC, Woodland Hills, CA) with linearly increasing speed (4-40 rpm in 300 s). After two training sessions, the length of time a mouse stays on the rotarod without falling was measured in 5 rotarod sessions per animal. Mice were placed back to their home cage for minimally 10 min in between the different test sessions.

3.15. Fluorescence-based inhibitor assay

The required recombinant enzyme amounts for all fluorescence-based inhibitor assays (FIAs) were identified in preliminary experiments by fluorescent substrate turnovers using different enzyme concentrations. All turnover reactions were run under conditions at which the relation of turnover rate to enzyme concentration and incubation time was linear. All FIAs were done below substrate saturating conditions (approximately 20% enzyme saturation).

Increasing MS-PPOH concentrations in 2 µl DMSO (final concentrations in 200 µl ranging from 0 to 100 µM) and recombinant enzyme (50 ng of human mEH, 50 ng of mouse mEH, 100 ng of rat mEH, 100 ng of human sEH, 100 ng of mouse sEH or 690 ng of rat sEH) were added to 100 µl Tris-buffer (20 mM Tris pH 7.4, 0.1% gelatin). The reaction was started by the addition of 100 µL of the respective substrate in Tris-buffer (final concentration in 200 µl: 1 µM for CMNMGC (Morisseau et al., 2011) or 5 µM for CMNPC (Jones et al., 2005)) and mixed well. The increase in fluorescence (FU) at an excitation wavelength of 330 nm and an emission wavelength of 465 nm was measured every 15 s for 10 min at 30 °C in a fluorescence reader (SpectraMAX GeminiXS microplate fluorescence reader, Molecular Devices, Sunnyvale, CA, USA). All measurements were done in quadruplicates.

3.16. Preparation of S9 fractions

200 mg of tissue (liver, brain, kidney or heart of C57BL/6J WT mice) were homogenized in 1 ml of chilled homogenization buffer (0.1 M potassium phosphate buffer pH 7.4, 0.125 M potassium chloride, 0.25 M sucrose and 1.0 mM EDTA) in a Teflon-glass homogenizer using 8-10 strokes. The homogenate was centrifuged at 600 g for 5 min and subsequently at 9000 g for 20 min at 4 °C (Eppendorf Centrifuge 5430R, rotor FA-45-30-11, Eppendorf AG, Hamburg, Germany). The supernatant, called S9 fraction,

was carefully transferred to a new Eppendorf tube without disturbing the loose pellet. The S9 fractions were aliquoted in the form of pearls formed by freezing droplets in liquid nitrogen and stored at -80 °C.

3.17. AA turnover assay with S9 fraction

Increasing MS-PPOH concentrations in 1.5 µl DMSO (final concentrations in 50 µl ranging from 0 to 300 µM) together with 3 µl of the respective S9 fraction and 1.5 µl AA (100 µM final concentration in 50 µl) were added to 37.7 µl microsomal buffer (0.05 M Tris pH 7.5, 10 mM magnesium chloride, 0.15 M potassium chloride containing 8 mM sodium isocitrate). The reaction was started by the addition of the regenerative system consisting of 5 µl 100 mM NADPH and 1.3 µl of isocitrate dehydrogenase (0.6 U/ml, Type IV from porcine heart). The reaction was incubated for 30 min at 37 °C and subsequently stopped by addition of 100 µl ethyl acetate containing 0.03 ng/µl deuterated analyte mix (5,6-EET d11, 8,9-EET d11, 11,12-EET d11, 14,15-EET d11 and corresponding DHETs d11) and immediate vortexing. Samples were centrifuged at 18'000 g (5 min, 4 °C), the upper, organic phase was collected in a fresh tube and extraction was repeated with another 100 µl of ethyl acetate. The pooled organic phase was dried under an N_2-stream and subsequently reconstituted with 100 µl of 50% (v/v) 20 mM Tris pH 7.4, 50% (v/v) methanol. The product formation (EETs and DHETs) was quantified by LC-MS/MS. Chromatography was performed on an Agilent 1100 system equipped with a Gemini-NX C18 reversed phase column (2 x 150 mm, 5 µm particle size, 110 Å pore size from Phenomenex, Torrance, CA, USA) with a corresponding Opti-Guard® guard column (Optimize Technologies, Inc., Oregon City, OR, USA). The mobile phase consisted of (A) 0.0125% NH_4OH in water and (B) 95% acetonitrile 5% methanol containing 0.0125% NH_4OH. The flow rate was set to 350 µl/min and the injection volume was 40 µl. Analytes were eluted with a three-step linear gradient from 16% B to 26% B in 2 min, 26% B to 36% B in 5 min and 36% B to 95% B in 0.7 min. The column was coupled to a QTrap 4000 hybrid quadrupole linear ion trap mass spectrometer (Sciex, Concord, Ontario, CA) with a Turbo V source and electrospray (ESI) interface. Analytes were recorded using multiple reaction monitoring (MRM) in negative mode (-MRM) using the following source specific parameters: gas 1, nitrogen (50 psi); gas 2, nitrogen (50 psi); ion spray voltage, -3800 V, ion-source temperature, 550 °C; curtain gas, nitrogen (30 psi); and collision gas set to medium. The transitions for each analyte and internal standard used and their individual detection conditions are specified in Table 14. Quantification was done using the deuterated internal standard and a corresponding external standard composed of 25 pg/µl of each analyte. Data analysis was done using MultiQuant Software (Sciex).

Table 14: Technical details of the EET and DHET detection by LC-MS-MS

Analyte	Q1 Mass [Da]	Q3 Mass [Da]	Time [msec]	DP [V]	CE [V]	CXP [V]	EP [V]
8,9-EET	319.2	68.9	50	-70	-30	-1	-10
11,12-EET	319.2	167.1	50	-65	-18	-13	-10
14,15-EET	319.2	218.8	50	-70	-16	-13	-10
8,9-DHET	337.2	126.8	50	-70	-28	-7	-10
11,12-DHET	337.2	166.8	50	-70	-26	-11	-10
14,15-DHET	337.2	206.9	50	-70	-26	-15	-10
8,9-EET d11	330.4	155.0	50	-60	-16	-15	-10
11,12-EET d11	330.4	167.0	50	-55	-20	-11	-10
14,15-EET d11	330.4	219.1	50	-55	-16	-1	-10
8,9-DHET d11	348.2	127.2	50	-85	-32	-1	-10
11,12-DHET d11	348.4	166.7	50	-65	-30	-10	-10
14,15-DHET d11	348.3	207.0	50	-55	-26	-9	-10

Time, dwell time; DP, declustering potential; CE, collision energy; CXP, collision exit potential; EP, entrance potential

4. Results

4.1. Deciphering the (patho)physiologic role of epoxide hydrolases by *ex vivo* cartography of their substrate landscape

4.1.1. Experimental strategy

The main project aimed to find the preferred *in vivo* substrates of six EHs. Point-mutated versions of the EHs, unable to release their substrate after covalent binding, were expressed in mice. The resulting enzyme-substrate complexes were retrieved from mouse tissue and analyzed by LC-MS/MS. The success of this approach is heavily dependent on high transgene expression *in vivo* and a reliable analytical method. Figure 14 shows an overview of the experimental strategy used to express the EH trapping mutants *in vivo* and identify bound substrates by LC-MS/MS. The depicted experimental strategy is explained in detail in the following.

In a first experimental series (Figure 14 left row) high amounts of recombinant WT EHs were produced in form of inclusion bodies as correct folding and functionality were not required to create LC-MS/MS methods on our in-house QTrap 4000 device. For this purpose, the pRSET vector was used and transgene expression was highly induced in BL21-AI *E. coli* by the addition of arabinose. The inclusion bodies were separated by centrifugation, solubilized with urea and digested with trypsin. Subsequently, the resulting tryptic peptide solution was used to optimize the LC-MS/MS methods to detect the unmodified CatNuc peptides in a complex proteolytic digest.

The trapping mutants were produced by site directed mutagenesis PCR of the pRSET constructs (Figure 14 top left). Three different mutants per EH were created. In the trapping mutant used during this work (HQ), the catalytic His (H) was replaced by Gln (Q). The HA trapping mutant constructs, where the catalytic His (H) was replaced with Ala (A), were produced in case the HQ variant would result in expression problems, since Ala has the simplest side chain and therefore a reduced tendency for misfolding. The third mutant DA serves as a negative control. In the DA mutant the CatNuc Asp (D) was replaced with Ala (A) leading to an enzyme incapable to perform the first catalytic step and thus unable to bind its substrate.

A strong mediator of *in vivo* transgene expression was required as the success of the *in vivo* substrate trapping (Figure 14 right row) depends on high trapping mutant expression in target organs of mice. Consequently, AAV was used as a viral vector for transgene delivery as it is well-known for its long-lasting and high transgene expression.

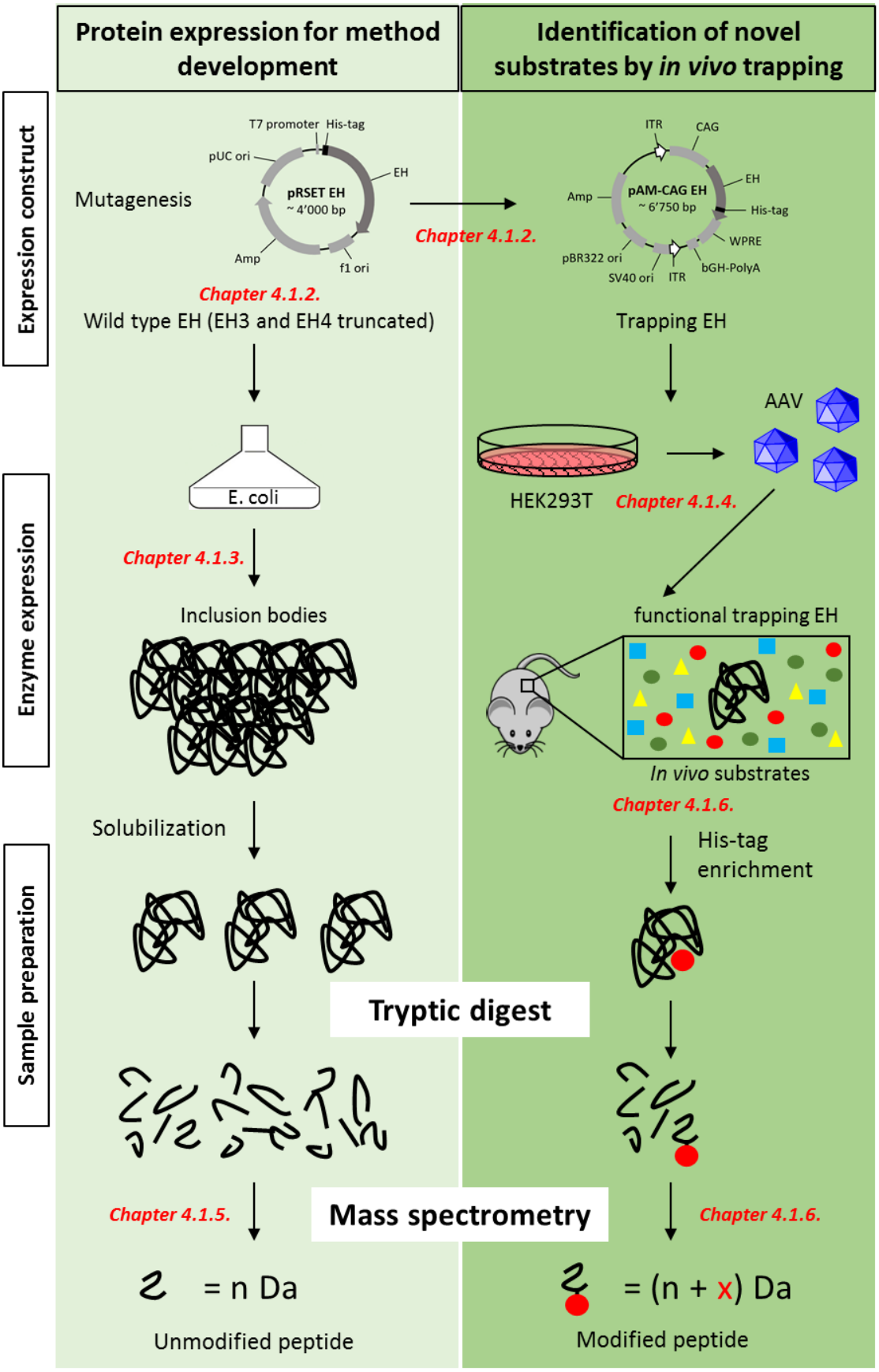

Figure 14: The initial strategy for the *in vivo* substrate trapping. The details are described in the text. The respective chapters of the results are marked in red. Adapted from Monika Dengler ETH Diss. No. 25663 (Dengler, 2019).

Moreover, AAV is non-pathogenic, shows low immunogenicity and can transduce dividing and non-dividing cells (Kaplitt et al., 1994, Lo et al., 1999, Mastakov et al., 2002). The EH variants were introduced into the pAM-CAG vector backbone for the AAV production. The translation efficiency was increased by introduction of a Kozak consensus sequence (GCCGCC), important for translation initiation, upstream of the start codon of the transgene (Kozak, 1984). The reported increase in transgene expression after introduction of a scaffold attachment region (SAR) into the pAM-CAG vector was tested. AAV exists in at least 11 different serotypes determining its tropism. In preliminary tests the most suitable AAV serotype achieving high transgene expression in mouse target organs (liver, brain, lung, kidney, heart) after tail vein injection was selected. Thereby more invasive techniques like direct brain or lung instillation were circumvented.

The EH trapping mutant enzymes expressed in target mouse organs were purified and enriched using His-tag based IMAC, trypsinized and analyzed for the substrate modified CatNuc peptide using LC-MS/MS. The chemical formula of the bound substrate can almost unequivocally be deduced from its exact mass measured by HRMS. Subsequently, the structure can potentially already be determined from the chemical formula or by release of the substrate from the trapping EH and further analysis.

4.1.2. Cloning

sEH, EH3 and EH4 were PCR amplified using the primers in Table 2 leading to amplicons flanked by the restriction sites required for ligation into the plasmid pRSET (detailed information in Table 2). The PCR products and empty pRSET plasmid were digested with the respective restriction endonucleases, ligated, and the sequence was verified by Sanger sequencing.

The primary sequences of EH3 and EH4 predict an N-terminal membrane anchor for both enzymes which may explain their previously observed poor bacterial expression (Decker et al., 2012). To improve the expression in *E. coli*, both enzymes were N-terminally truncated. Therefore, two additional constructs, pRSET EH3k and pRESET EH4k, were constructed which translate to an EH3 protein missing the first 117 amino acids and an EH4 protein missing the first 55 amino acids, respectively.

ThepRSET EH WT constructs were then used to generate trapping mutant (HQ, HA) and negative control (DA) constructs. Site-directed mutagenesis PCR was performed with the primers in Table 3. The sequence of the new constructs was verified by Sanger sequencing.

The primers in Table 4 were then used to ampify and insert the different EH genes into the pAM-CAG vector. Additionally, the Kozak consensus sequence (GCCGCC) was introduced upstream of the start codon of the transgene. At the C-terminus, the primers were used to remove the stop-codon and to insert the gene in frame with the following His-tag. All 24 pAM-CAG EH constructs were verified by

Sanger sequencing. Table 15 summarizes the calculated protein masses obtained with the different constructs. The mass differences are due to amino acids that were added N- or C-terminally due to the cloning strategy.

The respective constructs for mEH, MEST and Cif were cloned by Monika Dengler (Dengler, 2019).

Table 15: Calculated enzyme masses with different expression constructs

Name	pAM-CAG [kDa]	pRSET [kDa]
mEH	54.6	59.7
sEH	64.3	69.3
EH3	42.5	49.4
EH3k	34.2	34.2
EH4	44.0	49.0
EH4k	42.2	42.2
MEST	40.5	46.9
Cif	37.8	43.3

EH3k and EH4k are truncated enzymes lacking the membrane anchor.

4.1.3. Protein expression

For LC-MS/MS method development on our in-house QTrap 4000, high amounts of adequately pure recombinant protein were required, whereas catalytic activity and correct folding of the enzyme was not necessary. To achieve this, all six enzymes were expressed with the pRSET EH WT constructs in *E.coli* overnight at 30 °C[4] with 1 mM arabinose. Under these conditions, most of the recombinant protein aggregated and formed inclusion bodies that could be separated from the soluble protein by centrifugation and resuspended with 8 M urea. Analysis with SDS-PAGE followed by Coomassie staining showed high protein expression for mEH, sEH, Cif and MEST. In order to obtain enough EH3 and EH4 protein, the N-terminally truncated enzymes were expressed with pRSET EH3k and pRSET EH4k resulting in substantial protein amounts (Figure 15). Due to the high specificity of mass spectrometry the other proteins present in the inclusion bodies were of no concern for method development.

[4] Higher expression temperatures unexpectedly reduced inclusion body amounts.

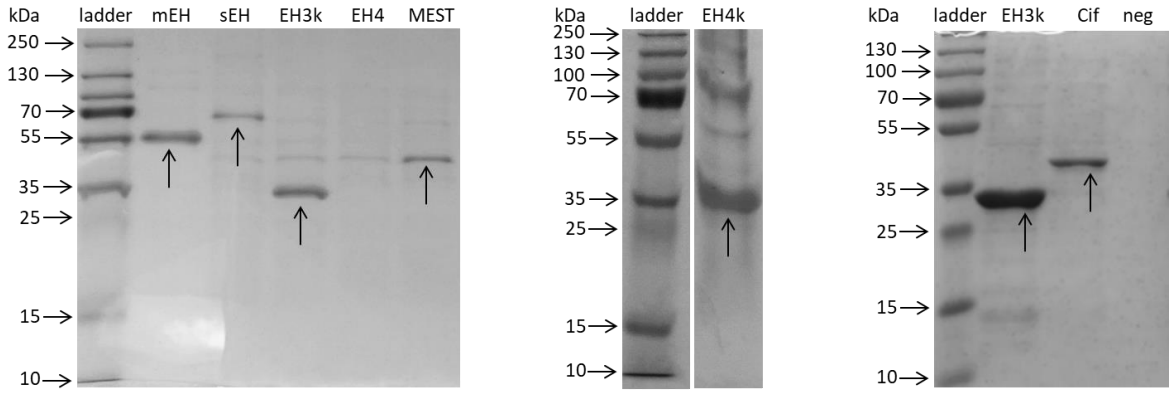

Figure 15: Coomassie stainings of EH inclusion body expression in BL21-AI *E. coli*. The different WT EHs were expressed as inclusion bodies with the pRSET constructs overnight at 30 °C induced with 1 mM arabinose. The inclusion bodies were separated from the soluble protein by centrifugation (4000 g, 15 min, 4 °C) and were analyzed by SDS-PAGE and Coomassie staining. EH3 and EH4 could only be expressed when the membrane anchor was truncated (EH3k and EH4k). Untransfected bacteria were used as negative control. 600 µl bacterial culture equivalent were loaded per lane. Adapted from Monika Dengler ETH Diss. No. 25663 (Dengler, 2019).

4.1.4. Virus production

The *in vivo* trapping approach in mice was based on transgene expression in different target tissues after AAV infection of mice. The following subchapters describe approaches to maximize transgene expression in the target tissue.

The virus production was initially planned to be done ourselves with the help of the Viral Vector Facility (VVF, University Zurich Irchel). Due to problems with the HEK293T cell transfection, this could not be accomplished in time, as we were not able to obtain adequate virus titers of at least 1 x 10^{11} vector genomes per ml (vg/ml). To clarify whether the transfection efficacy in our HEK293T cells was our main issue during AAV production, we received cells already transfected with pAM-CAG GFP/AAV-PHP.B helper plasmid from the Viral Vector Facility for purification. With these AAV-PHP.B GFP expressing cells, we performed the virus enrichment and purification by iodixanol ultracentrifugation and subsequent diafiltration and could successfully reach adequate titers of 5.55 x 10^{12} vg/ml of AAV-PHP.B GFP, confirming that the virus production before had failed due to transfection problems. In consequence, the AAVs used during this work were produced by the Viral Vector Facility.

4.1.4.1. SAR fragment does not increase viral transgene expression

Previous studies showed that inclusion of the SAR of the human interferon beta gene into the expression cassette increased retroviral transgene expression in primary human lymphocytes (Agarwal et al., 1998). To test whether inclusion of SAR into the expression cassette can increase transgene expression, it was inserted in our pAM-CAG construct in either direction, leading to the two new constructs pAM-CAG-SARsense and pAM-CAG-SARantisense which were confirmed by Sanger

sequencing. To evaluate the influence of the SAR on transgene expression, three GFP reporter constructs were produced: pAM-CAG GFP, pAM-CAG-SARsense GFP and pAM-CAG-SARantisense GFP. HEK293T cells in 24-well plates were transfected with the different constructs. After 48 h, GFP fluorescence was analyzed visually and quantified after lysis of the cells in a plate reader. Inclusion of SAR did not increase GFP expression which was in line with the subjective visual analysis (Figure 16). The smaller construct lacking the SAR was used for virus production as the length of DNA that can be packed into viral particles is limited.

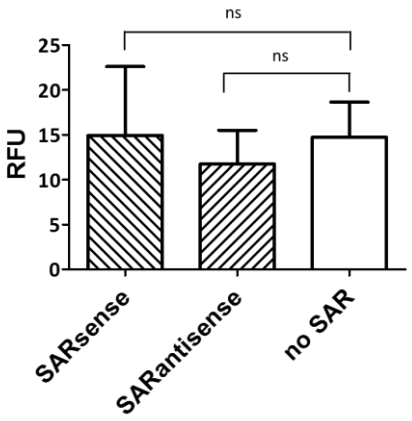

Figure 16: Inclusion of a SAR into the expression construct pAM-CAG GFP did not change transgene expression in HEK293T cells. HEK293T cells transfected with the different GFP encoding constructs were lysed 48 h post-transfection and GFP fluorescence was quantified in a plate reader (excitation wavelength 480 nm, emission wavelength 510 nm). One-way ANOVA revealed no significant difference between the constructs (F (2,6) = 0.3207, p = 0.7374). The error bars show the standard deviation of the separate determinations. n = 3

4.1.4.2. 11 bp deletion in the ITR does not impair virus titer and infectivity

After finishing the construction of all AAV expression constructs, we identified together with the Viral Vector Facility (University of Zurich) an 11 bp deletion within the 3'-ITR present in all our pAM-CAG constructs. The 145 bp long palindromic ITRs build hairpins that frame the genome of the AAV. They form the origin of replication and are required as packaging and integration signals (Mezzina and Merten, 2011). As the only *cis*-acting sequence, they are necessary for high-titer viral vector production (Ojala et al., 2015). The predicted structure (RNA structure prediction tool from CLC Main Workbench 7) of the corrupted ITR showed a shortening of one arm of the hairpin structure but no further changes (Figure 17).

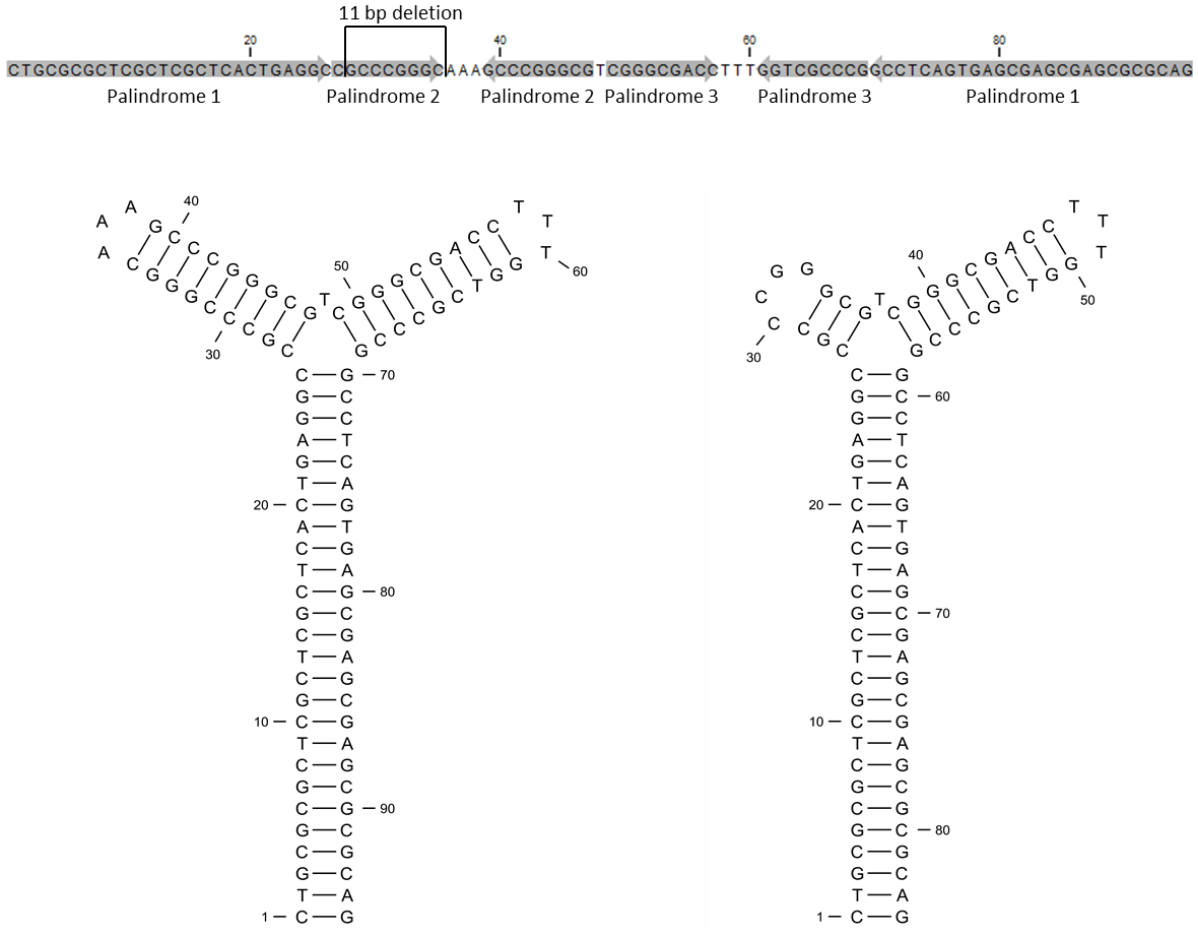

Figure 17: Sequence (top) and predicted structure of the intact ITR (left) and the ITR after an 11 bp deletion (right). Deletion of 11 bp in the 3'-ITR of the pAM-CAG construct is predicted to result in a shortening of one arm of the hairpin structure. Prediction was done with the RNA structure prediction tool from CLC Main Workbench 7.

To investigate whether this deletion affects virus production or virus infectivity, we compared the virus AAV-5 sEHcorr containing the restored ITR with the virus AAV-5 sEHdel with the corrupted ITR. The serotype AAV-5 was chosen as it was available in time and the serotype for the actual experiment had not been elected yet. We chose sEH as transgene because it has the longest sequence of all our EHs and therefore bears the highest risk for packaging problems. To repair the 11 bp deletion, the correct ITR was cut out of the p58 plasmid (kindly provided by J.-C. Paterna) and ligated into the pUC vector containing convenient restriction sites for the following exchange of the corrupted ITR in the pAM-CAG sEH vector. As the 11 bp deletion in the ITR was frequently observed when using TOP10 *E. coli,* all cloning and plasmid preparation was done in the *E. coli* strain MDS42, which was developed to improve integrity of isolated plasmid DNA (Csörgő et al., 2012). The titers of the correct virus AAV-5 sEHcorr and the virus with the deletion AA5 sEHdel were comparable with 5 x 10^{12} vg/ml and 8.5 x 10^{12} vg/ml, respectively. This confirmed that the deletion did not affect virus production. To check for potential infectivity shortcomings due to the deletion, an *in vitro* infectivity assay was performed. To find a

suitable system, SH-SY5Y, HEK293T and U87 cell lines were infected with the reporter virus AAV-5 GFP generously provided by the Viral Vector Facility. Best transgene expression was achieved in U87 glioma cells which was then used for the following infectivity assays. U87 glioma cells were infected with the viruses AAV-5 sEHcorr or AA-5 sEHdel using MOIs (multiplicity of infection) of 100'000 (1 x 10^9 vg/well) and 1'000'000 (1 x 10^{10} vg/well). After incubation for two or three days, cells were harvested and sEH expression was analyzed by Western blot (Figure 18).

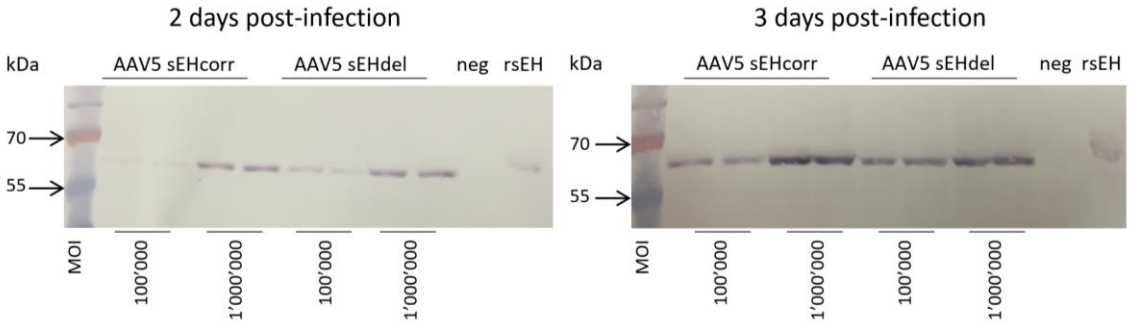

Figure 18: Western blot of sEH expression in U87 glioma cells after infection with an intact AAV-5 virus (AAV-5 sEHcorr) and an AAV-5 missing 11 bp in the ITR sequence (AAV-5 sEHdel). U87 cells were infected with the viruses with different MOIs and analyzed after two or three days by Western blotting using an anti His-tag antibody. Higher MOI and incubation for three days increased sEH expression. No difference was observed between the correct virus and the virus with an 11 bp deletion. neg = negative control, uninfected U87 cells and rsEH = recombinantly expressed sEH. Primary antibody: anti His-tag, secondary antibody: anti rabbit AP

AAV-5 sEHcorr and AAV-5 sEHdel showed comparable transgene expression after two as well as after three days post-infection. The use of higher MOIs and longer incubation time increased sEH expression. The results confirmed that the 11 bp depletion had no effect on infectivity and virus titer, therefore the already produced constructs were used for virus production.

4.1.4.3. Serotypes AAV-rh10 and AAV-PHP.B lead to high transgene expression

Different AAV serotypes are known to infect tissues with variable efficiency. Therefore, we first had to determine which serotypes are suitable for our target tissues. Considering the native expression patterns of EHs, we were mainly interested in liver, brain, kidney, lung, heart, stomach and muscle. To reduce stress for the animals, a virus targeting all organs of interest after tail vein injection was optimal. Serotype AAV-rh10 was the most promising candidate for our organs of interest except for the brain. It was shown to induce significantly higher transgene expression compared to the natural AAV serotypes 1-9 in all mouse tissues of interest except for the brain after tail vein injection in neonatal mice (Hu et al., 2010). The recently developed serotype AAV-PHP.B, which is based on serotype AAV-9, showed high transgene expression in the brain after i.v. application in mice (Deverman et al., 2016). These two serotypes were selected for *in vivo* characterization using GFP as reporter transgene. Five

female C57BL/6J mice per serotype were injected via tail vein (100 µl, 1-4 x 10^{12} vg/ml) and euthanized 1 to 14 days post-injection. Two non-injected mice were sacrificed at day zero as negative controls (experimental time line in Figure 19). GFP expression was analyzed by Western blot and IHC of mouse tissue after perfusion.

Figure 19: Experimental time line. Five mice per virus serotype were injected with 100 µl of the respective virus into the tail vein. On days 1, 3, and 14 post-injection one mouse per serotype and on day 7 two mice were perfused to analyze GFP expression in different tissues. Two mice were not injected to serve as negative controls.

Tissue Western blots of the different time points revealed first GFP expression after 3 days in the liver and after 7 days in the brain and highest expression in both 14 days post-injection (Figure 20 A). The serotype AAV-rh10 induced highest transgene expression in the liver followed by the heart, the stomach and the kidneys. AAV-PHP.B GFP led to GFP expression in the brain, the liver and the heart. There was no GFP expression observed in the Western Blot analysis of muscle and lung tissue (Figure 20 B).

To analyze the cell type selectivity of the virally mediated GFP expression in different organs, tissue sections were analyzed for GFP fluorescence. Both serotypes led to high GFP expression in the liver with the same expression pattern (Figure 21 A and B). Hepatocytes, identified by their characteristic shape, are extensively infected whereas other cells, for example endothelial cells, seem to be spared (Figure 21 B).

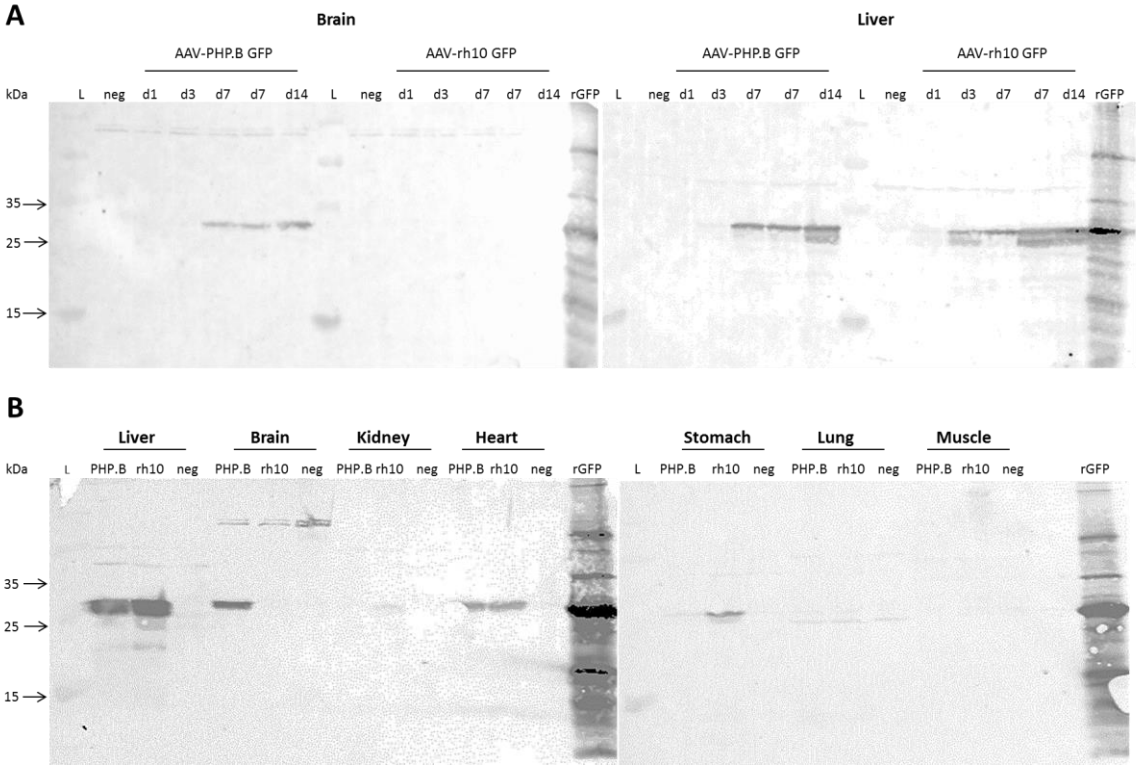

Figure 20: GFP expression in different mouse tissues after tail vein injection of the viruses AAV-rh10 GFP and AAV-PHP.B GFP. 100 µl virus were injected into the tail vein of C57BL/6J mice and GFP expression was analyzed by Western blot using anti-GFP antibody. 400 µg tissue lysate was loaded per lane. rGFP = recombinantly expressed GFP used as positive control, neg = tissue from uninfected mice as negative control. (A) Analysis of liver and brain tissue, the organs with highest expression, at all time points. (B) Analysis of all organs from animals perfused after 14 days. Primary antibody: anti GFP, secondary antibody: Odyssey 680.

Infection with AAV-PHP.B mediated GFP expression throughout the whole brain with particularly high and reproducible expression in the CA2 region of the hippocampus (Figure 21 C and E). Judging from the shape of the GFP positive cells, the virus mainly targeted neurons (Figure 21 D, E, G) but also labelled astrocytes were found (Figure 21 F). A more detailed analysis would require co-staining with cell type specific markers. However, the ratio of gain of information to effort is small and we decided to omit these experiments. Due to substantial native fluorescence in kidney and heart tissue, GFP fluorescence was not visible (data not shown).

Based on these findings, serotype AAV-PHP.B was used to target the brain and serotype AAV-rh10 was used to target the liver and other peripheral organs. Animals were scheduled for euthanasia 14 days post-injection to take out liver, brain, heart, kidney, lung, stomach and muscle because at that time point the highest signal was observed.

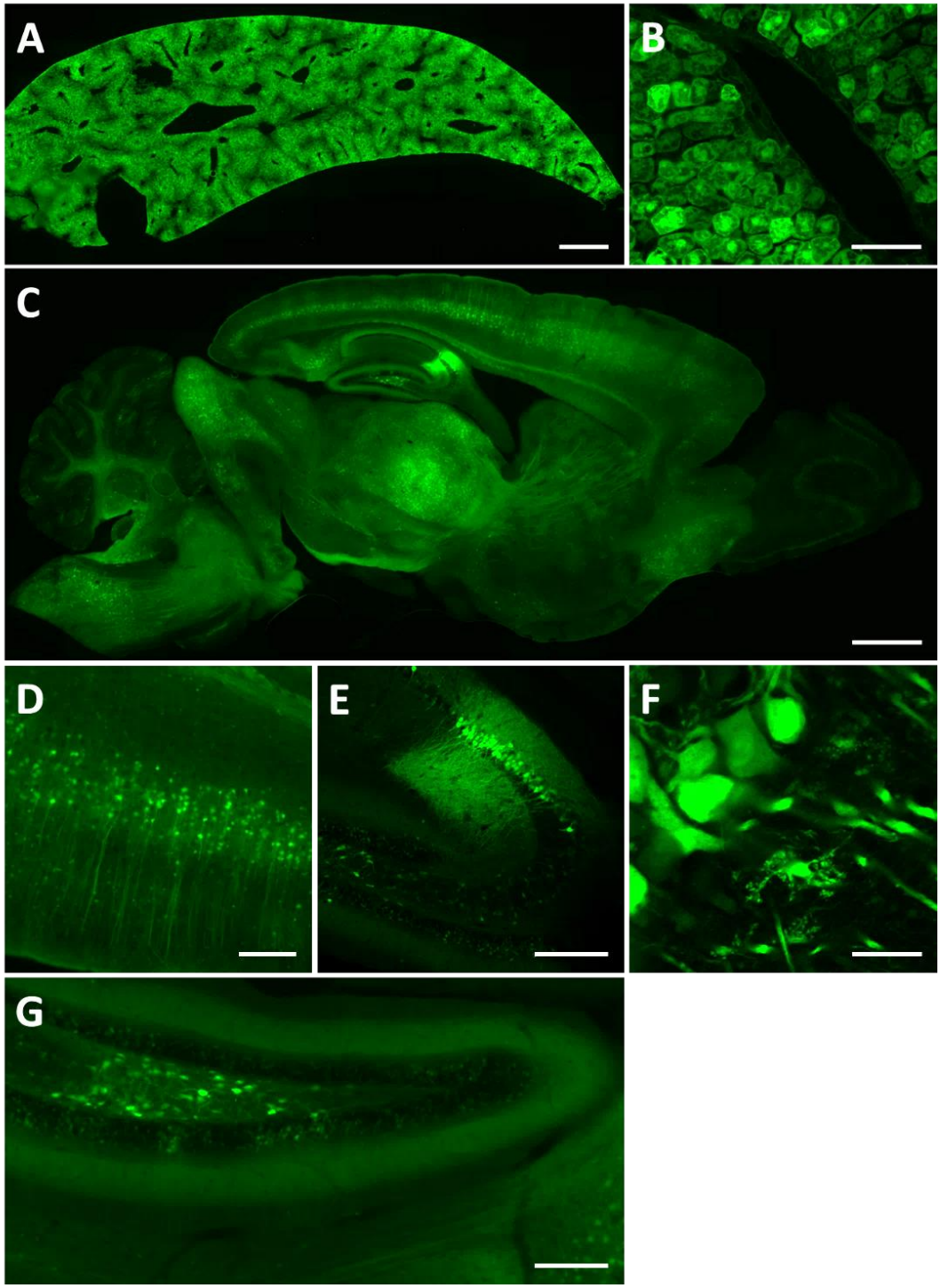

Figure 21: GFP expression in brain and liver slices after AAV PHP.B GFP tail vein injection. Liver and brain of mice perfused 14 days post-injection were sliced and GFP fluorescence revealed GFP expression. (A) Representative image shows homogenous GFP expression throughout the whole liver. (B) Representative liver cross section through a vessel or duct indicates expression mainly in hepatocytes. (C) Representative image of a whole brain section reveals variable GFP expression throughout the brain. Representative images of (D) cortex, (E, F) CA2 region of the hippocampus and (G) dentate gyrus indicate GFP expression mainly in neurons. Scale bar: A, C = 1 mm, B = 50 µm, D, E, G = 200 µm and F = 20 µm.

4.1.5. LC-MS/MS method development and characterization

First LC-MS/MS methods for the unmodified EH3, MEST and Cif CatNuc peptides could be developed on our in-house QTrap 4000 device. This was achieved with high amounts of recombinantly expressed trapping mutant EHs in form of inclusion bodies digested by trypsin. Subsequently, missing methods for tryptic mEH, sEH and EH4 CatNuc peptides were developed and the existing EH3, MEST and Cif methods were optimized with commercially available, pure synthetic peptides (synthetic peptide information see Table 7).

Method development was challenging as we were not mainly interested in the detection of the unmodified CatNuc peptides but in detecting them modified with a potentially unknown substrate. The fragmentation pattern and the parent ion mass (*m/z)* of the unmodified CatNuc peptides are predictable from the respective peptide sequence. However, the CatNuc peptides modified with an unknown substrate are likely to have another retention time and will definitively have an unknown parent ion mass (*m/z*). They can only be identified by their MS/MS fragmentation patterns as the key fragments stay the same. Thus, we required a method where the detection was triggered based on a fragment and not based on the parent ion mass. This, however, failed on the QTrap 4000 and we decided to analyze our samples with a TripleTOF 6600 (HRMS) of our collaborators (Institute of Forensic Medicine, University of Zurich, Zurich, Switzerland). Intense method development on the TripleTOF device operated in SWATH mode was not required as all parent ions and resulting fragments are detected. An LC program able to separate the six synthetic CatNuc peptides was developed and precision, linearity and detection limits of the method were characterized with the synthetic CatNuc peptides. The MEST CatNuc was the best detectable peptide with a detection limit of 3 ng. The other CatNuc peptides had a detection limit of 11 ng on the TripleTOF 6600.

More detailed information and data of the LC-MS/MS method development and characterization can be found in the ETH Diss. No. 25663 of Monika Dengler (Dengler, 2019).

4.1.6. *In vivo* substrate trapping in female C57BL/6J mice

To trap relevant *in vivo* substrates, the trapping EHs needed to be expressed in the same tissue as their native counterparts. As observed in section 4.1.4.3., the serotype AAV-rh10 led to transgene expression in peripheral organs including liver, heart, stomach, and kidneys and AAV-PHP.B primarily showed expression in brain, liver, and heart. For the EHs which are known to be expressed in the brain (mEH, sEH, EH4, and MEST) both serotypes were produced. In case of Cif and EH3, only serotype AAV-rh10 was produced. Mice were injected via tail vein (100 µl, 1-4 x 10^{12} vg/ml) and transgene expression was allowed for 14 days which had been determined as appropriate expression period (4.1.4.3.). C57BL/6J WT mice infected with AAV-PHP.B mEH HQ had to be euthanized preterm because

they developed severe trembling (4.1.8). An overview of the performed animal experiments is shown in Table 16.

Table 16: Summary of AAV injections in mice

AAVs	Exp. 1	Exp.2	Exp. 3	Exp. 4	Exp. 5	Total mice per virus
AAV-PHP.B sEH HQ	2		5			7
AAV-rh10 sEH HQ			4			4
AAV-PHP.B mEH HQ	2	3		1	2+2*	8+2*
AAV-rh10 mEH HQ		2				2
AAV-PHP.B mEH WT					1+2*	1+2*
AAV-rh10 EH3 HQ	2		3			5
AAV-PHP.B EH4 HQ	2	4				6
AAV-PHP.B MEST HQ	2	4				6
AAV-rh10 Cif HQ	2					2
Total mice per exp.	**12**	**13**	**12**	**1**	**7**	***41+4****

Female C57BL/6J WT mice except 4 animals (*) C57BL/6J mEH KO

4.1.6.1. Western blot analysis confirmed successful transgene expression

Transgene expression 14 days post-infection was visualized by Western blot. The GFP virus infections in section 4.1.4.3. showed highest transgene expression for both serotypes in liver tissue and for AAV-PHP.B in brain, thus we decided to first focus on the analysis of liver and brain tissue of infected mice.

The Western blot of homogenized liver samples revealed highest expression of sEH HQ for both serotypes, followed by mEH HQ and only weak expression of MEST HQ with the AAV-PHP.B virus (Figure 22). EH3 HQ, EH4 HQ and Cif HQ (Cif data not shown) were not detectable. In the homogenized brain tissues only AAV-PHP.B sEH HQ led to transgene expression visible in the Western blot. Therefore, LC-MS/MS analysis was first focused on liver samples with mEH HQ, sEH HQ and MEST HQ expression. MEST was also chosen due to the good LC-MS/MS detection properties for its CatNuc peptide (Dengler, 2019).

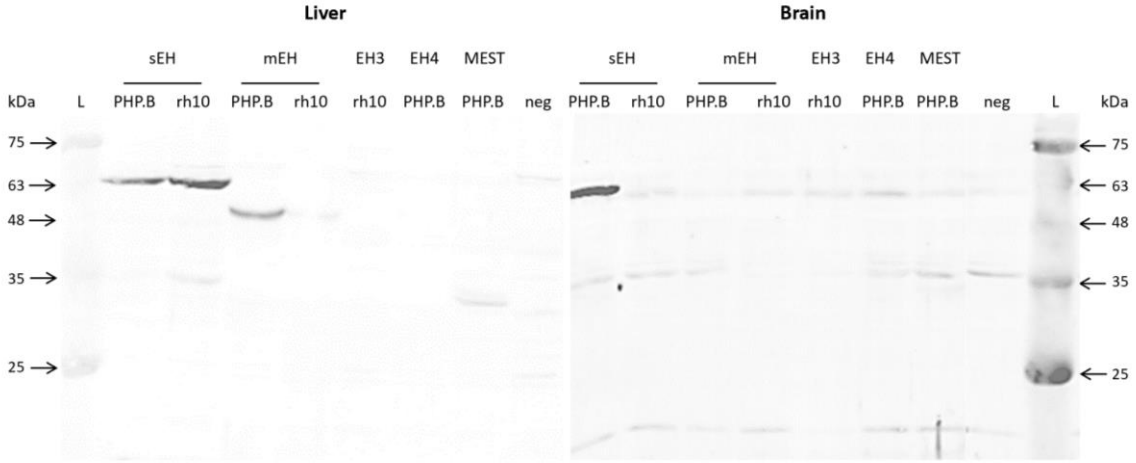

Figure 22: Transgene expression in liver and brain of mice 14 days after i.v. virus injection. Western blot analysis of 400 µg tissue revealed high expression of sEH and mEH in liver (both serotypes) and brain (only with AAV-PHP.B). A weak signal was observed in the liver of animals injected with AAV-PHP.B MEST HQ. Primary antibody: anti His-Tag, secondary antibody: Odyssey 680.

As all virally expressed EHs carry a C-terminal His-tag, an anti His-tag antibody was used for detection. However, quantification was difficult as His-tag detection varied between different proteins. Furthermore, it is possible that the His-tag was cleaved off after translation making it impossible to detect. The well characterized mEH and sEH antibodies of our group could not be used to detect our virally expressed EHs due to lack of species specificity. The signal of the natural mouse EH predominated the signal of the trapping EH. Other His-tag antibodies and Ni-NTA conjugates that bind the His-tag were tested without success. From multiple Western blots, the recombinant EH amount expressed in liver tissue was semi-quantitatively estimated to 50-100 ng/mg tissue for sEH HQ and 25-50 ng/mg tissue for mEH HQ. The detection limit of the TripleTOF 6600 method for both CatNuc peptides was 11 ng which corresponds to approximately 200 ng of protein. Assuming efficient sample preparation, the analysis of 4-8 mg tissue should be sufficient to detect the modified CatNuc peptides of mEH HQ and sEH HQ. To digest and analyze higher amounts of tissue via in-gel digest, the sample was loaded on multiple lanes of the gel and the excised gel pieces were combined. However, the analysis of up to 8 mg of sEH HQ expressing liver tissue was not successful. To increase the amount of trapping EH available for digestion, the tissue samples were enriched using IMAC. After enrichment of up to 400 mg liver or brain tissue, the expression of all trapping mutants could be confirmed by Western blot, except for EH3 (wrong size compared to control) in liver and MEST in brain tissue (Figure 23).

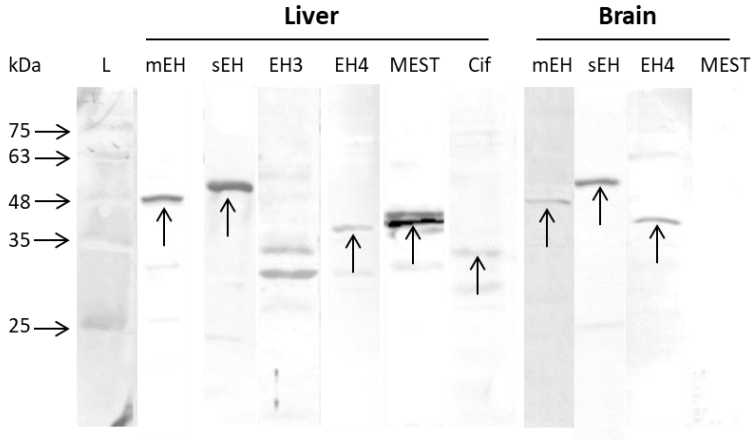

Figure 23: Western blot analysis of liver and brain samples enriched by His-tag purification. Approximately 400 mg liver or brain tissue from mice infected with either AAV-PHP.B (mEH HQ, sEH HQ, EH4 HQ and MEST HQ) or AAV-rh10 (EH3 and Cif) were manually His-tag enriched using a 1 ml HisTrap FF column. Peak fractions were analyzed by Western blot. Primary antibody: anti His-Tag, secondary antibody: Odyssey 800.

The Coomassie stained SDS-PAGE gel of sEH HQ and mEH HQ showed an additional band of expected size (arrows Figure 24), which is not visible in the negative control, indicating that this corresponds to the trapping EHs. With the assumption that these bands represent 1 µg sEH and 0.5 µg mEH (derived from the marker bands which represent 0.5-1 µg peptide), an initial tissue concentration prior enrichment of 100-200 ng/mg tissue sEH HQ and 50-100 ng/mg tissue mEH HQ was calculated, in line with the conclusions drawn from the previous Western blot. The expression of the other EHs in the analyzed tissue was lower. Estimated through comparison with mEH and sEH expression, MEST HQ expression lies in the range of 1-5 ng/mg liver tissue and EH4 HQ and Cif HQ expression in the range of 0.1-0.5 ng/mg liver or brain tissue.

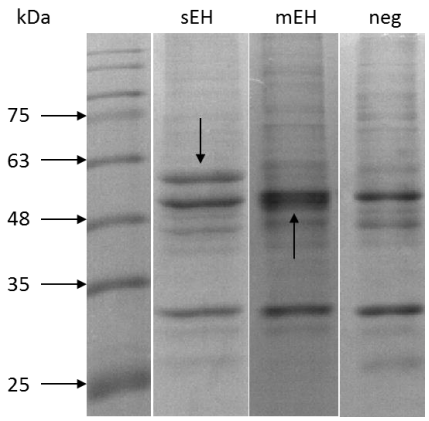

Figure 24: Coomassie stained SDS-PAGE gel of liver samples enriched by His-tag purification. 200-500 mg liver tissue from mice infected with AAV-rh10 (sEH, mEH and EH4) were manually His-tag enriched using a 1 ml HisTrap FF column. For mEH and sEH, bands of the expected size (arrow) are visible that are absent in the negative control.

4.1.6.2. IHC analysis of transgene expression in liver and brain

To characterize the AAV mediated transgene expression of the trapping EHs on a cellular level in liver and brain, tissue sections of mEH KO mice infected with AAV-PHP.B mEH HQ were stained for human mEH.

According to the cell shape, the human mEH HQ expression in liver was primarily prominent in hepatocytes, while other cell types seem to be spared (Figure 25 A). There was a clear discrimination between the infected mouse liver slice and the identically stained, uninfected liver slice. Although there was a slight mEH signal in the uninfected liver (Figure 25 B), no specific staining of single cells was visible, indicating unspecific staining of the first antibody, confirmed by Figure 25 C, where the background signal could be eradicated by skipping the first antibody.

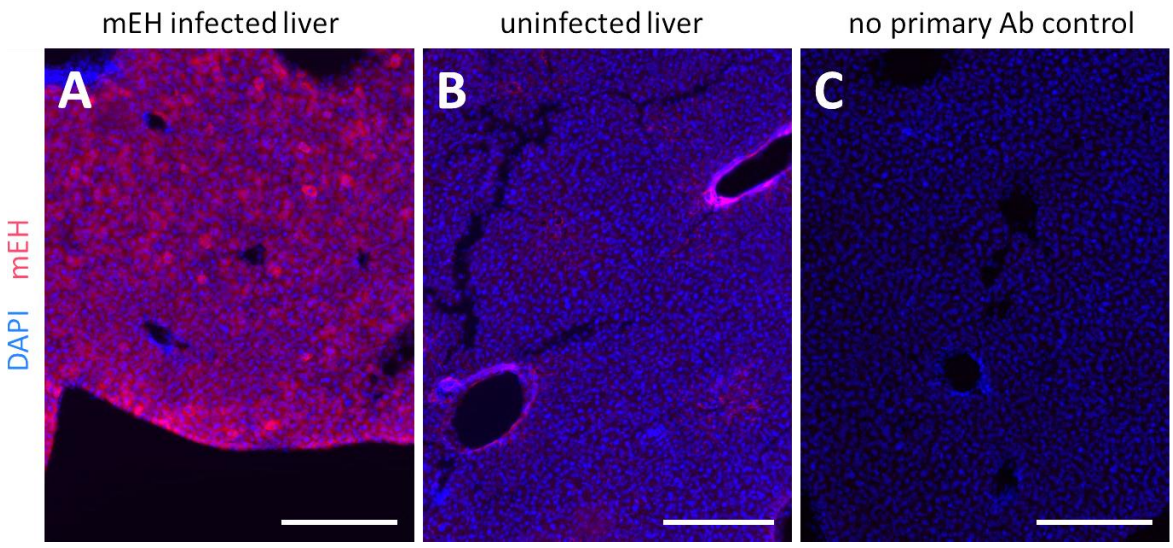

Figure 25: Virus-mediated expression of mEH HQ in the liver. Immunostainings on liver slices of (A) mEH KO mice infected with AAV-PHP.B mEH HQ and (B) uninfected mEH KO mice reveal mEH HQ expression throughout the liver. (C) represents a control where no primary antibody was applied. Mice were euthanized 14 days post-injection and liver slices were stained using a primary anti human mEH antibody. Scale bar 20 µm

The virus-mediated transgene expression throughout the whole brain, clearly marking single cells (Figure 26 A-C) compared to the uninfected brain tissue, which only showed unspecific background staining (Figure 26 E-G). According to their shape, the main cell type infected by AAV-PHP.B mEH HQ were neurons (Figure 26 B-D), with the same specific expression pattern in the CA2 region of the hippocampus (Figure 26 C) observed before with the GFP reporter virus (Figure 21 C, E). To draw a conclusion on exact cell types, co-stainings with specific markers would be required.

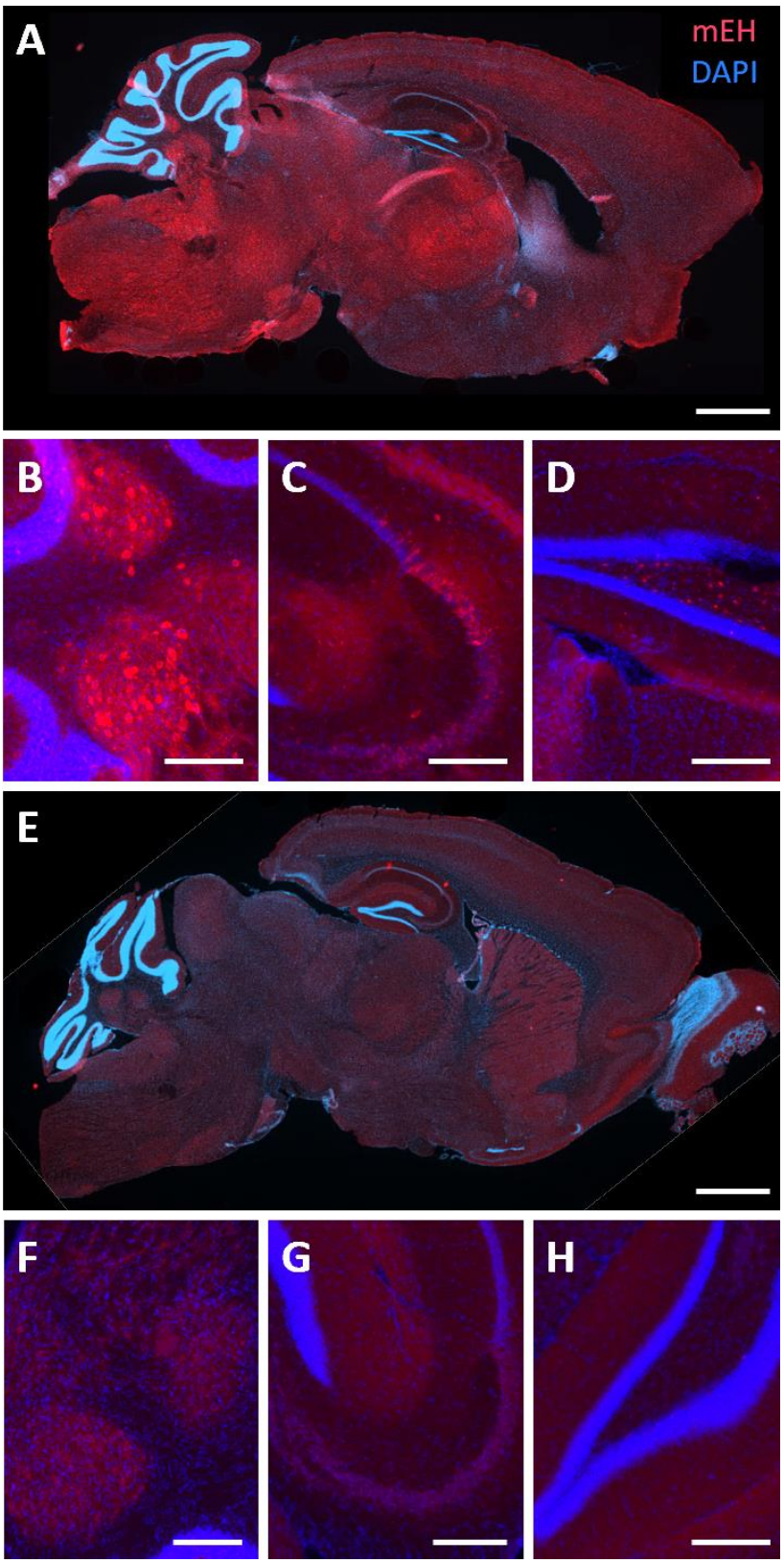

Figure 26: AAV-mediated expression of mEH HQ in the brain. Immunostaining on brain sections of (A-D) mEH KO mice infected with AAV-PHP.B mEH HQ and (E-H) uninfected mEH KO mice reveal mEH HQ expression throughout the brain. (B) shows expression in the cerebellum, (C) shows expression in hippocampus, (D) shows expression in dentate gyrus. Mice were euthanized 14 days post-injection and brain sections were stained using an anti-human mEH antibody. Scale bar: 200 µm except A and E: 1 mm

4.1.6.3. MS analysis of trapped substrates

The sample preparation for LC-MS/MS analysis of trapped substrates was done by FASP after His-tag enrichment and purification (IMAC) of the trapping EHs expressed in mouse tissues.

In a first set of LC-MS/MS measurements the presence of mEH HQ, sEH HQ, MEST HQ and Cif HQ could be confirmed by the detection of 2 to 8 protein specific peptides (Table 17). It was primarily checked for peptides present in trypsin-based peptide libraries (PeptideAtlas) and thus only for a subset of peptides per EH. The CatNuc peptide, however, could only be detected in an unmodified form for mEH HQ and MEST HQ. According to the detection limit for the sEH HQ CatNuc peptide of 11 ng and the approximate amount of 250 ng injected into the MS it remains unclear why it could not be detected in any form (unmodified, modified). EH3 HQ, EH4 HQ and the CatNuc peptide of Cif HQ could not be detected at all, but this goes in line with very low tissue expression (4.1.6.1) and the comparably high detection limit of 11 ng. More detailed Information and the corresponding calculations can be found in the ETH Diss. No. 25663 of Monika Dengler (Dengler, 2019).

Table 17: Detected peptides of the trapping EHs in mouse liver or brain

Trapping EH	Detected peptides	CatNuc peptide	Mouse organ
mEH	8	yes	liver, brain
sEH	6	no	liver, brain
EH3	-	-	liver
EH4	-	-	brain
MEST	2	yes	liver
Cif	2	no	liver

The subsequent search for substrate modified CatNuc peptides remained unsuccessful. One example of the mEH HQ CatNuc peptide is further elaborated on in the ETH Diss. No. 25663 of Monika Dengler (Dengler, 2019).

4.1.7. Trouble shooting

The *in vivo* substrate trapping emerged to be challenging. Especially the LC-MS/MS based analysis for trapped substrates was unsuccessful. In case of sEH HQ even amounts 20 times above the detection limit of the TripleTOF 6600 method did not result in the detection of the CatNuc peptide. An underlying cause could probably be that the peptide was selectively lost during sample preparation. Furthermore, the CatNuc peptides of MEST HQ and mEH HQ could only be detected in the unmodified form. This raises the question if they are only partially modified or even misfolded and unable to trap their substrates.

Because of the aforementioned reasons, intense trouble shooting was performed. The LC-MS/MS sample preparation was analyzed step by step to guarantee efficient production and recovery of the trapping EH CatNuc peptides. The trapping mutant EHs were also recombinantly expressed in HEK293T cells and in *E. coli* and analyzed with the TripleTOF 6600 to gain experience with complex samples. As a proof of principle and functionality of the used trapping mutants mEH HQ, sEH HQ and Cif HQ *in vitro* trapping experiments were performed, as they can be expressed as active proteins and some of their substrates are known and available.

The results of the different trouble shooting experiments are described in the following subchapters.

4.1.7.1. Tissue sample preparation optimization

Detailed information and data of the trouble shooting done on the optimization of tissue sample preparation can be found in the ETH Diss. No. 25663 of Monika Dengler (Dengler, 2019). The most important findings are summarized in the following.

The functionality and specificity of the used trypsin could be demonstrated with a Foerster resonance energy transfer (FRET)-based assay developed in our group.

In another set of experiments, the LC-MS/MS sample preparation techniques in-gel digestion and FASP digestion were compared in processing MEST HQ infected mouse liver tissue. The slightly better outcome in the LC-MS/MS analysis after FASP digestion resulted in short-term faveolization of FASP digestion for mouse tissue sample preparation.

In a third experiment it was checked for peptide loss after every step in FASP sample preparation using the synthetic CatNuc peptides of interest. Whereas the CatNuc peptides of Cif and MEST could be recovered in high amounts after every step, the ones of mEH, sEH, EH3 and EH4 were selectively lost already after the first evaporation step. Different measures like coating tubes and filters with 5% TWEEN, eluting the filter with ACN or under acidic conditions did not increase the recovery of sEH, EH3 and EH4 CatNuc peptides. The recovery of the mEH CatNuc peptide could be highly increased after 5% TWEEN coating, but surprisingly it was the only peptide susceptible to trypsin digestion. Based on these results future tissue samples were processed by in-gel trypsin digestion.

4.1.7.2. Expression of functional EHs in HEK293T cells

To gain experience and optimize the LC-MS/MS analysis of our tissue samples, trapping and WT EHs were expressed in HEK293T cells to obtain a comparably complex matrix. The recombinant expression of trapping EHs in HEK293T cells was also used for *in vitro* trappings with known substrates (4.1.7.4). The Western blot analysis showed successful expression of all WT and HQ trapping EHs except EH3 (Figure 27, EH3 data not shown). It has been shown before that the recombinant expression of EH3 is

difficult and was only successful after removal of the N-terminal membrane anchor or by baculovirus-mediated expression in insect cells (Decker et al., 2012).

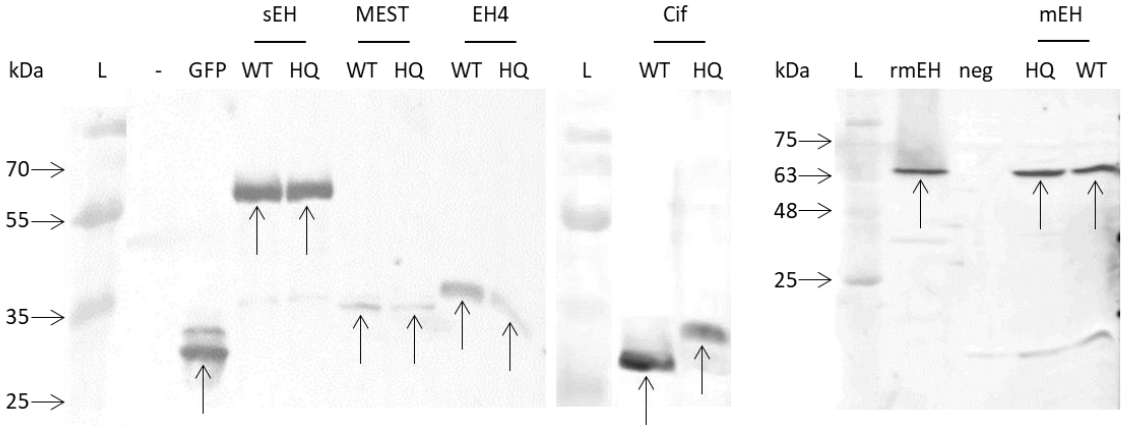

Figure 27: Expression of WT and HQ trapping EHs in HEK293T cells. Western blot analysis of lysed HEK293T cells. A 10 cm dish of transfected HEK293T cells was resuspended in 1 ml PBS and 6 µl of the cell suspension loaded per lane, followed by SDS-PAGE. Primary antibody: anti His-tag, secondary antibody: Odyssey 680.

Surprisingly, expression of the HQ variants of EH4 and MEST is weaker compared to their WT versions, indicating that the point mutation reduces expression efficiency or triggers proteolytic degradation. In the case of Cif, the HQ variant shows an increased size.

4.1.7.3. Cloning, expression and purification of active EHs in *E. coli*

To express functional trapping and WT EHs, the respective genes were inserted into the low copy number pET vector where transgene expression can be gradually induced by arabinose. By using low arabinose concentrations, expression of correctly folded, active enzyme that otherwise tends to inclusion body formation is possible. The vector contains a C-terminal His-tag which allows efficient protein enrichment/purification by IMAC.

The expression of WT and HQ trapping variants of mEH, sEH and Cif was performed in *E. coli* BL21-AI overnight with 10 µM arabinose at RT. Purification of the His-tagged proteins by IMAC on an ÄKTA setup was monitored by SDS-PAGE. Figure 28 shows representative Coomassie stainings of a sEH WT and a mEH HQ purification. The expression of active Cif HQ trapping mutant failed. Folding problems led to the formation of inclusion bodies.

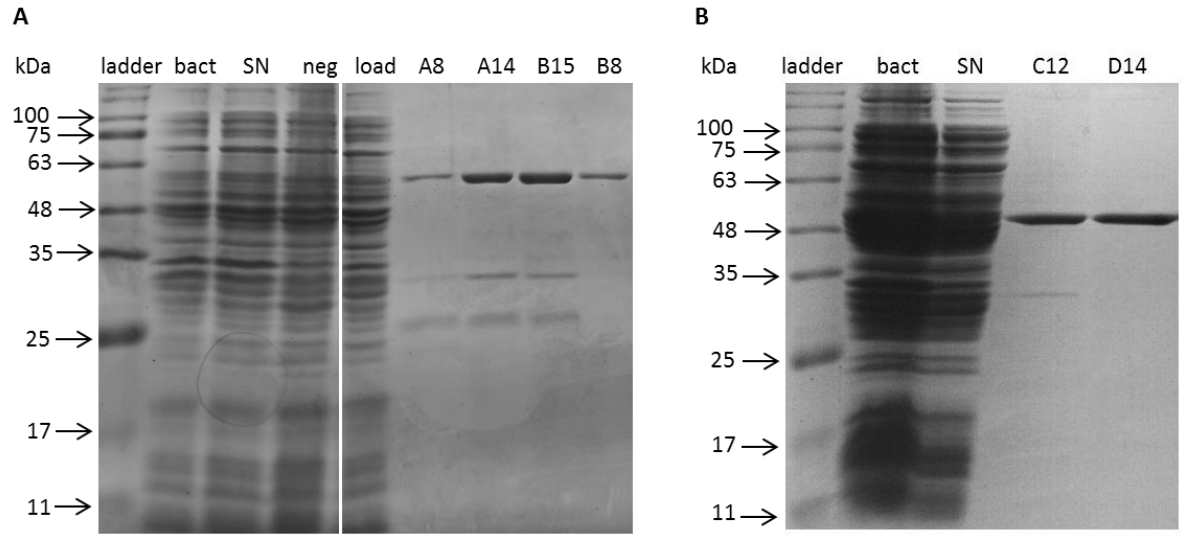

Figure 28: Visualization of purified sEH WT (A, 64 kDa) and mEH HQ (B, 54.5 kDa). Different fractions were collected during the His-tag purification process and analyzed by SDS-PAGE and Coomassie staining. Bact = intact bacteria, SN = supernatant after French press and centrifugation, neg = intact bacteria that were not transformed, load = flow-through collected during loading of the sample, A8-D14 = peak fractions collected during elution of the protein.

The recombinant proteins were obtained with a purity >90% as judged by the impurities visible in the Coomassie stained SDS-PAGE. The impurities are of no concern for further *in vitro* trapping experiments.

4.1.7.4. *In vitro* trapping

The *in vitro* trapping was performed with recombinant trapping mEH and sEH expressed in *E. coli* and with HEK293T cells expressing the trapping mutants after transient transfection. Pure recombinant trapping enzymes were incubated with a known substrate, 11,12-EET for mEH or 14,15-EET for sEH, or cultured HEK293T cells expressing the trapping mutants were incubated with the corresponding substrate. After in-gel trypsin digestion samples were analyzed with LC-MS/MS. The 14,15-EET-modified CatNuc peptide of sEH could be detected with both expression systems, whereas the trapping mEH CatNuc peptide could only be detected in the unmodified form. This goes in line with the *in vivo* substrate trapping for mEH HQ and indicates a potential disability to bind its substrate.
The detailed LC-MS/MS analysis demonstrating these results can be found in the ETH Diss. No. 25663 of Monika Dengler (Dengler, 2019).

4.1.8. Trembling phenotype of AAV-PHP.B mEH HQ infected mice

A total of 8 C57BL/6J WT and 2 C57BL/6J mEH KO female mice were injected with the brain-infecting AAV-PHP.B mEH HQ virus (Table 16). 7 out of the 8 injected WT mice and all mEH KO mice unexpectedly developed a progressing trembling phenotype after 8 days and 12 days, respectively. In particular,

animals showed an insecure, tipsy walk and strong shaking especially of the head while resting and moving. WT mice with trembling onset after 8 days were euthanized preterm around 11 days post-injection, as food and water intake was not guaranteed anymore. Preterm euthanasia of mEH KO mice injected with AAV-PHP.B mEH HQ was not necessary, and mice showed only very mild trembling at the last day of the experiment.

Interestingly this phenotype was only observed when the AAV-PHP.B mEH HQ virus was injected. Control experiments carried out with AAV-PHP.B mEH WT virus and the non-brain-infecting AAV-rh10 mEH HQ (Figure 20) did not elicit any aberrant behavior in the injected mice, pointing to the fact that indeed the trapping variant underlies the observed phenotype. The possibility that contaminations in the AAV-PHP.B mEH HQ virus caused the trembling phenotype was ruled out by purchasing a new virus batch. However, injections with the fresh virus batch showed the same result. The single WT mouse injected with AAV-PHP.B mEH HQ that did not develop the trembling phenotype was studied in more detail for the virus-mediated transgene expression. Interestingly, IHC of brain slices with an anti His-tag antibody revealed that in this particular animal the virus did not lead to any transgenic expression (data not shown); mEH HQ expression was also absent in a liver tissue Western blot (Figure 29).

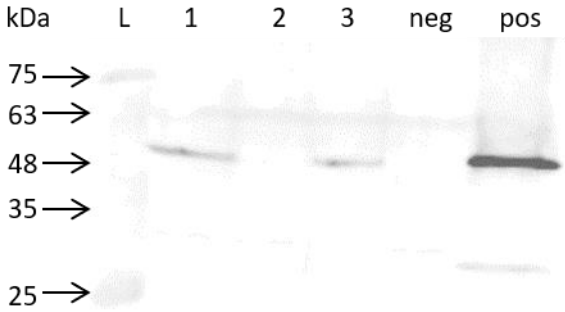

Figure 29: Western blot analysis of liver tissue of the non-trembling mEH HQ mouse. 400 µg liver tissue of two AAV-PHP.B mEH HQ injected trembling mice, the non-trembling AAV-PHP.B mEH HQ injected mouse and a non-injected mouse were loaded per lane. L = ladder, 1 = mEH HQ trembling mouse 1, 2 = mEH HQ non-trembling mouse, 3 = mEH HQ trembling mouse 2, neg = uninfected mouse liver, pos = ca. 20 ng recombinant mEH HQ. Primary antibody: anti His-tag, secondary antibody: Odyssey 800.

To further investigate the trembling phenotype, in a set of preliminary experiments a small number of non-injected control mice and mice injected with AAV-PHP.B mEH WT or AAV-PHP.B mEH HQ were tested for their sensorimotor coordination and motor learning by Monika Dengler. This was addressed by rotarod, where the latency of fall for every animal was recorded. Due to the small sample size no statistical analysis was performed but a clear trend for AAV-PHP.B mEH HQ infected mice performing worse was visible (Figure 30). This suggests that the AAV-PHP.B mEH HQ infected mice suffer from motor impairment. Grip strength was tested by letting the animals cling to the cage grid and pulling

them until they lose grip. No difference was observed between the three groups (subjective analysis). Moreover, no sign of pain was observed (subjective analysis).

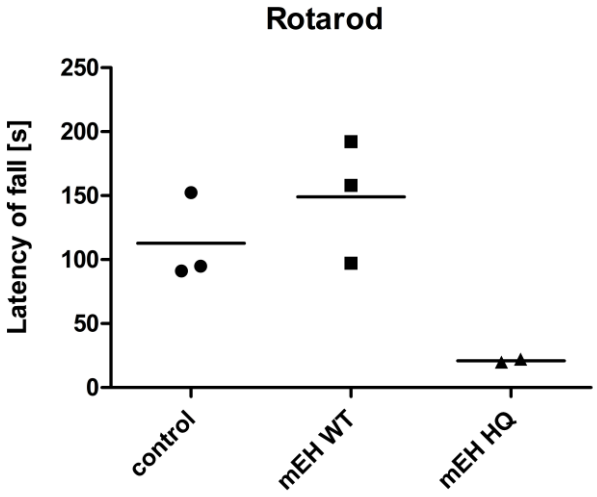

Figure 30: Rotarod performance of non-injected control mice, AAV-PHP.B mEH HQ injected and AAV-PHP.B mEH WT injected mice. Values were recorded 14 days post-injection in 5 trials per animal (C57BL/J6 WT). Mice were trained the day before and in the morning of the trial. The investigator was not blinded during the study. The plotted values represent means of the 5 repeated measurements and horizontal lines indicate means of the group. Because of the small sample size (n < 3) statistical analysis was omitted. Mean ± SEM control: 112.8 +/- 19.8 s, n=3; mEH WT: 149.1 +/- 27.78 s, n=3; mEH HQ: 21.00 +/- 1.2 s, n=2. Reproduced from Monika Dengler ETH Diss. No. 25663 (Dengler, 2019).

The striking trembling phenotype of the AAV-PHP.B mEH HQ infected mice raised the question if brain regions and cells relevant for motor coordination are infected by the virus. Deverman et al. reported significant virus expression in striatum, substantia nigra (SN) and cerebellum (Deverman et al., 2016). Brain slices were obtained from mEH KO mice injected with AAV-PHP.B mEH HQ and AAV-PHP.B mEH WT and stained for human mEH (Figure 31). In accordance with the study of Deverman et al. and our previous results obtained with AAV-PHP.B GFP (Figure 21), virus-mediated mEH HQ and mEH WT expression was indeed observed in the striatum (Figure 31 B, C), in the SN (Figure 31 E, F) and in the cerebellum (data not shown). These results suggest a possible effect of transgene expression on the dopaminergic neurons of the SN and the striatum. Anyway, to identify exact cell types, co-staining with specific markers (e.g. against dopaminergic neurons, TH antibody) is indispensable.

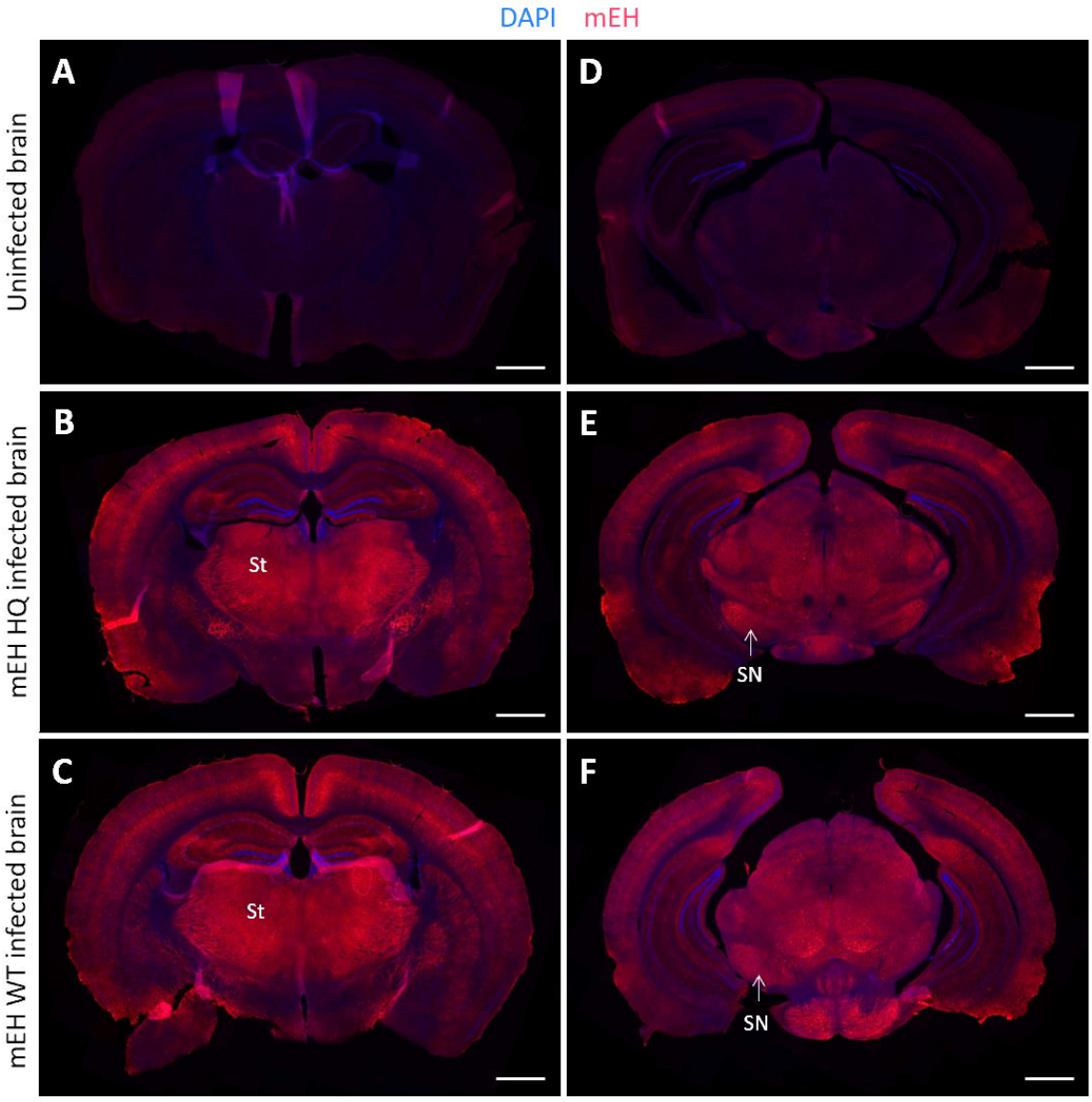

Figure 31: mEH expression in brains of non-injected (A, D), AAV-PHP.B mEH HQ (B, E) and AAV-PHP.B mEH WT (C, F) mEH KO mice. C57BL/6J mEH KO mice were injected with the respective virus and euthanized 14 days post-injection. Brain slices showing striatum (St) (left panel) and slices showing substantia nigra (SN) (right panel) were stained using an anti-human mEH antibody. Scale bar 1 mm

4.2. The CYP blocker MS-PPOH is an inhibitor of sEH

4.2.1. MS-PPOH does not affect mEH but inhibits sEH

In a first series of experiments, the potency of MS-PPOH as an inhibitor of human, mouse and rat mEH was assessed. Unexpectedly, MS-PPOH did not affect mEH activity of any of the three species at any measured concentration (Figure 32 A). A similar analysis was run in a second series of experiments for human, mouse and rat sEH. In these experiments, MS-PPOH displayed substantial inhibition of sEH. The calculated IC_{50} values for all three species are in the nanomolar range (Figure 32 B).

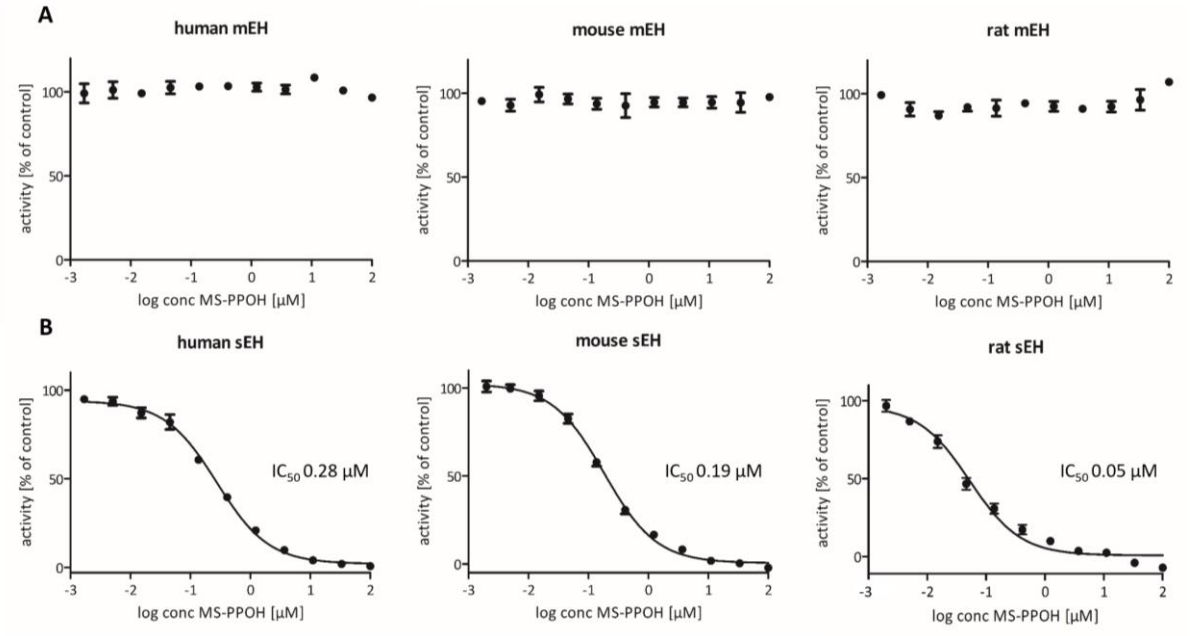

Figure 32: MS-PPOH inhibition curves for human, mouse and rat mEH (A) and sEH (B). Recombinant human, mouse and rat mEH or sEH were incubated with CMNMGC or CMNPC, respectively, in the presence of increasing MS-PPOH concentrations. Enzyme activity is expressed as the percentage of activity measured in the absence of inhibitor. The resulting IC_{50} values are: 0.28 µM (human sEH, $CI_{95\%}$ 0.24 to 0.32 µM); 0.19 µM (mouse sEH, $CI_{95\%}$ 0.16 to 0.21 µM); 0.05 µM (rat sEH, $CI_{95\%}$ 0.04 to 0.07 µM).

As all measurements were done well below enzyme saturation (approximately 20% enzyme saturation) the measured IC_{50} values can be expected to be reasonably close to the Ki values of the enzymes (Decker et al., 2012). As expected from its structure (Figure 7), PPOH did not show any sEH inhibition in a similar series of experiments (Figure 33).

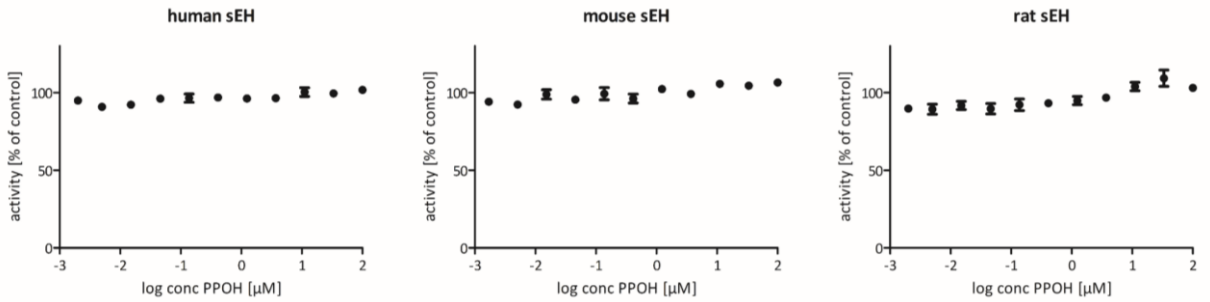

Figure 33: Non-inhibition of human, mouse and rat sEH by PPOH. Recombinant human, mouse and rat sEH was incubated with CMNPC in the presence of increasing PPOH concentrations. Enzyme activity is expressed as the percentage of activity measured in the absence of inhibitor. No sEH inhibition by PPOH was detected.

4.2.2. MS-PPOH treatment increases EET levels after AA turnover in tissue homogenates

To test the inhibitory capacity of MS-PPOH in a system which combines CYP and EH activities and therefore more closely resembles the conditions *in vivo*, an AA-turnover assays using S9 fractions (supernatant of tissue lysates after centrifugation at 9000 g) obtained from different mouse organs was performed. The S9 fraction contains both microsomal and cytosolic proteins, thus harboring CYPs, mEH and sEH. S9 fractions from mouse liver, brain, kidney and heart were incubated with AA and increasing MS-PPOH concentrations and the formation of 8,9-, 11,12- and 14,15-EET and their corresponding DHETs was measured by LC-MS/MS.

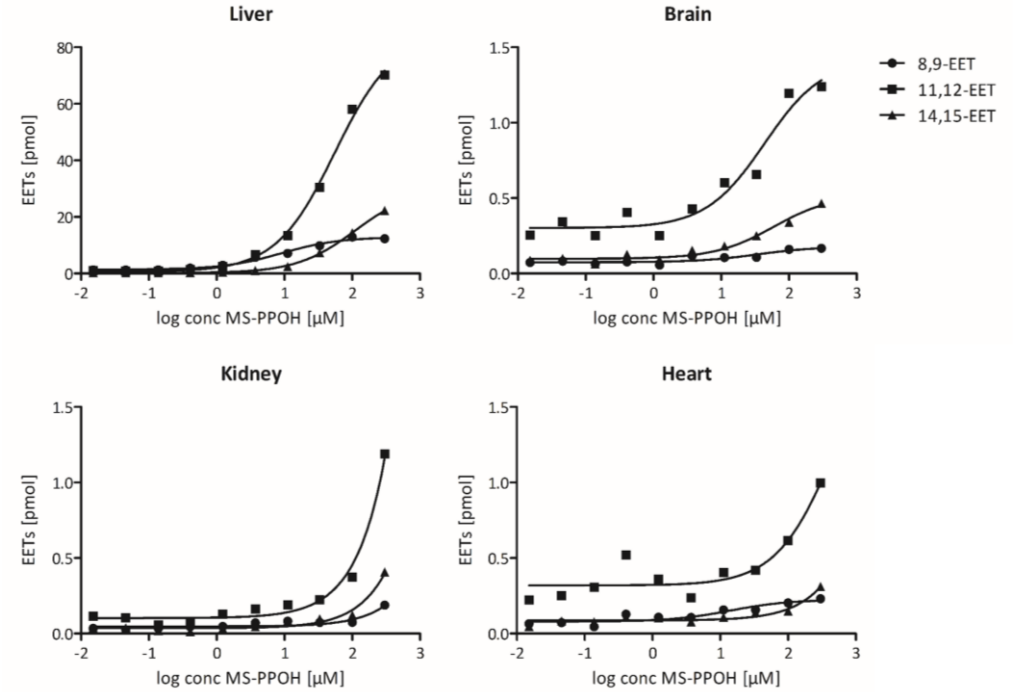

Figure 34: EET accumulation upon increasing MS-PPOH concentrations. EET regioisomer formation was measured after AA turnover in S9 fractions of liver, brain, kidney and heart from C57BL/6J WT mice in the presence of increasing MS-PPOH concentrations. An increase of EETs due to the presence of MS-PPOH becomes evident, starting at concentrations between 1 and 100 µM, depending on the organ and the regioisomer. Importantly, at no concentration of the inhibitor is the EET amount below the respective value measured in the absence of the inhibitor.

AA turnover assays with S9 fractions from all four organs showed an accumulation of 8,9-, 11,12- and 14,15-EET starting to appear at MS-PPOH concentrations around 1-100 µM, depending on the organ and regioisomer (Figure 34). Importantly, at no concentration of the inhibitor is the EET amount below the respective value measured in the absence of the inhibitor. This correlates well with the decrease of 8,9-, 11,12- and 12,14-DHET in the same samples (Figure 35).

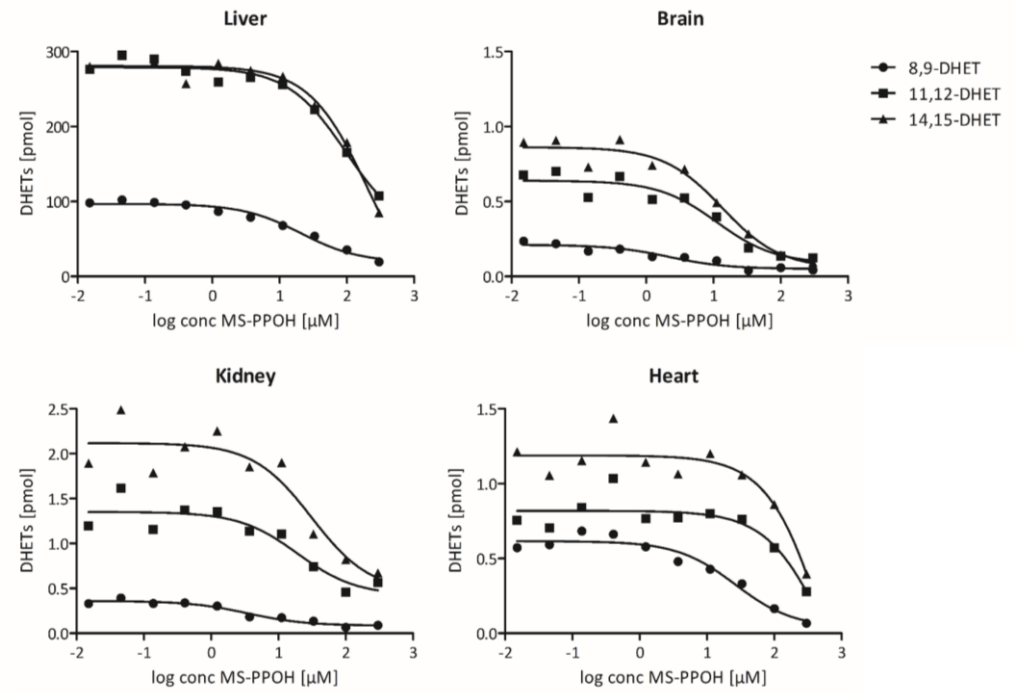

Figure 35: Reduced DHET formation with increasing MS-PPOH concentrations. DHET regioisomer amounts measured in the samples shown in Figure 34. The decreased formation of these EET metabolites corresponds well with the observed increase in EETs.

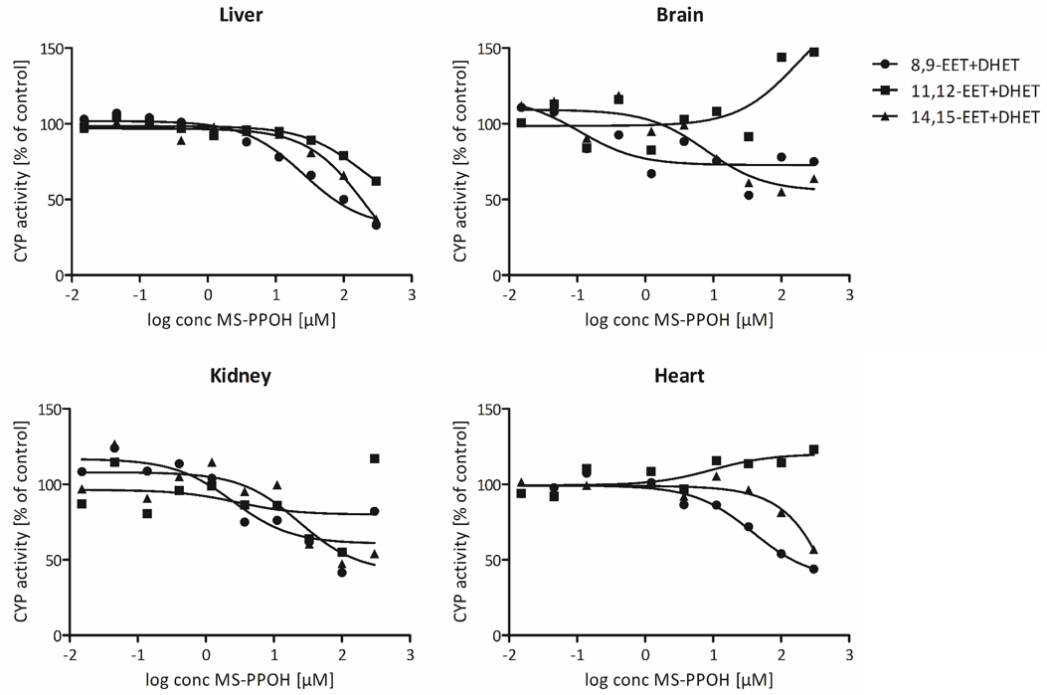

Figure 36: Total CYP activity at different MS-PPOH concentrations. CYP activity is expressed as the percentage of the sum of EET regioisomers and corresponding DHET regioismers to their sum measured in the absence of MS-PPOH from the samples shown in Figure 34 and 35.

To quantify the actual AA epoxygenation rate, the sum of EETs and their corresponding DHETs was related to the MS-PPOH concentration in the experiment. AA epoxygenation is inhibited in the liver for all three EET regioisomers, starting at MS-PPOH concentrations between 3 and 30 µM, while the other organs present a less uniform picture. Due to the much lower formation rate of EETs in these organs, the precision of the analysis is not as accurate as with the liver sample. Yet there is a common tendency essentially showing an absence of inhibition of 11,12-EET formation by MS-PPOH in lung, kidney and heart, while there is some evidence for inhibition of the formation of the other two regioisomers (Figure 36).

5. Discussion

5.1. Deciphering the (patho)physiologic role of epoxide hydrolases by *ex vivo* cartography of their substrate landscape

This doctoral thesis was motivated by the desire to gain new insight into the roles of α/β hydrolase fold EHs in mammalian physiology, to provide new leads for the development of novel therapeutic strategies. Although the newly developed trapping technique did not yet produce conclusive results, it provides a first step to identify the real contribution of the respective EH under investigation in the *in vivo* situation in an unbiased manner.

The underlying causes for failing to detect any *in vivo* substrates and potential measures to improve the technique are discussed in the following. In section 5.2. the role of the different α/β hydrolase fold EHs in mammalian physiology is discussed based on current hypotheses and unanswered questions. A successful, unbiased *in vivo* substrate trapping approach would be an enormously powerful tool to answer many open questions not only in regard to EHs but also to study other enzymes, that form covalent intermediates with their substrates.

5.1.1. Detection of the CatNuc peptides with LC-MS/MS

The most challenging aspect of our *in vivo* trapping approach concerning the LC-MS/MS detection was the fact that we were not interested in identifying an unknown protein by means of an arbitrary subset of characteristic peptides but in identifying one single peptide of a protein. Moreover, this single peptide is modified with an unknown substrate which results in an unknown parent ion mass and thus requires identification through its fragmentation pattern.

A potential problem in early LC-MS/MS method development with inclusion bodies was the risk of peptide modifications during recombinant expression in *E. coli* (e.g. post-translational modification) or during sample preparation (e.g. carbamylation after solubilization in 8 M urea (Sun et al., 2014b)). This was avoided in the subsequent LC-MS/MS method development by using synthetic versions of our CatNuc peptides of interest. The trapping EHs expressed in mouse tissue did not indicate any post-translational or preparation indebted modifications as the mEH HQ and the MEST HQ CatNuc peptides could be detected in mouse tissue lysates (Table 17) and the CatNuc peptides of mEH HQ, sEH HQ and Cif HQ (Cif data not shown) were detected when expressed in HEK293T cells. In case of EH3 and EH4 trapping mutants, peptide modification cannot be excluded but most probably they could not be detected because of their low AAV-mediated tissue expression (Figure 22, Figure 23).

Besides that, most of our tryptic CatNuc peptides were quite long with a length of 19-30 amino acids (Table 7). In classical proteomics it is known that peptides ideally have a length of 7-20 amino acids to be well-detectable (Hoofnagle et al., 2016). The only peptide fulfilling this criterion is the MEST CatNuc peptide with a length of 19 amino acids. In addition, MEST and mEH CatNuc peptides are the only ones appearing in trypsin-based peptide libraries (PeptideAtlas) indicating that they are the best detectable ones. This goes in line with our *in vivo* trapping results and the lowest detection limit measured for the MEST CatNuc peptide of 3 ng compared to 11 ng for the others (4.1.5). To obtain shorter peptides one could use another protease or a combination of proteases. This was checked with chymotrypsin and GluC but none of them did bring any improvement (Dengler, 2019). Chymotrypsin digestion resulted in to short peptides of 4-8 amino acids. The Cif CatNuc peptide with 8 amino acids was the only detectable one. GluC would lead to adequate peptide size but on the other hand it cleaves after Asp (D) including the CatNuc. Thus, trypsin remained the protease of choice also because it is generally used in large scale proteomics and it is the basis of all known peptide libraries.

5.1.2. AAV serotypes

The virally mediated transgene expression was highest in liver and brain, therefore LC-MS/MS analysis was focused on these two organs. These are not the appropriate organs for substrate trapping with EH3 and Cif but due to highest transgene expression in these organs they were used to test the detection capacity of our LC-MS/MS method. Furthermore, the identification of a new substrate would in any case help to better understand the function of the six EHs. This is especially the case for EH4 and MEST where identification of an epoxide substrate would proof their EH activity. In the following section we discuss how the serotype specific expression would affect the relevance of a trapped substrate.

For mEH and sEH, substrate trapping in the liver and brain are of major interest. Liver tissue sections suggested transgene expression mainly in hepatocytes (Figure 21 A and B, Figure 25), which was also shown to be the expression site for mEH and sEH (Coller et al., 2001, Enayetallah et al., 2004). Thus, both serotypes are appropriate for the *in vivo* trapping with sEH and mEH in the liver. In the brain, native GFP fluorescence and IHC staining of brain slices infected with the AAV-PHP.B showed neurons to be the primarily infected cell population and to lesser extent astrocytes (Figure 21 D-G). However, to reveal exact cell types further co-stainings with cell specific markers are indispensable. Nevertheless, Deverman et al. reported infection of astrocytes, different neuronal subtypes, endothelial cells and oligodendrocytes by AAV-PHP.B (Deverman et al., 2016). Native mEH expression was shown to be present in neurons whereas sEH is mainly present in astrocytes (Marowsky et al., 2009). The PHP.B serotype is therefore primarily appropriate for mEH. To more efficiently target

astrocytes to trap relevant substrates for sEH, expression could be increased by direct brain instillation of the virus.

EH3 is natively expressed in lung, skin and upper gastro intestinal tract. The used AAV-rh10 and AAV-PHP.B serotypes did not reach the relevant organs except the stomach where expression was low (Figure 20). The lung could probably be reached through direct lung instillation of the virus. Due to its proposed function in barrier formation, substrate trapping with EH3 in a barrier forming cell line (e.g. keratinocytes) could be another successful approach.

In case of EH4, which is almost exclusively expressed in the brain, AAV-PHP.B-mediated transgene expression seems to be appropriate to trap relevant substrates (Figure 20). Nevertheless, EH4 HQ transgene expression in the brain was low. This could potentially be addressed by direct brain instillation of AAV-PHP.B EH4 HQ.

Substrate trapping for MEST is of highest interest in the brain due to the behavioral phenotype of MEST KO mice and the AAV-PHP.B serotype is suitable as MEST is reported to be highest expressed in neuron-enriched areas of the brain (Lefebvre et al., 1998). However, MEST is widely expressed throughout the whole organism and identification of a substrate trapped in any organ would be a breakthrough, thus both serotypes AAV-PHP.B and AAV-rh10 are appropriate. Direct brain instillation could be considered to reach detectable MEST HQ transgene expression.

Cif is secreted during *P. aeruginosa* infection in the lung but neither of the two virus serotypes AAV-rh10 and AAV-PHP.B did infect the relevant organ. Thus, direct lung instillation of the purchased AAV-rh10 Cif HQ or first substrate trapping experiments in a CFTR expressing lung cell line could be promoting.

5.1.3. Substrate trapping in mouse tissue

The LC-MS/MS method used for *in vivo* substrate identification on the TripleTOF 6600 was established and optimized for our six CatNuc peptides of interest with commercially available synthetic versions of these peptides. *In vitro* trappings with recombinant sEH HQ and its known substrate (14,15-EET) resulted in successful detection of the EET-modified CatNuc peptide confirming the functionality of the used approach. Unexpectedly, however, we were unable to detect any substrate-modified CatNuc peptide isolated from mouse tissue.

The probable reasons for this outcome differ between the six different trapping EHs. In case of mEH HQ we assume that the trapping mutant was unable to bind its substrate. This was evidenced by the fact that the CatNuc peptide was only detected in the unmodified form, in both the *in vivo* and *in vitro* trapping experiments. Residual activity of recombinantly expressed mEH trapping mutant in *E. coli* could neither be observed (data not shown), which indicates its inability of covalent substrate binding

Another possibility that the covalent ester bound was cleaved during sample preparation is unlikely as it did not happen to the 14,15-EET-sEH CatNuc peptide complex in the sEH HQ *in vitro* trapping experiment. This, however, was unexpected as the functionality of the mEH HQ trapping mutant was demonstrated in preliminary experiments of our group with rat mEH and was reported earlier for the related *A. niger* EH (Arand et al., 1999b). In case of Cif we probably had the same problem of a misfolded protein unable to bind its substrate, which was supported by inclusion body formation upon expression in bacteria (4.1.7.3). Moreover, AVV-mediated Cif HQ expression in the lung, as the target tissue, was low or inexistent (Figure 20). During that time Filtter et al. reported a functional Cif trapping mutant, namely Cif E153Q (Flitter et al., 2016). Therefore, future trapping approaches for Cif should be performed with Cif E153Q. First attempts should be performed in a CFTR expressing lung cell line as relevant, new substrates might be revealed independent of the subcellular localization already in this system. Thus, it was not surprising to see that MEST HQ, the most promising candidate because of its LC-MS/MS detection properties (Dengler, 2019), also seemed to be non-functional and unable to bind its substrate. The AAV-mediated expression in liver and peptide recovery during sample preparation was high enough to detect the CatNuc peptide by LC-MS/MS but only in the unmodified form. Other possible reasons like hydrolyzation of the enzyme-substrate complex during sample preparation (was not a problem in sEH *in vitro* trapping), residual hydrolytic activity or that no substrate was present are rather unlikely. MEST is widely expressed throughout the whole organism, thus substrates should also be present in the liver. However, considering the aforementioned mEH and Cif trapping mutants, a misfolded MEST trapping mutant unable to bind its substrate seems plausible. To perform a successful *in vivo* substrate trapping experiment it is essential to find functional trapping mutants for the EHs under investigation. These trapping mutants should be tested *in vitro* prior to *in vivo* administration. Unfortunately, this is not possible in case of EH4 and MEST as none of their substrates are known.

sEH HQ was the only trapping mutant of which the ability to trap substrates was confirmed by LC-MS/MS analysis of *in vitro* trappings with its known substrate 14,15-EET. Nonetheless, the sEH CatNuc peptide was not detected in mouse tissue samples in any form (modified, unmodified). The two most probable reasons for this outcome are the fact that the sEH CatNuc peptide was substantially lost after evaporation steps during sample preparation (Dengler, 2019) and the potential trapping of several different substrates lowering the MS signal of each enzyme-substrate complex below the detection limit. This is also supported by the fact that the unmodified peptide was not detected, excluding issues yielding unmodified peptide. Furthermore, it is known that hydrophobic peptides tend to adsorb to tips, vials and parts of the detection system (Hoofnagle et al., 2016). According to the RPLC elution profile of our TripleTof 6600 LC-MS/MS method the sEH CatNuc peptide is the most hydrophobic peptide. To reduce adsorption to different surfaces we used low binding tips and tubes

and pretreated FASP filters and all used vials and tubes with 5% TWEEN. Moreover, peptide elution was performed under acidic conditions or with high amounts of organic solvent (Dengler, 2019). The taken measures needed to be compatible with LC-MS/MS analysis (Kovalchuk et al., 2015, Hoofnagle et al., 2016). However, none of them did improve sEH HQ CatNuc peptide recovery.

EH3 HQ and EH4 HQ CatNuc peptides were not detectable at all. Peptide recovery during LC-MS/MS sample preparation was also a major issue for EH3 and EH4 CatNuc peptides. Like the sEH CatNuc peptide they were significantly lost during FASP sample preparation and peptide recovery could not be increased by any measure described above. However, this was further impaired by low AAV-mediated tissue expression of EH3 HQ and EH4 HQ, which is probably due to a shorter half-life of these enzymes compared to the other trapping mutants (Figure 22). Furthermore, EH3 and EH4 are proposed to be membrane bound, which could impair recombinant expression. Both were reported to cause problems in different expression systems (Decker et al., 2012, Decker, 2010) and we had to truncate their membrane anchor for successful recombinant expression in *E. coli* (4.1.3). Anyway, this should not be of concern in mice, where everything required for natural EH expression is present.

To avoid the evaporation step during FASP sample preparation, which resulted in sEH, EH3 and EH4 CatNuc peptide loss, the tryptic digest could be directly measured after elution from the FASP filter as no MS detrimental agents are in the eluting buffer.

5.1.4. Trembling phenotype in AAV-PHP.B mEH HQ infected mice

We did not expect to affect the animals in any way as we expressed EHs without hydrolytic activity in a system where the natural EHs are intact. Every single translated trapping EH traps only one substrate molecule, thus reducing the pool of available epoxides to an, at best, very moderate extend. On top, as the viral expression occurs over a period of many days, we expect no relevant reduction of endogenously available epoxides. Furthermore, AAVs are well-known for their highly favorable characteristics like non-pathogenicity and low immunogenicity (Mezzina and Merten, 2011, Cearley and Wolfe, 2006).

Unexpectedly, however, WT and mEH KO mice injected with AAV-PHP.B mEH HQ developed an eye-catching trembling phenotype. The phenotype is characterized by resting tremor and postural instability. While WT mice injected with AAV-PHP.B mEH HQ showed first signs already 8 days post-injection, they were only observed after 12 days in mEH KO mice. Moreover, neither mice injected with AAV-PHP.B mEH WT (encoding active mEH) nor mice injected with the non-brain-infecting AAV-rh10 mEH HQ did develop any apparent phenotype. Thus, virus-mediated expression of mEH HQ in the brain seems to be the underlying cause but not mEH WT transgene expression in the brain. In addition, mEH KO mice appear to be less susceptible compared to WT mice.

As reported by Deverman et al. the AAV-PHP.B mediates transgene expression in the dopaminergic, TH^+ neurons of the substantia nigra pars compacta (SNpc) (Deverman et al., 2016), a loss or change of these cells upon mEH HQ transgene expression could be a very likely explanation for the observed trembling phenotype. To pick up on this, very recently, a small set of IHC stainings with a combination of an anti mEH and an anti TH antibody were done on brain slices of mEH KO mice infected with AAV-PHP.B mEH HQ by another member of the Arand lab. TH catalyzes the conversion of L-tyrosine to the dopamine precursor L-DOPA. A substantial loss of TH^+ dopaminergic neurons could be observed in the SNpc of AAV-PHP.B mEH HQ injected mice compared to untreated WT control mice.

Dopaminergic neurons from the SNpc synapse in the striatum. They build the nigrostriatal dopaminergic pathway and allow physiologic motor function (Figure 37 red arrows). Thus, a loss of SNpc neurons results in dopamine deficiency in the striatum, which is well-recognized as the underlying cause of Parkinson's disease (Blesa and Przedborski, 2014). There are two pathways of movement the indirect inhibiting movement and the direct enabling movement. Under physiologic conditions dopamine inhibits the indirect pathway via D2 receptors and it excites the direct pathway via D1 receptors. The dopamine deficit in the striatum in Parkinson's disease results in hyperactivity of the inhibitory D2 indirect pathway and reduced activity of the activating D1 direct pathway leading to an imbalance und thus an inhibition of voluntary movements (Figure 37) (Belujon et al., 2007). Some of the resulting typical Parkinson symptoms such as resting tremor and postural instability could also be observed in our mice.

Surprisingly, only mEH HQ expression in the brain induced motor function impairment, but not mEH WT expression. Other than mEH WT the mEH HQ is intended to trap substrates in a covalent ester-bond, thus reducing diol formation rate. However, as mEH KO mice seem to be less susceptible compared to WT mice, decreased tissue diol levels are unlikely to be the underlying cause for the loss of dopaminergic neurons. A more likely explanation involves the already mentioned potential misfolding of mEH HQ which potentially leads to aggregate formation and thus neuronal toxicity. This is reinforced by the unsuccessful mEH HQ *in vitro* and *in vivo* trappings and the fact that HEK293T cells transfected with pAM-CAG mEH HQ showed higher cell death compared to cells transfected with other constructs (subjective impression).

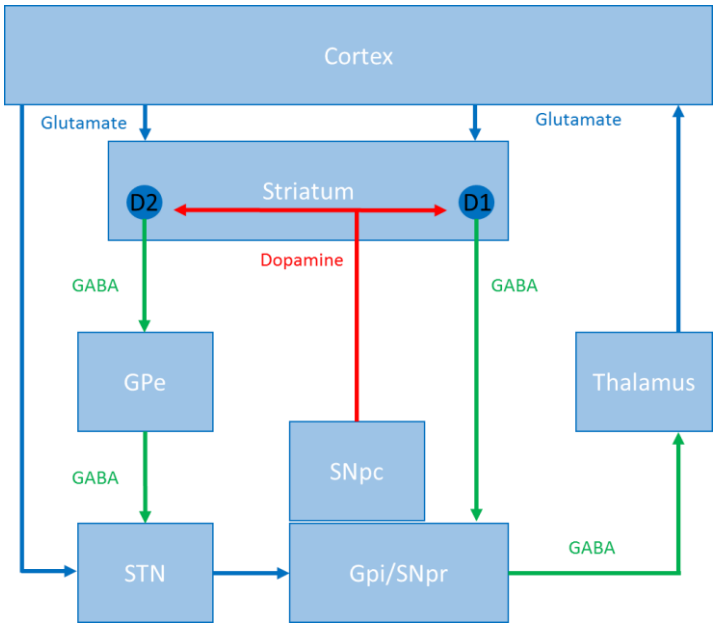

Figure 37: Direct and indirect pathway of motor function. Under physiologic conditions the indirect pathway (left side) prevents movement and the direct pathway enables movement. The dopamine (red) from the substantia nigra pars compacta (SNpc) acts in the striatum as an inhibitor of the indirect pathway via activation of D2 receptors and as an activator of the direct pathway via activation of D1 receptors. Thus, dopamine is a prerequisite for movement. STN = subthalamic nucleus, GPe/I = globus pallidus externa/interna, SNpr = substantia nigra pars reticularis. Adapted from (Belujon et al., 2007).

The delayed onset and the slower progression of the trembling in mEH KO mice could possibly be explained by higher EET tissue levels in these mice. In WT mice the mEH is naturally expressed in the substantia nigra pars reticulate (SNpr), but not in the dopaminergic neurons of the SNpc (Marowsky et al., 2009). mEH KO mice do not exhibit any phenotypic abnormalities (Miyata et al., 1999). Blood-flow in mEH KO mouse brains is increased after whisker stimulation compared to WT mice, thus mEH seems to be involved in brain vasodynamics (manuscript in preparation). This goes in line with higher EET levels in mEH KO mice (Edin et al., 2018, Marowsky et al., 2009). Moreover, both mEH and sEH KO mice seem to be less susceptible to MPTP treatment. TH^+ neuronal cell death was significantly reduced in these mice compared to WT control mice (Liu et al., 2008, Qin et al., 2015). MPTP is widely used in a toxin based Parkinson model to induce gradual cell death of dopaminergic neurons in the SNpc (Blesa and Przedborski, 2014). This is in line with our findings of more resistant dopaminergic neurons in mEH KO mice after AAV-mediated expression of potentially cell toxic proteins. Thus, increased EET levels in mEH KO may elicit a neuroprotective effect. EETs actually seem to be neuroprotective through several pathways e.g. inhibition of neuronal apoptosis or reduction of neuroinflammation (Wang et al., 2018).

In conclusion, AAV-PHP.B mEH HQ treated mice might provide a valuable approach for a Parkinson model system, as none of the existing models is able to reproduce the human condition. Especially the tremor phenotype is missing in most Parkinson models (Blesa and Przedborski, 2014). However, other

Parkinson characteristics like Lewy body inclusions in neurons, depression and sleep disturbance need to be further studied either by α-synuclein stainings or behavioral tests.

5.2. Epoxide hydrolases in mammalian physiology

Traditionally, EHs mainly have been regarded as detoxifying enzymes (Oesch, 1973, Ota and Hammock, 1980). In particular, mEH was shown to be the crucial enzyme in xenobiotic detoxification of epoxide intermediates of chemicals and pharmaceuticals (Fretland and Omiecinski, 2000, Wang et al., 2017) and sEH is seen as the key enzyme in FAE metabolism. To date, a large body of evidence demonstrates the involvement of sEH in many physiologic processes, mainly because of its ability to efficiently hydrolyze EETs. Small molecule inhibitors of sEH have become a novel therapeutic strategy in the treatment of diseases like hypertension, inflammation, chronic pain and diabetes (Campbell et al., 2017, Wagner et al., 2017).

5.2.1. Three for one: mEH, sEH and EH3 in fatty acid epoxide hydrolysis

During the last decades, however, evidence has accumulated that not only sEH but also other EHs are involved in physiologic processes via the turnover of endogenous FAEs. Especially mEH, which exhibits slow FAE hydrolysis compared to sEH *in vitro* (Marowsky et al., 2009), was shown to contribute significantly to their hydrolysis *in vivo* (Marowsky et al., 2017, Edin et al., 2018). Thus, the long-time postulated division of roles between sEH and mEH is slowly dissolving. Moreover, the most recently identified member of the α/β hydrolase fold EH family, EH3, was shown to have the highest specific activity for EET hydrolysis and is the best catalyst in leukotoxin turnover reported *in vitro* for EHs so far (Decker et al., 2012). Only because of its lower affinity (higher K_m), EH3 has a catalytic efficiency for EETs in the range of sEH, the supposed key enzyme in EET turnover (Zeldin et al., 1993).

This, however, raises the question why there are at least three different EHs for the hydrolysis of bioactive FAEs. The most obvious reasons are their different expression patterns in different tissues and cell types and that they slightly differ in their substrate preferences concerning the different FAE regioisomers. Another important point is their individual subcellular localization. While sEH is present in the cytosol and peroxisomes, EH3 and mEH are ER resident and thus profit from their close proximity to the epoxide forming CYPs, which are also ER resident (Decker et al., 2012). Potential substrate channeling between CYPs and ER resident EHs may result in a significant kinetic advantage for the 'low affinity' EH3 and the 'slow' mEH. In case of mEH, this could be demonstrated with CYP2J5 (Orjuela Leon et al., 2017). The ER resident mEH and EH3 differ in respect to their affinity (K_m) for the different FAEs with mEH being the one with higher affinity (lower K_m), but their catalytic efficiency is in the same range. Thus, mEH seems to be more relevant at low substrate concentrations and when slow diol

formation is desired, whereas EH3 would be the most appropriate EH if high diol formation rate with only minimal FAE leakage is needed (Decker et al., 2012). Considering the fact that also the diol products may elicit biologic activity, potentially even opposing the epoxide's actions, as was reported for leukotoxin (Moghaddam et al., 1997b), already slight differences in local epoxide/diol ratios may lead to differential physiologic effects, thus the presence of three slightly different EHs might be meaningful.

Evidence for the dual role of mEH in detoxification and the regulation of endogenous signaling molecules could potentially be given by the fact that mEH is the only mammalian EH possessing a Glu as an acidic residue in the charge relay system. In case of mEH, the Glu is responsible for the slower diol formation rates compared to other EHs. No higher species is known to have a mEH with Asp as acidic residue like in the other known mammalian α/β hydrolase fold EHs. Former studies showed that exchanging the catalytic Glu of mEH with Asp resulted in an up to 40-fold increase in turnover rates with different mEH substrates. At the same time K_m increased, indicating that the speed of the second hydrolytic step increased due to the mutation. The detoxification capacity of mEH mainly depends on the first, ester-forming step, thus faster diol formation does not necessarily increase its detoxification capacity as long as mEH is well in excess over its substrate, which is usually the case, especially in the liver (Arand et al., 1999a). However, the obvious preference for an apparently less efficient enzyme by nature must have a reason. The 'fast' Asp-variant is absent in mammals, indicating that diol formation is not only of relevance in xenobiotic metabolism. Probably, the slow diol formation is beneficial in the turnover of an endogenous mEH substrate of yet unknown function. Interestingly, another, moderately high activity human mEH genotype has been related to the development of hereditary disorders like pre-eclampsia (Groten et al., 2014, Zusterzeel et al., 2001, Laasanen et al., 2002), which could potentially be linked to endogenous vasoactive mEH substrates. In a mEH Glu404Asp mouse model, significantly higher DHETs/EETs ratios were observed in various tissues suggesting a broad impact of mEH on EET metabolism. Because EETs are strong vasodilators in the brain, this also resulted in impaired cerebral blood flow regulation (Marowsky et al., 2016). This reveals the physiologic importance of the 'slow' diol formation by mEH. Further studies are required to define the exact role of mEH in FAE metabolism and the related physiological processes.

The relevance of EH3 *in vivo* is even less clear as EH3 KO mice did not show any overt phenotype when compared to WT mice (Hoopes et al., 2017). Possibly sEH and mEH were able to compensate for the anyway very low expressed EH3 in this case, thus further *in vivo* studies with different double or triple KO mice would provide more information on the respective participation. According to its expression pattern, a role in detoxification would also be tempting for EH3. However, such a role is not supported by the narrow substrate spectrum observed for EH3 (Decker et al., 2012). Altered EH3 expression levels were related to different tumors in the gastrointestinal tract and skin (Yamashita et al., 2006, Øster et

al., 2011, Furuta et al., 2006). Concerning the fact that EETs are proangiogenic (Michaelis et al., 2005, Fleming, 2007), EH3 but also other EETs converting EHs may potentially be important in the prevention of tumor malignancy. Thus, depending on their expression patterns, different EHs could be of relevance at different sites. One could also speculate on a potential role of EH3 in barrier formation, as highest expression was reported in tissues forming contact surfaces with the outside (Decker et al., 2012). In addition, EH3 was related to ichthyosis (Ala et al., 2008) and most recent evidence effectively revealed a potential role in epidermal water barrier formation (Yamanashi et al., 2018). In the latter study, EH3 and sEH were shown to be able to hydrolyze a skin-related epoxide (9*R*,10*R*-*trans*-epoxy-13*R*-hydroxy-octadeca-11*E*-enoic acid) involved in a crucial step in sealing the epidermal water barrier. However, EH3 hydrolyzed the mentioned epoxide up to 31-fold faster than 14,15-EET and would thus potentially outperform sEH. At a first glance it would be tempting to speculate that EH3 is the main candidate involved in this very important process, also because of its high expression in the skin (Decker et al., 2012) and especially in the outer epidermis (Toulza et al., 2007), where the skin water barrier formation takes place. Nonetheless, concerning the fact that EH3 expression is generally very low compared to other EHs and sEH is also highly expressed in skin (Enayetallah et al., 2004), the contribution of sEH cannot be neglected. This redundancy is probably also a reason why sEH and EH3 single KO mice did not show any skin-related phenotype. Moreover, the used model did not take into account that the tested epoxide is coupled to a skin-ceramide under natural conditions, which might affect its hydrolysis by both EHs. Thus, the next step would be to check the impact of each enzyme under *in vivo* conditions using sEH and EH3 KO and double KO mice (Yamanashi et al., 2018).

In addition, EH3 is the most efficient EH in leukotoxin metabolism and is highly expressed in the lung. This suggests that EH3 potentially contributes to leukotoxin toxicity in the lung, as the resulting leukotoxin-diol was reported to be a strong promoter of acute respiratory distress syndrome (ARDS) (Moghaddam et al., 1997b). However, sEH was also reported to be involved in the leukotoxin-diol induced development of ARDS. Inhibition of sEH was even found to decrease the leukotoxin induced mortality *in vivo* (Zheng et al., 2001). Considering the fact that EH3 was shown to be susceptible to many sEH inhibitors (Decker et al., 2012), it cannot be excluded that the used sEH inhibitor also blocked EH3. Finally, at least a dualistic participation may be the cause for leukotoxin-diol induced development of ARDS and further experiments will expand our knowledge.

5.2.2. The two orphans EH4 and MEST

According to the expression pattern of EH4 and its close relation to EH3, a role in the metabolism of endogenous signaling molecules, especially FAEs, seems likely (Decker et al., 2009). The inability to recombinantly express EH4 efficiently in an active form, however, hinders its characterization and the

better understanding of its potential functions. Thus, probably the only hint in this direction was the recently reported potential role of EH4 in lipid metabolism of sebaceous glands (Dahlhoff et al., 2015). EH4 was shown to be significantly enriched on the surface of lipid droplets (LD) of different sebocyte cell lines, indicating that EH4 is an LD-associated protein. Lipid synthesis is the hallmark of sebaceous gland cell differentiation and lipid metabolism depends on LD, which are cytoplasmic structures encircled by a protein-rich phospholipid monolayer originating from the ER. siRNA-mediated downregulation of EH4 resulted in increased LD size and sebaceous lipogenesis. Thus, EH4, as a protein in sebaceous lipogenesis, may be a potential target for the treatment of sebaceous gland-related diseases such as acne (Dahlhoff et al., 2015). However, as EH4 is most highly expressed in the brain, it likely also fulfills an important role there. The biologic roles of LDs are numerous in many different cell types, also in the brain. They are involved in lipid storage and energy homeostasis but also in lipid signaling and eicosanoid formation and thus play an important role in the host immune system. Concerning the brain, it was suggested that disrupted LD function can contribute to neurodegeneration (Welte, 2015). A potential role of EH4 in these processes does not seem unrealistic. Anyway, the exact catalytic activity of EH4 needs to be elucidated before drawing any premature conclusion.

MEST is highly conserved in mammals and primarily seems to be important in early development. EH activity of MEST is not yet evidenced, and it is thus early to speculate on a physiologic EH function for MEST. However, MEST was related to lipid metabolism, as it was shown to be associated with adipose tissue expansion. MEST expression in adipose tissue was induced and expression levels correlated with the expansion of fat mass in mice kept on a positive energy diet (Nikonova et al., 2008b). Additionally, global depletion of MEST and focused depletion in adipose tissue resulted in reduced fat mass accumulation with high-fat diet compared to WT mice, which suggests that MEST facilitates lipid accumulation (Anunciado-Koza et al., 2017). However, as mentioned before, a direct connection between a specific catalytic activity of MEST and adipose tissue expansion has not yet been identified. It is possible that MEST acts as an EH on FAEs. Further studies are required to clarify the catalytic activity of MEST and its possible biologic roles.

5.2.3. Targeting the *P. aeruginosa* epoxide hydrolase Cif

P. aeruginosa infection contributes significantly to the mortality of acute and chronic lung diseases even when treated with the appropriate antibiotics. Thus, novel drug targets are most welcome to ameliorate the treatment options. In cystic fibrosis patients, *P. aeruginosa* infection is a leading cause of morbidity and mortality (Parkins et al., 2018). The exact role of the bacterially secreted EH Cif in the pathogenicity of *P. aeruginosa* is still unclear but it is reported to interfere with host CFTR trafficking. Thus, Cif seems to be a promising target for the treatment of *P. aeruginosa* lung infections, especially

in patients with cystic fibrosis, where CFTR activity and thus mucociliary clearance is already reduced. The inhibition of Cif might compromise *P. aeruginosa* colonization and reduce pulmonary infections. Nonetheless, concerning therapeutic intervention targeting Cif, it must be considered that Cif is only one amongst a potpourri of virulence factors of *P. aeruginosa* (Bleves et al., 2010). Thus, depending on the lung disease, there is a possibility that targeting Cif in the treatment of *P. aeruginosa* infections does not lead to the wanted outcome and might even interfere with host epoxide metabolism. Concerning the fact that EETs act as vasoconstrictors in the lung, this would not be acceptable. Anyway, the identification of the epoxide or diol involved in CFTR recycling and targeted by Cif would shed light onto the understanding of the recycling mechanism and regulation of CFTR expression in general.

5.3. The CYP blocker MS-PPOH is an inhibitor of sEH

MS-PPOH is widely used as a selective CYP inhibitor to block EET formation to study or specifically eliminate EET functions. EETs, however, are rapidly converted by EHs to their usually less active vicinal diols (DHETs). MS-PPOH shows strong structural similarity to the amide class of mEH inhibitors (Morisseau et al., 2001). However, we could not observe any inhibitory effect on mEH at any MS-PPOH concentration used in our FIAs (Figure 32 A). While it did not block mEH, MS-PPOH did inhibit its sister enzyme sEH (Figure 32 B). This is even more relevant, concerning the fact that sEH is generally recognized as the major player in EET metabolism (Yu et al., 2000). The obtained IC_{50} values are in the nanomolar range for sEH of all tested species (Figure 32 B) and are therefore below the reported values for some CYP isoforms, which range from 11 to 300 µM (VanAlstine and Hough, 2011, Brand-Schieber et al., 2000, Wang et al., 1998). This fact implicates that the inhibitory effect is higher on EET breakdown than on EET production which should rather increase than decrease EET levels upon MS-PPOH treatment. This hypothesis could subsequently be supported in an S9 fraction-based AA turnover assay, where sEH and CYPs are both present. In all tested S9 fractions a substantial accumulation of 8,9-, 11,12-, and 14,15-EET becomes evident, starting at MS-PPOH concentrations between 1 and 100 µM, depending on the organ and the regioisomer (Figure 34), confirming sEH inhibition by MS-PPOH. The decreased levels of DHET (Figure 35) are in line with sEH inhibition but could also be explained by CYP inhibition. This latter effect of MS-PPOH on CYPs is represented in the sum of EETs and DHETs which is only reduced with MS-PPOH concentrations above 30 µM. These results suggest that CYP inhibition potentially requires higher MS-PPOH concentrations than the ones effectively used in previous *in vitro* and *in vivo* trials (Wang et al., 1998, Bhardwaj et al., 2000, Brand-Schieber et al., 2000, Zhu et al., 2000, Peng et al., 2002, Conroy et al., 2010). Furthermore, although the inhibition of CYPs might reduce the sum of EETs and DHETs at high MS-PPOH concentrations, the concurrent

inhibition of sEH shifts the ratio of EETs and DHETs to the side of EETs, resulting in a net increase of EET levels.

The fluctuations of the calculated CYP activities in brain, kidney and heart (Figure 36) can be explained by the low EETs and DHETs amounts measured in these tissues, scratching at the detection limit of our analytical system. The much higher EET and DHET amounts detected in the liver S9 samples can be attributed to the higher abundance of the relevant CYP epoxygenases in mouse liver and additionally high sEH expression (Imig, 2012, Renaud et al., 2011). Anyway, the differential EET regioisomer production in the four organs is a result of the differing CYP isozyme expression and each CYP isozyme shows its own MS-PPOH sensitivity. The two orders of magnitude higher MS-PPOH concentrations needed to inhibit sEH and also CYPs in the S9 fraction assay compared to the experiments with purified enzymes could possibly be explained with the hydrophobicity of MS-PPOH and the resulting binding to protein surfaces (Brand-Schieber et al., 2000). Thus, the unspecifically bound MS-PPOH is no longer available to inhibit CYPs or sEH, resulting in an increase of the needed concentrations to see an effect. Another possibility is, that MS-PPOH is less stable than reported and thus metabolically eliminated in the S9 fraction. However, our assay is an endpoint determination, thus we cannot judge on this.

In essence, our results reveal that MS-PPOH blocks sEH more efficiently than CYPs, therefore unexpectedly rather increasing than decreasing EET tissue levels. This suggests that *in vivo* experiments with MS-PPOH, carried out with the intention to reduce endogenous EET levels, are based on a wrong overall assumption and erroneous conclusions are likely drawn from their results, now requiring careful revision in the light of our present findings. Nonetheless, additional studies to examine the *in vivo* relevance of our *in vitro* results are of major importance to further substantiate the net effect of MS-PPOH *in vivo* application on EET steady state levels in tissues.

6. Future directions

Concerning the developed *in vivo* trapping approach in the main project of this thesis, sEH with its functional trapping mutant is the most promising candidate to continue. Thus, it would be necessary to increase the peptide recovery during sample preparation. For that purpose, evaporation steps should be avoided which is possible using FASP digestion and directly analyzing the eluting fraction after trypsin digestion. Functional trapping mutants for mEH, EH3 and Cif should first be confirmed *in vitro* as some of their substrates are known. In case of Cif the reported functional trapping mutant Cif E153Q (Flitter et al., 2016) should be tested. The *in vitro* trapping experiments are at the same time important to further improve the sample preparation. In case of EH3 and Cif first trapping experiments could be performed in a lung cell line or in barrier-forming keratinocytes (EH3) as the AAV-mediated transgene expression did not reach these tissues. To reach the relevant tissues for EH3 and Cif *in vivo* direct lung instillation or another AAV serotype could be considered. The mutations resulting in functional trapping mutants for the aforementioned EHs can subsequently be tested for EH4 and MEST *in vitro*. Thereby, the still open question whether these two orphans effectively act as EHs can potentially be answered. After successful establishment of the trapping technique, it could be extended to other organs like adipose tissue for MEST or kidney and heart for sEH. The extend by which mEH and sEH are occupied with detoxification could be assessed in another set of experiments by challenging the animals with xenobiotic precursors of these EHs.

The progressive trembling phenotype in mice after AAV-mediated mEH HQ expression in the brain needs further investigation. Besides the tremor phenotype, other typical Parkinson related symptoms like depression or sleep disturbance should be addressed through behavioral tests and the characteristical Lewy body formation in dopaminergic neurons should be checked by α-synuclein stainings of brain slices. Furthermore, the course of the phenotype should be observed for a longer time period (> 14 d) in mEH KO mice and in sEH KO mice additionally as these have even higher plasma EET levels and are thus potentially more resistant than mEH KO mice. Moreover, to check if the underlying cause really is dopamine deficiency in the striatum it would be obvious to test whether the trembling stops upon L-DOPA treatment.

Concerning the more general discussion about the important role of EHs in mammalian physiology, comparison studies of different mEH, sEH and EH3 KO mice including double and triple KO mice would be of major interest as at least these EHs seem to be involved in FAE hydrolysis and are potentially able to compensate for each other. Moreover, to further expand our understanding, it is important to identify the molecular high affinity receptors for the substrates and products of the EH reactions, primarily for EETs. This would enable the development of experimental models to study an array of physiologic processes and promote drug development in the respective fields.

Referring to the smaller side project that revealed MS-PPOH as an inhibitor of sEH, additional studies to examine the *in vivo* relevance of sEH inhibition are of major importance to further substantiate the net effect of MS-PPOH *in vivo* application on EET steady state levels in tissues.

7. References

AGARWAL, M., AUSTIN, T. W., MOREL, F., CHEN, J., BOHNLEIN, E. & PLAVEC, I. 1998. Scaffold attachment region-mediated enhancement of retroviral vector expression in primary T cells. *Journal of virology,* 72**,** 3720-8.

ALA, U., PIRO, R. M., GRASSI, E., DAMASCO, C., SILENGO, L., OTI, M., PROVERO, P. & DI CUNTO, F. 2008. Prediction of human disease genes by human-mouse conserved coexpression analysis. *PLOS computational biology,* 4**,** e1000043.

ANUNCIADO-KOZA, R. P., MANUEL, J., MYNATT, R. L., ZHANG, J., KOZAK, L. P. & KOZA, R. A. 2017. Diet-induced adipose tissue expansion is mitigated in mice with a targeted inactivation of mesoderm specific transcript (Mest). *PLOS ONE,* 12**,** e0179879.

ARAND, M., CRONIN, A., OESCH, F., MOWBRAY, S. L. & JONES, T. A. 2003c. The telltale structures of epoxide hydrolases. *Drug metabolism reviews,* 35**,** 365-83.

ARAND, M., GRANT, D. F., BEETHAM, J. K., FRIEDBERG, T., OESCH, F. & HAMMOCK, B. D. 1994. Sequence similarity of mammalian epoxide hydrolases to the bacterial haloalkane dehalogenase and other related proteins. Implication for the potential catalytic mechanism of enzymatic epoxide hydrolysis. *FEBS Letters,* 338**,** 251-6.

ARAND, M., HEMMER, H., DURK, H., BARATTI, J., ARCHELAS, A., FURSTOSS, R. & OESCH, F. 1999b. Cloning and molecular characterization of a soluble epoxide hydrolase from Aspergillus niger that is related to mammalian microsomal epoxide hydrolase. *Biochemical journal,* 344 Pt 1**,** 273-80.

ARAND, M., HERRERO PLANA, M., HENGSTLER, J. G., LOHMANN, M., CRONIN, A. & OESCH, F. 2003a. Detoxification strategy of epoxide hydrolase the basis for a threshold in chemical carcinogenesis. *EXCLI Journal,* 2**,** 22-30.

ARAND, M., KNEHR, M., THOMAS, H., ZELLER, H. D. & OESCH, F. 1991. An impaired peroxisomal targeting sequence leading to an unusual bicompartmental distribution of cytosolic epoxide hydrolase. *FEBS letters,* 294**,** 19-22.

ARAND, M., MÜLLER, F., MECKY, A., HINZ, W., URBAN, P., POMPON, D., KELLNER, R. & OESCH, F. 1999a. Catalytic triad of microsomal epoxide hydrolase: replacement of Glu404 with Asp leads to a strongly increased turnover rate. *Biochemical journal,* 337**,** 37-43.

ARAND, M., WAGNER, H. & OESCH, F. 1996. Asp333, Asp495, and His523 form the catalytic triad of rat soluble epoxide hydrolase. *Journal of biological chemistry,* 271**,** 4223-9.

ARGIRIADI, M. A., MORISSEAU, C., HAMMOCK, B. D. & CHRISTIANSON, D. W. 1999. Detoxification of environmental mutagens and carcinogens: structure, mechanism, and evolution of liver epoxide hydrolase. *Proceedings of the national academy of sciences,* 96**,** 10637-10642.

ARMSTRONG, R. N. 1999. Kinetic and chemical mechanism of epoxide hydrolase. *Drug metabolism reviews,* 31**,** 71-86.

ARMSTRONG, R. N. & CASSIDY, C. S. 2000. New structural and chemical insight into the catalytic mechanism of epoxide hydrolases. *Drug metabolism reviews,* 32**,** 327-338.

BAHL, C. D., HVORECNY, K. L., BOMBERGER, J. M., STANTON, B. A., HAMMOCK, B. D., MORISSEAU, C. & MADDEN, D. R. 2015. Inhibiting an Epoxide Hydrolase Virulence Factor from Pseudomonas aeruginosa Protects CFTR. *Angewandte Chemie internationale Edition Englisch,* 54**,** 9881-5.

BAHL, C. D. & MADDEN, D. R. 2012. Pseudomonas aeruginosa Cif defines a distinct class of α/β epoxide hydrolases utilizing a His/Tyr ring-opening pair. *Protein and peptide letters,* 19**,** 186-193.

BAHL, C. D., MORISSEAU, C., BOMBERGER, J. M., STANTON, B. A., HAMMOCK, B. D., O'TOOLE, G. A. & MADDEN, D. R. 2010. Crystal structure of the cystic fibrosis transmembrane conductance regulator inhibitory factor Cif reveals novel active-site features of an epoxide hydrolase virulence factor. *Journal of bacteriology,* 192**,** 1785-95.

BELAND, F. A. & POIRIER, M. C. 1993. Significance of DNA adduct studies in animal models for cancer molecular dosimetry and risk assessment. *Environmental health perspectives,* 99**,** 5.

BELUJON, P., LODGE, D. J. & GRACE, A. A. 2007. Dopamine Systems in Parkinson's Disease and L-DOPA-induced Dyskinesia—What Goes Wrong? *Dopamine Systems in Parkinson's Disease and L-DOPA-induced Dyskinesia—What Goes Wrong?*

BHARDWAJ, A., NORTHINGTON, F. J., CARHUAPOMA, J. R., FALCK, J. R., HARDER, D. R., TRAYSTMAN, R. J. & KOEHLER, R. C. 2000. P-450 epoxygenase and NO synthase inhibitors reduce cerebral blood flow response to N-methyl-D-aspartate. *American journal of physiology-heart and circulatory physiology,* 279**,** H1616-H1624.

BLESA, J. & PRZEDBORSKI, S. 2014. Parkinson's disease: animal models and dopaminergic cell vulnerability. *Frontiers in neuroanatomy,* 8**,** 155.

BLEVES, S., VIARRE, V., SALACHA, R., MICHEL, G. P., FILLOUX, A. & VOULHOUX, R. 2010. Protein secretion systems in Pseudomonas aeruginosa: a wealth of pathogenic weapons. *International journal of medical microbiology,* 300**,** 534-543.

BOMBERGER, J. M., ELY, K. H., BANGIA, N., YE, S., GREEN, K. A., GREEN, W. R., ENELOW, R. I. & STANTON, B. A. 2014. Pseudomonas aeruginosa Cif protein enhances the ubiquitination and proteasomal degradation of the transporter associated with antigen processing (TAP) and reduces major histocompatibility complex (MHC) class I antigen presentation. *Journal of biological chemistry,* 289**,** 152-62.

BOMBERGER, J. M., MACEACHRAN, D. P., COUTERMARSH, B. A., YE, S., O'TOOLE, G. A. & STANTON, B. A. 2009. Long-distance delivery of bacterial virulence factors by Pseudomonas aeruginosa outer membrane vesicles. *PLOS Pathogens,* 5**,** e1000382.

BRAND-SCHIEBER, E., FALCK, J. F. & SCHWARTZMAN, M. 2000. Selective inhibition of arachidonic acid epoxidation in vivo. *Journal of physiology and pharmacology,* 51**,** 655-72.

CAMPBELL, W. B., IMIG, J. D., SCHMITZ, J. M. & FALCK, J. R. 2017. Orally Active Epoxyeicosatrienoic Acid Analogs. *Journal of cardiovascular pharmacology,* 70**,** 211-224.

CAPDEVILA, J., GIL, L., ORELLANA, M., MARNETT, L. J., MASON, J. I., YADAGIRI, P. & FALCK, J. R. 1988. Inhibitors of cytochrome P-450-dependent arachidonic acid metabolism. *Archives of biochemistry and biophysics,* 261**,** 257-63.

CAPDEVILA, J. H., FALCK, J. & ESTABROOK, R. W. 1992. Cytochrome P450 and the arachidonate cascade. *FASEB Journal,* 6**,** 731-736.

CARRATT, S. A., MORIN, D., BUCKPITT, A. R., EDWARDS, P. C. & VAN WINKLE, L. S. 2016. Naphthalene cytotoxicity in microsomal epoxide hydrolase deficient mice. *Toxicology Letters,* 246**,** 35-41.

CEARLEY, C. N. & WOLFE, J. H. 2006. Transduction characteristics of adeno-associated virus vectors expressing cap serotypes 7, 8, 9, and Rh10 in the mouse brain. *Molecular therapy : the journal of the american society of gene therapy,* 13**,** 528-37.

CHEN, D., WHITCOMB, R., MACINTYRE, E., TRAN, V., DO, Z. N., SABRY, J., PATEL, D. V., ANANDAN, S. K., GLESS, R. & WEBB, H. K. 2012. Pharmacokinetics and pharmacodynamics of AR9281, an inhibitor of soluble epoxide hydrolase, in single- and multiple-dose studies in healthy human subjects. *Journal of clinical pharmacology,* 52**,** 319-28.

COLLER, J. K., FRITZ, P., ZANGER, U. M., SIEGLE, I., EICHELBAUM, M., KROEMER, H. K. & MÜRDTER, T. E. 2001. Distribution of microsomal epoxide hydrolase in humans: an immunohistochemical study in normal tissues, and benign and malignant tumours. *The histochemical journal,* 33**,** 329-336.

CONROY, J. L., FANG, C., GU, J., ZEITLIN, S. O., YANG, W., YANG, J., VANALSTINE, M. A., NALWALK, J. W., ALBRECHT, P. J. & MAZURKIEWICZ, J. E. 2010. Opioids activate brain analgesic circuits through cytochrome P450/epoxygenase signaling. *Nature neuroscience,* 13**,** 284.

CRONIN, A., HOMBURG, S., DURK, H., RICHTER, I., ADAMSKA, M., FRERE, F. & ARAND, M. 2008. Insights into the catalytic mechanism of human sEH phosphatase by site-directed mutagenesis and LC-MS/MS analysis. *Journal of molecular biology,* 383**,** 627-40.

CRONIN, A., MOWBRAY, S., DURK, H., HOMBURG, S., FLEMING, I., FISSLTHALER, B., OESCH, F. & ARAND, M. 2003. The N-terminal domain of mammalian soluble epoxide hydrolase is a phosphatase. *Proceedings of the national academy of sciences,* 100**,** 1552-7.

CSÖRGŐ, B., FEHÉR, T., TÍMÁR, E., BLATTNER, F. R. & PÓSFAI, G. 2012. Low-mutation-rate, reduced-genome Escherichia coli: an improved host for faithful maintenance of engineered genetic constructs. *Microbial cell factories,* 11**,** 11.

CUI, P. H., PETROVIC, N. & MURRAY, M. 2011. The ω-3 epoxide of eicosapentaenoic acid inhibits endothelial cell proliferation by p38 MAP kinase activation and cyclin D1/CDK4 down-regulation. *British journal of pharmacology,* 162**,** 1143-1155.

DAHLHOFF, M., FROHLICH, T., ARNOLD, G. J., MULLER, U., LEONHARDT, H., ZOUBOULIS, C. C. & SCHNEIDER, M. R. 2015. Characterization of the sebocyte lipid droplet proteome reveals novel potential regulators of sebaceous lipogenesis. *Experimental cell research,* 332**,** 146-55.

DECKER, M., 2010. *PhD thesis: Expression and characterization of the novel human epoxide hydrolases EH3 and EH4.* University of Zurich.

DECKER, M., ADAMSKA, M., CRONIN, A., DI GIALLONARDO, F., BURGENER, J., MAROWSKY, A., FALCK, J. R., MORISSEAU, C., HAMMOCK, B. D., GRUZDEV, A., ZELDIN, D. C. & ARAND, M. 2012. EH3 (ABHD9): The first member of a new epoxide hydrolase family with high activity for fatty acid epoxides. *Journal of lipid research,* 53**,** 2038-45.

DECKER, M., ARAND, M. & CRONIN, A. 2009. Mammalian epoxide hydrolases in xenobiotic metabolism and signalling. *Archives of toxicology,* 83**,** 297-318.

DENGLER, M., 2019. *ETH Diss. No. 25663: Trapped: Developing an unbiased approach to identify epoxide hydrolase substrates in vivo.* ETH Zürich.

DEVERMAN, B. E., PRAVDO, P. L., SIMPSON, B. P., KUMAR, S. R., CHAN, K. Y., BANERJEE, A., WU, W. L., YANG, B., HUBER, N., PASCA, S. P. & GRADINARU, V. 2016. Cre-dependent selection yields AAV variants for widespread gene transfer to the adult brain. *Nature biotechnology,* 34**,** 204-9.

DOMON, B. & AEBERSOLD, R. 2006. Mass spectrometry and protein analysis. *Science,* 312**,** 212-217.

EDIN, M. L., GHOLIPOUR HAMEDANI, B., GRUZDEV, A., GRAVES, J. P., LIH, F. B., ARBES, S. J., SINGH, R., ORJUELA LEON, A. C., BRADBURY, J. A., DEGRAFF, L. M., HOOPES, S. L., ARAND, M. & ZELDIN, D. 2018. Epoxide hydrolase 1 (EPHX1) hydrolyzes epoxyeicosanoids and impairs cardiac recovery after ischemia. *Journal of biological chemistry*.

ENAYETALLAH, A. E., FRENCH, R. A., BARBER, M. & GRANT, D. F. 2006. Cell-specific subcellular localization of soluble epoxide hydrolase in human tissues. *Journal of histochemistry & cytochemistry,* 54**,** 329-335.

ENAYETALLAH, A. E., FRENCH, R. A., THIBODEAU, M. S. & GRANT, D. F. 2004. Distribution of soluble epoxide hydrolase and of cytochrome P450 2C8, 2C9, and 2J2 in human tissues. *Journal of histochemistry & cytochemistry,* 52**,** 447-454.

FENN, J. B., MANN, M., MENG, C. K., WONG, S. F. & WHITEHOUSE, C. M. 1989. Electrospray ionization for mass spectrometry of large biomolecules. *Science,* 246**,** 64-71.

FISSLTHALER, B., POPP, R., KISS, L., POTENTE, M., HARDER, D. R., FLEMING, I. & BUSSE, R. 1999. Cytochrome P450 2C is an EDHF synthase in coronary arteries. *Nature,* 401**,** 493.

FLEMING, I. 2007. Epoxyeicosatrienoic acids, cell signaling and angiogenesis. *Prostaglandins & other lipid mediators,* 82**,** 60-67.

FLITTER, B. A., HVORECNY, K. L., ONO, E., EDDENS, T., YANG, J., KWAK, D. H., BAHL, C. D., HAMPTON, T. H., MORISSEAU, C., HAMMOCK, B. D., LIU, X., LEE, J. S., KOLLS, J. K., LEVY, B. D., MADDEN, D. R. & BOMBERGER, J. M. 2016. Pseudomonas aeruginosa sabotages the generation of host proresolving lipid mediators. *Proceedings of the national academy of sciences*.

FRETLAND, A. J. & OMIECINSKI, C. J. 2000. Epoxide hydrolases: biochemistry and molecular biology. *Chemico-biological interactions,* 129**,** 41-59.

FRIEDBERG, T., LÖLLMANN, B., BECKER, R., HOLLER, R. & OESCH, F. 1994. The microsomal epoxide hydrolase has a single membrane signal anchor sequence which is dispensable for the catalytic activity of this protein. *Biochemical journal,* 303**,** 967-972.

FURUTA, J., NOBEYAMA, Y., UMEBAYASHI, Y., OTSUKA, F., KIKUCHI, K. & USHIJIMA, T. 2006. Silencing of Peroxiredoxin 2 and aberrant methylation of 33 CpG islands in putative promoter regions in human malignant melanomas. *Cancer research,* 66**,** 6080-6086.

GONZALEZ, F. 1988. The molecular biology of cytochrome P450s. *Pharmacological reviews,* 40**,** 243-288.

GRIEGER, J. C., CHOI, V. W. & SAMULSKI, R. J. 2006. Production and characterization of adeno-associated viral vectors. *Nature protocols,* 1**,** 1412-28.

GROTEN, T., SCHLEUSSNER, E., LEHMANN, T., REISTER, F., HOLZER, B., DANSO, K. & ZEILLINGER, R. 2014. eNOSI4 and EPHX1 polymorphisms affect maternal susceptibility to preeclampsia: analysis of five polymorphisms predisposing to cardiovascular disease in 279 Caucasian and 241 African women. *Archives of gynecology and obstetrics,* 289**,** 581-593.

GUO, A., DURNER, J. & KLESSIG, D. F. 1998. Characterization of a tobacco epoxide hydrolase gene induced during the resistance response to TMV. *The plant journal,* 15**,** 647-656.

HAMMOCK, B. D., GILL, S. S., STAMOUDIS, V. & GILBERT, L. I. 1976. Soluble mammalian epoxide hydratase: action on juvenile hormone and other terpenoid epoxides. *Comparative biochemistry and physiology part B: Comparative biochemistry,* 53**,** 263-265.

HARRIS, T. R., ARONOV, P. A., JONES, P. D., TANAKA, H., ARAND, M. & HAMMOCK, B. D. 2008. Identification of two epoxide hydrolases in Caenorhabditis elegans that metabolize mammalian lipid signaling molecules. *Archives of biochemistry and biophysics,* 472**,** 139-149.

HARRIS, T. R. & HAMMOCK, B. D. 2013. Soluble epoxide hydrolase: gene structure, expression and deletion. *Gene,* 526**,** 61-74.

HASEGAWA, L. S. & HAMMOCK, B. D. 1982. Spectrophotometric assay for mammalian cytosolic epoxide hydrolase using trans-stilbene oxide as the substrate. *Biochemical pharmacology,* 31**,** 1979-1984.

HEREDIA, A. 2003. Biophysical and biochemical characteristics of cutin, a plant barrier biopolymer. *Biochimica et biophysica acta -General Subjects,* 1620**,** 1-7.

HOLLER, R., ARAND, M., MECKY, A., OESCH, F. & FRIEDBERG, T. 1997. The membrane anchor of microsomal epoxide hydrolase from human, rat, and rabbit displays an unexpected membrane topology. *Biochemical and biophysical research communications,* 236**,** 754-9.

HOLMQUIST, M. 2000. Alpha beta-hydrolase fold enzymes structures, functions and mechanisms. *Current protein and peptide science,* 1**,** 209-235.

HOOFNAGLE, A. N., WHITEAKER, J. R., CARR, S. A., KUHN, E., LIU, T., MASSONI, S. A., THOMAS, S. N., TOWNSEND, R. R., ZIMMERMAN, L. J. & BOJA, E. 2016. Recommendations for the generation, quantification, storage, and handling of peptides used for mass spectrometry–based assays. *Clinical chemistry,* 62**,** 48-69.

HOOPES, S. L., GRUZDEV, A., EDIN, M. L., GRAVES, J. P., BRADBURY, J. A., FLAKE, G. P., LIH, F. B., DEGRAFF, L. M. & ZELDIN, D. C. 2017. Generation and characterization of epoxide hydrolase 3 (EPHX3)-deficient mice. *PLOS ONE,* 12**,** e0175348.

HU, C., BUSUTTIL, R. W. & LIPSHUTZ, G. S. 2010. RH10 provides superior transgene expression in mice when compared with natural AAV serotypes for neonatal gene therapy. *The journal of gene medicine,* 12**,** 766-778.

HVORECNY, K. L., BAHL, C. D., KITAMURA, S., LEE, K. S. S., HAMMOCK, B. D., MORISSEAU, C. & MADDEN, D. R. 2017. Active-Site Flexibility and Substrate Specificity in a Bacterial Virulence Factor: Crystallographic Snapshots of an Epoxide Hydrolase. *Structure,* 25**,** 697-707.e4.

IMIG, J. D. 2012. Epoxides and soluble epoxide hydrolase in cardiovascular physiology. *Physiological reviews,* 92**,** 101-130.

IMIG, J. D. 2015. Epoxyeicosatrienoic acids, hypertension, and kidney injury. *Hypertension,* 65**,** 476-482.

INCEOGLU, B., SCHMELZER, K. R., MORISSEAU, C., JINKS, S. L. & HAMMOCK, B. D. 2007. Soluble epoxide hydrolase inhibition reveals novel biological functions of epoxyeicosatrienoic acids (EETs). *Prostaglandins & other lipid mediators,* 82**,** 42-9.

JACKSON, K. L., DAYTON, R. D., DEVERMAN, B. E. & KLEIN, R. L. 2016. Better Targeting, Better Efficiency for Wide-Scale Neuronal Transduction with the Synapsin Promoter and AAV-PHP.B. *Frontiers in molecular neuroscience,* 9**,** 116.

JONES, P. D., WOLF, N. M., MORISSEAU, C., WHETSTONE, P., HOCK, B. & HAMMOCK, B. D. 2005. Fluorescent substrates for soluble epoxide hydrolase and application to inhibition studies. *Analytical biochemistry,* 343**,** 66-75.

KAPLITT, M. G., LEONE, P., SAMULSKI, R. J., XIAO, X., PFAFF, D. W., O'MALLEY, K. L. & DURING, M. J. 1994. Long-term gene expression and phenotypic correction using adeno-associated virus vectors in the mammalian brain. *Nature genetics,* 8**,** 148.

KIM, I.-H., PARK, Y.-K., HAMMOCK, B. D. & NISHI, K. 2011. Structure− Activity Relationships of Cycloalkylamide Derivatives as Inhibitors of the Soluble Epoxide Hydrolase. *Journal of medicinal chemistry,* 54**,** 1752-1761.

KNEHR, M., THOMAS, H., ARAND, M., GEBEL, T., ZELLER, H. D. & OESCH, F. 1993. Isolation and characterization of a cDNA encoding rat liver cytosolic epoxide hydrolase and its functional expression in Escherichia coli. *Journal of biological chemistry,* 268**,** 17623-7.

KOBAYASHI, S., KOHDA, T., MIYOSHI, N., KUROIWA, Y., AISAKA, K., TSUTSUMI, O., KANEKO-ISHINO, T. & ISHINO, F. 1997. Human PEG1/MEST, an imprinted gene on chromosome 7. *Human molecular genetics,* 6**,** 781-786.

KOVALCHUK, S. I., ANIKANOV, N. A., IVANOVA, O. M., ZIGANSHIN, R. H. & GOVORUN, V. M. 2015. Bovine serum albumin as a universal suppressor of non-specific peptide binding in vials prior to nano-chromatography coupled mass-spectrometry analysis. *Analytica chimica acta,* 893**,** 57-64.

KOZAK, M. 1984. Point mutations close to the AUG initiator codon affect the efficiency of translation of rat preproinsulin in vivo. *Nature,* 308**,** 241.

KRÄMER, A., FRANK, H., SETIABUDI, F., OESCH, F. & GLATT, H. 1991. Influence of the level of cytosolic epoxide hydrolase on the induction of sister chromatid exchanges by trans-β-ethylstyrene 7, 8-oxide in human lymphocytes. *Biochemical pharmacology,* 42**,** 2147-2152.

LAASANEN, J., ROMPPANEN, E.-L., HILTUNEN, M., HELISALMI, S., MANNERMAA, A., PUNNONEN, K. & HEINONEN, S. 2002. Two exonic single nucleotide polymorphisms in the microsomal epoxide hydrolase gene are jointly associated with preeclampsia. *European journal of human genetics,* 10**,** 569.

LAUGHLIN, L. T., TZENG, H. F., LIN, S. & ARMSTRONG, R. N. 1998. Mechanism of microsomal epoxide hydrolase. Semifunctional site-specific mutants affecting the alkylation half-reaction. *Biochemistry,* 37**,** 2897-904.

LEFEBVRE, L., VIVILLE, S., BARTON, S. C., ISHINO, F., KEVERNE, E. B. & SURANI, M. A. 1998. Abnormal maternal behaviour and growth retardation associated with loss of the imprinted gene Mest. *Nature genetics,* 20**,** 163.

LIU, M., HUNTER, R., NGUYEN, X. V., KIM, H. C. & BING, G. 2008. Microsomal epoxide hydrolase deletion enhances tyrosine hydroxylase phosphorylation in mice after MPTP treatment. *Journal of neuroscience research,* 86**,** 2792-801.

LO, W. D., QU, G., SFERRA, T. J., CLARK, R., CHEN, R. & JOHNSON, P. R. 1999. Adeno-associated virus-mediated gene transfer to the brain: duration and modulation of expression. *Human gene therapy,* 10**,** 201-213.

LUO, B., NORRIS, C., BOLSTAD, E. S., KNECHT, D. A. & GRANT, D. F. 2008. Protein quaternary structure and expression levels contribute to peroxisomal-targeting-sequence-1-mediated peroxisomal import of human soluble epoxide hydrolase. *Journal of molecular biology,* 380**,** 31-41.

LURIA, A., WELDON, S. M., KABCENELL, A. K., INGRAHAM, R. H., MATERA, D., JIANG, H., GILL, R., MORISSEAU, C., NEWMAN, J. W. & HAMMOCK, B. D. 2007. Compensatory mechanism for homeostatic blood pressure regulation in Ephx2 gene-disrupted mice. *The Journal of biological chemistry,* 282**,** 2891-8.

MACEACHRAN, D. P., YE, S., BOMBERGER, J. M., HOGAN, D. A., SWIATECKA-URBAN, A., STANTON, B. A. & O'TOOLE, G. A. 2007. The Pseudomonas aeruginosa secreted protein PA2934 decreases apical membrane expression of the cystic fibrosis transmembrane conductance regulator. *Infection and immunity,* 75**,** 3902-12.

MANHIANI, M., QUIGLEY, J. E., KNIGHT, S. F., TASOOBSHIRAZI, S., MOORE, T., BRANDS, M. W., HAMMOCK, B. D. & IMIG, J. D. 2009. Soluble epoxide hydrolase gene deletion attenuates renal injury and inflammation with DOCA-salt hypertension. *American journal of physiology-renal physiology,* 297**,** F740-8.

MAROWSKY, A., BURGENER, J., FALCK, J., FRITSCHY, J.-M. & ARAND, M. 2009. Distribution of soluble and microsomal epoxide hydrolase in the mouse brain and its contribution to cerebral epoxyeicosatrienoic acid metabolism. *Neuroscience,* 163**,** 646-661.

MAROWSKY, A., CRONIN, A., FRÈRE, F., ADAMSKA, M. & ARAND, M. 2010. Mammalian Epoxide Hydrolases. *Comprehensive toxicology,* 4**,** 275-294.

MAROWSKY, A., HAENEL, K., BOCKAMP, E., HECK, R., RUTISHAUSER, S., MULE, N., KINDLER, D., RUDIN, M. & ARAND, M. 2016. Genetic enhancement of microsomal epoxide hydrolase improves metabolic detoxification but impairs cerebral blood flow regulation. *Archives of toxicology,* 90**,** 3017-3027.

MAROWSKY, A., MEYER, I., ERISMANN-EBNER, K., PELLEGRINI, G., MULE, N. & ARAND, M. 2017. Beyond detoxification: a role for mouse mEH in the hepatic metabolism of endogenous lipids. *Archives of toxicology,* 91**,** 3571-3585.

MASTAKOV, M. Y., BAER, K., SYMES, C. W., LEICHTLEIN, C. B., KOTIN, R. M. & DURING, M. J. 2002. Immunological aspects of recombinant adeno-associated virus delivery to the mammalian brain. *Journal of virology,* 76**,** 8446-8454.

MESMAN, S., VAN HOOFT, J. A. & SMIDT, M. P. 2017. Mest/Peg1 is essential for the development and maintenance of a SNc neuronal subset. *Frontiers in molecular neuroscience,* 9**,** 166.

MEZZINA, M. & MERTEN, O.-W. 2011. Adeno-associated viruses. *Viral vectors for gene therapy*. Springer.

MICHAELIS, U. R., FISSLTHALER, B., BARBOSA-SICARD, E., FALCK, J. R., FLEMING, I. & BUSSE, R. 2005. Cytochrome P450 epoxygenases 2C8 and 2C9 are implicated in hypoxia-induced endothelial cell migration and angiogenesis. *Journal of cell science,* 118**,** 5489-5498.

MIYATA, M., KUDO, G., LEE, Y. H., YANG, T. J., GELBOIN, H. V., FERNANDEZ-SALGUERO, P., KIMURA, S. & GONZALEZ, F. J. 1999. Targeted disruption of the microsomal epoxide hydrolase gene. Microsomal epoxide hydrolase is required for the carcinogenic activity of 7,12-dimethylbenz[a]anthracene. *Journal of biological chemistry,* 274**,** 23963-8.

MOGHADDAM, M. F., GRANT, D. F., CHEEK, J. M., GREENE, J. F., WILLIAMSON, K. C. & HAMMOCK, B. D. 1997a. Bioactivation of leukotoxins to their toxic diols by epoxide hydrolase. *Nature medicine,* 3**,** 562.

MOGHADDAM, M. F., GRANT, D. F., CHEEK, J. M., GREENE, J. F., WILLIAMSON, K. C. & HAMMOCK, B. D. 1997b. Bioactivation of leukotoxins to their toxic diols by epoxide hydrolase. *Nature medicine,* 3**,** 562-6.

MOODY, D. E., LOURY, D. N. & HAMMOCK, B. D. 1985. Epoxide metabolism in the liver of mice treated with clofibrate (ethyl-α-(p-chlorophenoxyisobutyrate)), a peroxisome proliferator. *Toxicology and applied pharmacology,* 78**,** 351-362.

MORISSEAU, C., BERNAY, M., ESCAICH, A., SANBORN, J. R., LANGO, J. & HAMMOCK, B. D. 2011. Development of fluorescent substrates for microsomal epoxide hydrolase and application to inhibition studies. *Analytical biochemistry,* 414**,** 154-62.

MORISSEAU, C. & HAMMOCK, B. D. 2005. Epoxide hydrolases: mechanisms, inhibitor designs, and biological roles. *Annual review of pharmacology and toxicology,* 45**,** 311-333.

MORISSEAU, C. & HAMMOCK, B. D. 2013. Impact of soluble epoxide hydrolase and epoxyeicosanoids on human health. *Annual review of pharmacology and toxicology,* 53**,** 37-58.

MORISSEAU, C., INCEOGLU, B., SCHMELZER, K., TSAI, H.-J., JINKS, S. L., HEGEDUS, C. M. & HAMMOCK, B. D. 2010. Naturally occurring mono epoxides of EPA and DHA are bioactive antihyperalgesic lipids. *Journal of lipid research***,** jlr. M006007.

MORISSEAU, C., NEWMAN, J. W., DOWDY, D. L., GOODROW, M. H. & HAMMOCK, B. D. 2001. Inhibition of microsomal epoxide hydrolases by ureas, amides, and amines. *Chemical research in toxicology,* 14**,** 409-415.

MULE, N. K., ORJUELA LEON, A. C., FALCK, J. R., ARAND, M. & MAROWSKY, A. 2017. 11,12 - Epoxyeicosatrienoic acid (11,12 EET) reduces excitability and excitatory transmission in the hippocampus. *Neuropharmacology,* 123**,** 310-321.

MULLEN, R. T., TRELEASE, R. N., DUERK, H., ARAND, M., HAMMOCK, B. D., OESCH, F. & GRANT, D. F. 1999. Differential subcellular localization of endogenous and transfected soluble epoxide hydrolase in mammalian cells: evidence for isozyme variants. *FEBS Letters,* 445**,** 301-5.

MULLER, F., ARAND, M., FRANK, H., SEIDEL, A., HINZ, W., WINKLER, L., HANEL, K., BLEE, E., BEETHAM, J. K., HAMMOCK, B. D. & OESCH, F. 1997. Visualization of a covalent intermediate between microsomal epoxide hydrolase, but not cholesterol epoxide hydrolase, and their substrates. *European journal of biochemistry,* 245**,** 490-6.

MULLIN, C. A. 1988. Adaptive relationships of epoxide hydrolase in herbivorous arthropods. *Journal of chemical ecology,* 14**,** 1867-1888.

NAKANISHI, H., SUDA, T., KATOH, M., WATANABE, A., IGISHI, T., KODANI, M., MATSUMOTO, S., NAKAMOTO, M., SHIGEOKA, Y. & OKABE, T. 2004. Loss of imprinting of PEG1/MEST in lung cancer cell lines. *Oncology reports,* 12**,** 1273-1278.

NARDINI, M. & DIJKSTRA, B. W. 1999. Alpha/beta hydrolase fold enzymes: the family keeps growing. *Current opinion in structural biology,* 9**,** 732-7.

NARDINI, M., RIDDER, I. S., ROZEBOOM, H. J., KALK, K. H., RINK, R., JANSSEN, D. B. & DIJKSTRA, B. W. 1999. The X-ray Structure of Epoxide Hydrolase from Agrobacterium radiobacter AD1 An enzyme to detoxify harmful epoxides. *Journal of biological chemistry,* 274**,** 14579-14586.

NEWMAN, J. W., MORISSEAU, C. & HAMMOCK, B. D. 2005. Epoxide hydrolases: their roles and interactions with lipid metabolism. *Progress in lipid research,* 44**,** 1-51.

NEWMAN, J. W., MORISSEAU, C., HARRIS, T. R. & HAMMOCK, B. D. 2003. The soluble epoxide hydrolase encoded by EPXH2 is a bifunctional enzyme with novel lipid phosphate phosphatase activity. *Proceedings of the national academy of sciences,* 100**,** 1558-1563.

NIKONOVA, L., KOZA, R. A., MENDOZA, T., CHAO, P.-M., CURLEY, J. P. & KOZAK, L. P. 2008a. Mesoderm-specific transcript is associated with fat mass expansion in response to a positive energy balance. *The FASEB Journal,* 22**,** 3925-3937.

NIKONOVA, L., KOZA, R. A., MENDOZA, T., CHAO, P. M., CURLEY, J. P. & KOZAK, L. P. 2008b. Mesoderm-specific transcript is associated with fat mass expansion in response to a positive energy balance. *FASEB journal,* 22**,** 3925-37.

NODE, K., HUO, Y., RUAN, X., YANG, B., SPIECKER, M., LEY, K., ZELDIN, D. C. & LIAO, J. K. 1999. Anti-inflammatory properties of cytochrome P450 epoxygenase-derived eicosanoids. *Science,* 285**,** 1276-1279.

OESCH, F. 1973. Mammalian epoxide hydrases: inducible enzymes catalysing the inactivation of carcinogenic and cytotoxic metabolites derived from aromatic and olefinic compounds. *Xenobiotica,* 3**,** 305-40.

OESCH, F. 1974. Purification and specificity of a human microsomal epoxide hydratase. *Biochemical journal,* 139**,** 77-88.

OESCH, F. & BENTLEY, P. 1976. Antibodies against homogeneous epoxide hydratase provide evidence for a single enzyme hydrating styrene oxide and benz(a)pyrene 4,5-oxide. *Nature,* 259**,** 53-5.

OESCH, F., HENGSTLER, J. G. & ARAND, M. 2004. Detoxication Strategy of Epoxide Hydrolase—The Basis for a Novel Threshold for Definable Genotoxic Carcinogens. *Nonlinearity in biology, toxicology, medicine,* 2**,** 15401420490426963.

OESCH, F., HERRERO, M. E., HENGSTLER, J. G., LOHMANN, M. & ARAND, M. 2000. Metabolic detoxification: implications for thresholds. *Toxicologic pathology,* 28**,** 382-387.

OJALA, D. S., AMARA, D. P. & SCHAFFER, D. V. 2015. Adeno-associated virus vectors and neurological gene therapy. *The neuroscientist : a review journal bringing neurobiology, neurology and psychiatry,* 21**,** 84-98.

OLLIS, D. L., CHEAH, E., CYGLER, M., DIJKSTRA, B., FROLOW, F., FRANKEN, S. M., HAREL, M., REMINGTON, S. J., SILMAN, I., SCHRAG, J. & ET AL. 1992. The alpha/beta hydrolase fold. *Protein engineering,* 5**,** 197-211.

ORJUELA LEON, A. C., MARWOSKY, A. & ARAND, M. 2017. Evidence for a complex formation between CYP2J5 and mEH in living cells by FRET analysis of membrane protein interaction in the endoplasmic reticulum (FAMPIR). *Archives of toxicology,* 91**,** 3561-3570.

ØSTER, B., THORSEN, K., LAMY, P., WOJDACZ, T. K., HANSEN, L. L., BIRKENKAMP-DEMTRÖDER, K., SØRENSEN, K. D., LAURBERG, S., ØRNTOFT, T. F. & ANDERSEN, C. L. 2011. Identification and validation of highly frequent CpG island hypermethylation in colorectal adenomas and carcinomas. *International journal of cancer,* 129**,** 2855-2866.

OTA, K. & HAMMOCK, B. D. 1980. Cytosolic and microsomal epoxide hydrolases: differential properties in mammalian liver. *Science,* 207**,** 1479-1481.

PARKINS, M. D., SOMAYAJI, R. & WATERS, V. J. 2018. Epidemiology, Biology, and Impact of Clonal Pseudomonas aeruginosa Infections in Cystic Fibrosis. *Clinical microbiology reviews,* 31.

PATERNA, J. C., MOCCETTI, T., MURA, A., FELDON, J. & BUELER, H. 2000. Influence of promoter and WHV post-transcriptional regulatory element on AAV-mediated transgene expression in the rat brain. *Gene therapy,* 7**,** 1304-11.

PEDERSEN, I. S., DERVAN, P. A., BRODERICK, D., HARRISON, M., MILLER, N., DELANY, E., O'SHEA, D., COSTELLO, P., MCGOLDRICK, A. & KEATING, G. 1999. Frequent loss of imprinting of PEG1/MEST in invasive breast cancer. *Cancer research,* 59**,** 5449-5451.

PENG, X., CARHUAPOMA, J. R., BHARDWAJ, A., ALKAYED, N. J., FALCK, J. R., HARDER, D. R., TRAYSTMAN, R. J. & KOEHLER, R. C. 2002. Suppression of cortical functional hyperemia to vibrissal stimulation in the rat by epoxygenase inhibitors. *American journal of physiology-heart and circulatory physiology,* 283**,** H2029-H2037.

PETROSYAN, H., ALESSI, V., SINGH, V., HUNANYAN, A., LEVINE, J. & ARVANIAN, V. 2014. Transduction efficiency of neurons and glial cells by AAV-1,-5,-9,-rh10 and-hu11 serotypes in rat spinal cord following contusion injury. *Gene therapy,* 21**,** 991-1000.

PIETROPAOLO, S., PATERNA, J.-C., BÜELER, H., FELDON, J. & YEE, B. K. 2007. Bidirectional changes in water-maze learning following recombinant adenovirus-associated viral vector (rAAV)-mediated brain-derived neurotrophic factor expression in the rat hippocampus. *Behavioural pharmacology,* 18**,** 533-547.

POKREISZ, P., FLEMING, I., KISS, L., BARBOSA-SICARD, E., FISSLTHALER, B., FALCK, J. R., HAMMOCK, B. D., KIM, I.-H., SZELID, Z. & VERMEERSCH, P. 2006. Cytochrome P450 epoxygenase gene function in hypoxic pulmonary vasoconstriction and pulmonary vascular remodeling. *Hypertension,* 47**,** 762-770.

PORTER, T. D., BECK, T. W. & KASPER, C. B. 1986. Complementary DNA and amino acid sequence of rat liver microsomal, xenobiotic epoxide hydrolase. *Archives of biochemistry and biophysics,* 248**,** 121-129.

QIN, X., WU, Q., LIN, L., SUN, A., LIU, S., LI, X., CAO, X., GAO, T., LUO, P. & ZHU, X. 2015. Soluble epoxide hydrolase deficiency or inhibition attenuates MPTP-induced parkinsonism. *Molecular neurobiology,* 52**,** 187-195.

RENAUD, H. J., CUI, J. Y., KHAN, M. & KLAASSEN, C. D. 2011. Tissue distribution and gender-divergent expression of 78 cytochrome P450 mRNAs in mice. *Toxicological sciences,* 124**,** 261-277.

SADO, T., NAKAJIMA, N., TADA, M. & TAKAGI, N. 1993. A Novel Mesoderm-Specific cDNA Isolated from a Mouse Embryonal Carcinoma Cell Line: (embryonal carcinoma cell/cDNA/in situ hybridization/mesoderm/mouse embryo). *Development, growth & differentiation,* 35**,** 551-560.

SCHAAF, T. K. & HESS, H. J. 1979. Synthesis and biological activity of carboxyl-terminus modified prostaglandin analogs. *Journal of medicinal chemistry,* 22**,** 1340-1346.

SHIMADA, T. 2006. Xenobiotic-metabolizing enzymes involved in activation and detoxification of carcinogenic polycyclic aromatic hydrocarbons. *Drug metabolism and pharmacokinetics,* 21**,** 257-76.

SINAL, C. J., MIYATA, M., TOHKIN, M., NAGATA, K., BEND, J. R. & GONZALEZ, F. J. 2000. Targeted disruption of soluble epoxide hydrolase reveals a role in blood pressure regulation. *Journal of biological chemistry,* 275**,** 40504-10.

SLADE, M. & ZIBITT, C. H. 1972. Metabolism of Cecropia juvenile hormone in insects and in mammals. *Insect Juvenile Hormones.* Elsevier.

SPECTOR, A. A. & NORRIS, A. W. 2006. Action of epoxyeicosatrienoic acids (EETs) on cellular function. *American journal of physiology-cell physiology*.

SUN, D., CUEVAS, A. J., GOTLINGER, K., HWANG, S. H., HAMMOCK, B. D., SCHWARTZMAN, M. L. & HUANG, A. 2014a. Soluble epoxide hydrolase-dependent regulation of myogenic response and blood pressure. *American journal of physiology-heart and circulatory physiology,* 306**,** H1146-53.

SUN, S., ZHOU, J.-Y., YANG, W. & ZHANG, H. 2014b. Inhibition of protein carbamylation in urea solution using ammonium-containing buffers. *Analytical biochemistry,* 446**,** 76-81.

SWIATECKA-URBAN, A., MOREAU-MARQUIS, S., MACEACHRAN, D. P., CONNOLLY, J. P., STANTON, C. R., SU, J. R., BARNABY, R., O'TOOLE, G. A. & STANTON, B. A. 2006. Pseudomonas aeruginosa inhibits endocytic recycling of CFTR in polarized human airway epithelial cells. *American journal of physiology-cell physiology,* 290**,** C862-72.

TOULZA, E., MATTIUZZO, N. R., GALLIANO, M.-F., JONCA, N., DOSSAT, C., JACOB, D., DE DARUVAR, A., WINCKER, P., SERRE, G. & GUERRIN, M. 2007. Large-scale identification of human genes implicated in epidermal barrier function. *Genome biology,* 8**,** R107.

VAN DER WERF, M. J., OVERKAMP, K. M. & DE BONT, J. A. 1998. Limonene-1, 2-epoxide hydrolase fromRhodococcus erythropolis DCL14 belongs to a novel class of epoxide hydrolases. *Journal of bacteriology,* 180**,** 5052-5057.

VANALSTINE, M. A. & HOUGH, L. B. 2011. Effects of acetylenic epoxygenase inhibitors on recombinant cytochrome p450s. *Drug metabolism and disposition***,** dmd. 110.037424.

VON DER HUDE, W., CARSTENSEN, S. & OBE, G. 1991. Structure-activity relationships of epoxides: induction of sister-chromatid exchanges in Chinese hamster V79 cells. *Mutation research/fundamental and molecular mechanisms of mutagenesis,* 249**,** 55-70.

WAGNER, K. M., MCREYNOLDS, C. B., SCHMIDT, W. K. & HAMMOCK, B. D. 2017. Soluble epoxide hydrolase as a therapeutic target for pain, inflammatory and neurodegenerative diseases. *Pharmacology & therapeutics,* 180**,** 62-76.

WANG, L., LUO, G., ZHANG, L.-F. & GENG, H.-X. 2018. Neuroprotective Effects of Epoxyeicosatrienoic Acids. *Prostaglandins & other lipid mediators*.

WANG, M.-H., BRAND-SCHIEBER, E., ZAND, B. A., NGUYEN, X., FALCK, J. R., BALU, N. & SCHWARTZMAN, M. L. 1998. Cytochrome P450-derived arachidonic acid metabolism in the rat kidney: characterization of selective inhibitors. *Journal of pharmacology and experimental therapeutics,* 284**,** 966-973.

WANG, Z., FANG, Y., TEAGUE, J., WONG, H., MORISSEAU, C., HAMMOCK, B. D., ROCK, D. A. & WANG, Z. 2017. In Vitro Metabolism of Oprozomib, an Oral Proteasome Inhibitor: Role of Epoxide Hydrolases and Cytochrome P450s. *Drug metabolism and disposition,* 45**,** 712-720.

WELTE, M. A. 2015. Expanding roles for lipid droplets. *Current biology,* 25**,** R470-R481.

WU, Z., ASOKAN, A. & SAMULSKI, R. J. 2006. Adeno-associated virus serotypes: vector toolkit for human gene therapy. *Molecular therapy,* 14**,** 316-327.

XU, X., ZHAO, C. X., WANG, L., TU, L., FANG, X., ZHENG, C., EDIN, M. L., ZELDIN, D. C. & WANG, D. W. 2010. Increased CYP2J3 expression reduces insulin resistance in fructose-treated rats and db/db mice. *Diabetes*.

YAMANASHI, H., BOEGLIN, W. E., MORISSEAU, C., DAVIS, R. W., SULIKOWSKI, G. A., HAMMOCK, B. D. & BRASH, A. R. 2018. Catalytic activities of mammalian epoxide hydrolases with cis and trans fatty acid epoxides relevant to skin barrier function. *Journal of lipid research***,** jlr. M082701.

YAMASHITA, S., TSUJINO, Y., MORIGUCHI, K., TATEMATSU, M. & USHIJIMA, T. 2006. Chemical genomic screening for methylation-silenced genes in gastric cancer cell lines using 5-aza-2′-deoxycytidine treatment and oligonucleotide microarray. *Cancer science,* 97**,** 64-71.

YANG, L., CHERIYAN, J., GUTTERMAN, D. D., MAYER, R. J., AMENT, Z., GRIFFIN, J. L., LAZAAR, A. L., NEWBY, D. E., TAL-SINGER, R. & WILKINSON, I. B. 2017. Mechanisms of Vascular Dysfunction in COPD and Effects of a Novel Soluble Epoxide Hydrolase Inhibitor in Smokers. *Chest,* 151**,** 555-563.

YU, Z., XU, F., HUSE, L. M., MORISSEAU, C., DRAPER, A. J., NEWMAN, J. W., PARKER, C., GRAHAM, L., ENGLER, M. M. & HAMMOCK, B. D. 2000. Soluble epoxide hydrolase regulates hydrolysis of vasoactive epoxyeicosatrienoic acids. *Circulation research,* 87**,** 992-998.

ZELDIN, D. C., KOBAYASHI, J., FALCK, J. R., WINDER, B. S., HAMMOCK, B. D., SNAPPER, J. R. & CAPDEVILA, J. H. 1993. Regio-and enantiofacial selectivity of epoxyeicosatrienoic acid hydration by cytosolic epoxide hydrolase. *Journal of biological chemistry,* 268**,** 6402-6407.

ZHANG, G., PANIGRAHY, D., MAHAKIAN, L. M., YANG, J., LIU, J.-Y., LEE, K. S. S., WETTERSTEN, H. I., ULU, A., HU, X. & TAM, S. 2013. Epoxy metabolites of docosahexaenoic acid (DHA) inhibit angiogenesis, tumor growth, and metastasis. *Proceedings of the national academy of sciences***,** 201304321.

ZHENG, J., PLOPPER, C. G., LAKRITZ, J., STORMS, D. H. & HAMMOCK, B. D. 2001. Leukotoxin-diol: a putative toxic mediator involved in acute respiratory distress syndrome. *American journal of respiratory cell and molecular biology,* 25**,** 434-8.

ZHU, D., BOUSAMRA, M., ZELDIN, D. C., FALCK, J. R., TOWNSLEY, M., HARDER, D. R., ROMAN, R. J. & JACOBS, E. R. 2000. Epoxyeicosatrienoic acids constrict isolated pressurized rabbit pulmonary arteries. *American journal of physiology-lung cellular and molecular physiology,* 278**,** L335-L343.

ZOU, J., HALLBERG, B. M., BERGFORS, T., OESCH, F., ARAND, M., MOWBRAY, S. L. & JONES, T. A. 2000. Structure of Aspergillus niger epoxide hydrolase at 1.8 A resolution: implications for the structure and function of the mammalian microsomal class of epoxide hydrolases. *Structure,* 8**,** 111-22.

ZUSTERZEEL, P. L., PETERS, W. H., VISSER, W., HERMSEN, K. J., ROELOFS, H. M. & STEEGERS, E. A. 2001. A polymorphism in the gene for microsomal epoxide hydrolase is associated with pre-eclampsia. *Journal of medical genetics,* 38**,** 234-237.

ACKNOWLEDGMENTS

Es war eine spannende und lehrreiche Zeit als PhD-Student und oft lagen Erfolg und Frustration nahe beieinander. Damit möchte ich mich bei allen bedanken, die mich unterstützt und auf ganz unterschiedliche Weise zu meiner Doktorarbeit beigetragen haben:

An erster Stelle bedanke ich mich bei meinem Supervisor Erni (Michael Arand), der mir die Möglichkeit gegeben hat an diesem Projekt zu arbeiten. Vielen Dank für dein scheinbar grenzenloses Wissen, die vielen motivierenden und weiterführenden Diskussionen und dein entgegengebrachtes Vertrauen.

Gleichermassen bedanke ich mich bei Monika Dengler, die das Hauptprojekt gemeinsam mit mir gemeistert hat. Du warst die beste Team-Partnerin, die ich mir vorstellen kann. Wir haben diese Arbeit als Studienkolleginnen begonnen und haben sie als Freunde beendet. Liebe Monika, danke für alles!

Vielen Dank auch an Prof. Dr. Hanns Ulrich Zeilhofer und Prof. Dr. Ursula Quitterer, die mein Komitee vervollständigen und damit einen wertvollen Beitrag zu dieser Arbeit geleistet haben.

Ein herzliches Dankeschön an alle Toxies! Liebe(r) Anne, Imke, Kira, Olga und Beau vielen Dank für eure Inputs, viele lehrreiche und unterhaltsame Gespräche, eure Unterstützung und die tolle Zeit mit euch. Danke Kira und Beau für das kritische Korrekturlesen und die vielen lustigen Bakkie-, Kuchen-, Playmobil-, Mittags- und Bierpausen. Ohne euch hätte das Ganze nur halb so viel Spass gemacht!

Vielen Dank an Dr. Jean-Charles Paterna für die Hilfe bei der Virusproduktion und an Mohammad Hleihil, Dr. Karen Haenraets, Ladina Hösli und Rebecca Das Gupta für die Hilfe bei den Perfusionen und Gewebefärbungen.

Vielen Dank an alle, die das Institut ausmachen und es zu einem tollen Arbeitsplatz machen. Herzlichen Dank auch allen Freunden und Kollegen ausserhalb des Instituts für‘s Kopf freimachen und Geniessen.

Danke Mami, Ätti, Evi und Meli, ihr seid die beste Familie auf dieser Kugel!

Danke Orlando, ohne Worte <3

CURRICULUM VITAE

PERSONAL DATA	
Last name	Hew
First name	Bettina
Date of birth	30. July, 1987
Citizen of	Klosters-Serneus, GR
Nationality	Swiss

EDUCATION

03/2014 - 11/2018	PhD student ETH in Toxicology at the Institute of Pharmacology and Toxicology, University of Zurich Irchel, Group of Prof. Dr. Michael Arand "Substrate identification and functional analysis of α/β hydrolase fold epoxide hydrolases" PhD committee: Prof. Dr. Hanns Ulrich Zeilhofer, Prof. Dr. Michael Arand, Prof. Dr. Ursula Quitterer
10/2013	Federal Pharmacist Diploma
09/2011 - 09/2013	Master's Degree in Pharmaceutical Sciences at the ETH Zurich Master thesis at the Institute of Pharmaceutical Sciences, ETH Zurich, group of Prof. Dr. med. Michael Detmar "The role of lymphatic metastasis in tumor progression"
09/2007 - 09/2011	Bachelor's Degree in Pharmaceutical Sciences at the ETH Zurich
08/2002 - 06/2006	Evangelische Mittelschule Schiers (GR) (high school) Specialization: Spanish, Supplementary subject: Geography

POSTERS, PRESENTATIONS AND MANUSCRIPTS

One-day Symposium Drug Discovery Network Zurich (DDNZ), February 10, 2017, Zurich, Switzerland. Poster: "The cytochrome P450 blocker MS-PPOH is a high affinity inhibitor of soluble epoxide hydrolase.", **B. Hew,** M. Arand

38th Colloquium on Toxicology, Swiss Society of Toxicology, May 16, 2017, Basel, Switzerland. Presentation: "Dreadful off-target effect of a pharmacologic *in vivo* inhibitor.", **B. Hew**, M. Arand

Manuscripts in preparation:
"The cytochrome P450 blocker MS-PPOH is an inhibitor of soluble epoxide hydrolase.", **B. Hew**, M. Dengler, M. Arand

"Kinetic analysis of the epoxide hydrolase Cif, a pathogenicity factor from *Pseudomonas aeruginosa*.", **M. Dengler**, B. Hew, M. Arand

"Characterization of microsomal epoxide hydrolase through *in vitro* substrate and inhibitor assessments.", **A. Marowsky**, B. Hew and others

RETREATS

PhD Program Predictive Toxicology Student Retreat, September 11-12, 2014, Vitznau, Switzerland. Presentation: "Deciphering the (patho)physiologic role of epoxide hydrolases by *ex vivo* cartography of their substrate landscape.", **B. Hew**, M. Dengler, M. Arand

PhD Program Predictive Toxicology Student Retreat, November 5-6, 2015, Engelberg, Switzerland. Presentation: "Deciphering the (patho)physiologic role of epoxide hydrolases by *ex vivo* cartography of their substrate landscape – Introduction and Virus Production.", **B. Hew**, M. Dengler, M. Arand

PhD Program Predictive Toxicology Student Retreat, June 27-28, 2016, Ittigen, Switzerland. Presentation: "Deciphering the (patho)physiologic role of epoxide hydrolases by *ex vivo* cartography of their substrate landscape – Introduction and Virus Production.", **B. Hew**, M. Dengler, M. Arand

PhD Program Predictive Toxicology Student Retreat, June 1-2, 2017, Stoos, Switzerland. Presentation: "Substrate landscape of epoxide hydrolases – Virus production and *in vivo* administration.", **B. Hew**, M. Dengler, M. Arand

CONTINUING EDUCATION

Weiterbildungsprogramm Fachtoxikologin/Fachtoxikologe GT, Deutsche Gesellschaft für experimentelle und klinische Pharmakologie und Toxikologie (DGPT):

Grundlagen der Organtoxikologie und -pathologie II, June 16-20, 2014, Erfurt, Germany.

Fremdstoffmetabolismus/ Toxikokinetik, August 25-29, 2014, Zurich, Switzerland.

Safety Pharmacology, February 2-6, 2015, Basel, Switzerland.

Grundlagen der Organtoxikologie und -pathologie I, February 23-27, 2015, Erfurt, Germany.

Molekulare Zelltoxikologie, March 16-20, 2015, Munich, Germany.

LTK Modul1, FELASA Category B, August 10-19, 2015, Zurich, Switzerland.

Lebensmitteltoxikologie, October 10-14, 2016, Hannover, Germany.

Epidemiologische Methoden, March 6-10, 2017, Hannover, Germany.

Klinische Toxikologie, September 11-15, 2017, Berlin, Germany.

Chemische Kanzerogenese und Mutagenese, November 27-December 2, 2017, Munich, Germany.